

# BIM based Cyber-physical System for Bridge Assessment

## cyberBridge

Project funded by the European Community under the  
Eurostars project E! 10925

## M8.2 Completion of all pilots

Responsible author: Tobias Mansperger  
Co-authors: Jan Cervenka, Markus Petschacher,

Status: final  
Type: software/pilot  
Access: public  
Version: 3.0  
Date: 5. 6. 2020

Available for download at  
<http://www.cyberBridge.eu>



## Executive summary:

The project cyberBridge develops a new cyber-physical bridge assessment system that allows at low cost allow continuous online monitoring and system identification beyond modal analysis on the level of crack propagation and hence considerably improve prognosis of bridge deterioration. We deliver a software system both as a product and as a service. Besides selling the system, continuous support and training, partial and complete bridge monitoring services and life cycle prognosis will be offered.

The goal is to radically improve bridge monitoring and forecasting. The main result is an innovative BIM based cyber-physical system for bridge assessment comprising continuous bridge and load monitoring, continuous vehicle load and bridge system identification for global and local crack propagation deterioration, and forecasting using mass simulation and probabilistic methods. It is provided as a continuous monitoring platform with online evaluation. The automated use of HPC (Cloud/Grid) power allows deep system identification at any time providing for much better understanding of the deterioration process and the impact of each deterioration event on the reliability of the bridge.

This report provides an overview of the proposed pilot tests. Three pilot bridges were proposed in Germany, Czech Republic and Austria. The bridges were equipped with an online monitoring system, which enables to measure the bridge response as well as the weight and type of the traffic using the bridge. This information was used to calibrate numerical models for the pilot bridges.

This information is used to make prognosis of the bridge behavior in the future. The prognosis development is part of WP 6 and is reported in deliverables from this WP [8].

## Revision history:

date	author	status	changes
07.04.2020	Tobias Mansperger	draft	First draft version
16.04.2020	Markus Petschacher	draft	Addition Austrian bridge (PSP)
23.04.2020	Tobias Mansperger	pre-final	Additions Vogelsang bridge
30.04.2020	Jan Cervenka	final	Minor editorial changes
5.6.2020	Jan Cervenka	Ver 3.0	Added figures on Wonka bridge and correction of incorrect captions

## Table of contents:

<b>REVISION HISTORY:</b> .....	<b>3</b>
<b>1 GENERAL</b> .....	<b>6</b>
<b>2 WONKA BRIDGE PARDUBICE, CZECH REPUBLIC (CER)</b> .....	<b>8</b>
2.1 MONITORING PROCEDURE AND RESULTS.....	10
2.2 ANALYSIS OF PRELIMINARY MEASUREMENTS .....	13
2.2.1 Introduction .....	13
2.2.2 Is our data set biased?.....	14
2.2.3 Vehicle Description.....	15
2.2.4 Temporal patterns.....	16
2.2.5 Damage description.....	18
2.3 DEVELOPMENT AND CALIBRATION OF THE NUMERICAL MODEL .....	18
2.3.1 Initial calibration using bridge load test data.....	19
2.3.2 Calibration on bridge monitoring .....	19
2.3.3 Prognosis of bridge load carrying capacity and durability modelling.....	30
<b>3 VOGELANGBRÜCKE ESSLINGEN, GERMANY (LAP)</b> .....	<b>34</b>
3.1 OVERVIEW.....	34
3.2 MAIN BRIDGE B1 & B2 OVER NECKAR RIVER.....	35
3.3 RAMPS C1 – C4.....	36
3.4 TWO-SPAN-BRIDGE D1 & D2 .....	38
3.5 BIM MODEL .....	39
3.6 MONITORING PROCEDURE AND RESULTS.....	41
3.7 ANALYSIS OF INITIAL DATA SET .....	44
3.7.1 Is the data set biased? .....	45
3.7.2 Vehicle Characteristics.....	47
3.7.3 Temporal Patterns.....	48
3.7.4 Damage Metrics .....	49
3.8 DEVELOPMENT AND CALIBRATION OF THE NUMERICAL MODEL .....	49
3.8.1 Model.....	49
3.8.2 Material parameters.....	50
3.8.3 Parametric study .....	51
3.8.4 Results .....	53
3.9 DURABILITY PROGNOSIS .....	55
3.9.1 General .....	55
3.9.2 Durability Study .....	55
3.9.3 Prediction of Reinforcement Corrosion in Existing Structure.....	56
3.9.4 Conclusions .....	60

---

<b>4</b>	<b>AUSTRIAN BRIDGE (PSP)</b> .....	<b>61</b>
4.1	MONITORING PROCEDURE AND RESULTS.....	63
4.2	DEVELOPMENT AND CALIBRATION OF THE NUMERICAL MODEL .....	65
4.3	INITIAL ANALYSIS OF DATA SET .....	65
4.3.1	Introduction .....	65
4.3.2	Bias.....	66
4.3.3	Vehicle Characteristics.....	67
4.3.4	Temporal Patterns.....	67
4.3.5	Damage Metrics .....	69
4.4	ETHICAL ISSUES.....	69
<b>5</b>	<b>REFERENCES</b> .....	<b>70</b>

# 1 General

The goal is to radically improve bridge monitoring and forecasting. The main result is an innovative BIM based cyber-physical system for bridge assessment comprising continuous bridge and load monitoring, continuous vehicle load and bridge system identification for global and local crack propagation deterioration, and forecasting using mass simulation and probabilistic methods. It is provided as a continuous monitoring platform with online evaluation. The automated use of HPC (Cloud/Grid) power allows deep system identification at any time providing for much better understanding of the deterioration process and the impact of each deterioration event on the reliability of the bridge.

The system is capable of continuously detecting micro cracks and the deterioration state as well as its changes on a much more precise level and a higher confidence than today's monitoring systems and keeps monitoring costs at about the same level. This is based on several new methods:

- 1) A new continuous simulation-based system identification method for global and local behaviour identification, using massive Grid/Cloud simulation,
- 2) Load monitoring systems for identification of individual vehicles and their synchronisation with the bridge behaviour monitored values,
- 3) Reliable, accurate prediction of the remaining lifespan and retrofit measures on the basis of the deeply identified system and massive Grid/Cloud sensitivity simulations and probabilistic methods
- 4) BIM, Multimodel and ontology-centred flexible and efficient mass information management and visualization of the results via a 3D bridge navigator enabling improved information and decision-making even for laypersons
- 5) Improved sensor system layout, modification and tuning process for global and local bridge system identification based on multiple virtual scenario simulations and ontology-based Multimodel information management.
- 6) Improved sensor network with max 1ms delay.

Target clients and products are:

## 1) Bridge Owners

Product (2): The cyberBridge system itself, including the system, installing equipment, training people for a fixed period, helpdesk support, consultancy on demand and continuous updates on annual fee basis.

Product (1): Consulting for bridge assessment. In this case, the cyberBridge system will be maintained by the partners. The clients will have full access on all data or only on some selected data depending on the specific

contract. The cyberBridge system will either be explicitly rented or will be offered as part of the consultant contract and price.

## 2) Monitoring and Assessment Companies

Product (3): The cyberBridge system. The complete system with all hardware and software components will be offered at a fixed price and an annual support as well as update fee. The latter concerns in particular the cyberBridge software components, i.e. the core platform services, the workflow system, the data management and storage system, the public Cloud access, the private Grid, the BIM filter and

navigator tools as well as the ATENA extended system and the system identification system, i.e. variation and fit algorithms and strategies.

### 3. Consultant Companies

This is essentially the same as for Bridge Owners, but the related contract is sub-contracting.

### 4. To all

Product (4): Education, system identification with cyber-physical systems is a new area in civil engineering, where up to now no courses are offered, except of traditional temporary monitoring and vibration modes fitting, i.e. with a strongly limited amount of parameters. Therefore, the results of cyberBridge will be offered as a new university and industry course by TUD as wells as for the training courses mentioned above.

Most important at the start of the development of the cyberBridge platform is the proper identification of all relevant requirements in accordance with the project scope and objectives, all relevant basic specifications to be used in the development work, with special emphasis on available standards or accepted industry norms, the envisaged users / clients of the system, and the respective practice-oriented usage scenarios. Requirements will be defined on the basis of the buildingSMART IDM methodology (ISO 29481-1:2010) to provide for early recognition of all data exchange and interoperability issues as a first substantial step towards Multimodel based information integration. Requirement gathering is thereby be split in three separate tasks, namely

- (1) computational engineering and system engineering,
- (2) monitoring and
- (3) ICT system,

in order to work out the most innovative use of the newly emerging technologies in each domain by one partner per task in accordance with the expertise and background knowledge of the partners.

## 2 Wonka Bridge Pardubice, Czech Republic (CER)

This pilot bridge is a prestressed box-girder concrete bridge of Mr. Pavel Wonka over the river Elbe in Pardubice, Czech Republic (see Fig. 2-1).

The bridge was designed and erected between 1956 and 1959. The structure is depicted in Fig. 2-2. The bridge consists of three arches, having spans 50 + 70 + 50 m. Average depth of cross sections is up to 3.5 m.

This was the first pilot bridge of the cyberBridge project. It was used for first tests and evaluations of the developed analytical and monitoring technologies.

The structure was analysed by program ATENA with implemented durability models [11]. The bridge is modelled by 4512 layered shell elements. The structure near supports and some other details are modelled by hexahedral and wedge solid elements. The pre-stressed tendons are realized by 3022 external cable truss elements, while the conventional reinforcement is introduced by embedded reinforcement within shell elements. A special material model for concrete and tendons has been employed with more details in [12].

The analysis of the bridge consists of three parts. The first analysis replicates in-situ load tests and measurements. The bridge was loaded by its self-weight and by tens of loaded trucks simulating a traffic load. It was used to calibrate the model of the bridge.

In the second part, numerical model was used to investigate service load state (SLS) and ultimate load state (ULS) of the bridge. Applied steps of the analysis and the associated loads were as follows:

1. Self-weight of the load-bearing structure and pre-stressing, (steps 1...10)
2. Weight of the top layers of the bridge, i.e. road etc., (steps 11...15)
3. Extra 35% of the load in the item 2, (steps 16...20)
4. 150% of the traffic load of the bridges according to ULS ČSN EN 1991-2, (steps 21...27)
5. Additional extra load according to the item 4. incremented up to failure of the bridge, (steps 28...78)



Fig. 2-1: Wonka bridge in Pardubice during the monitoring installation in August 2018

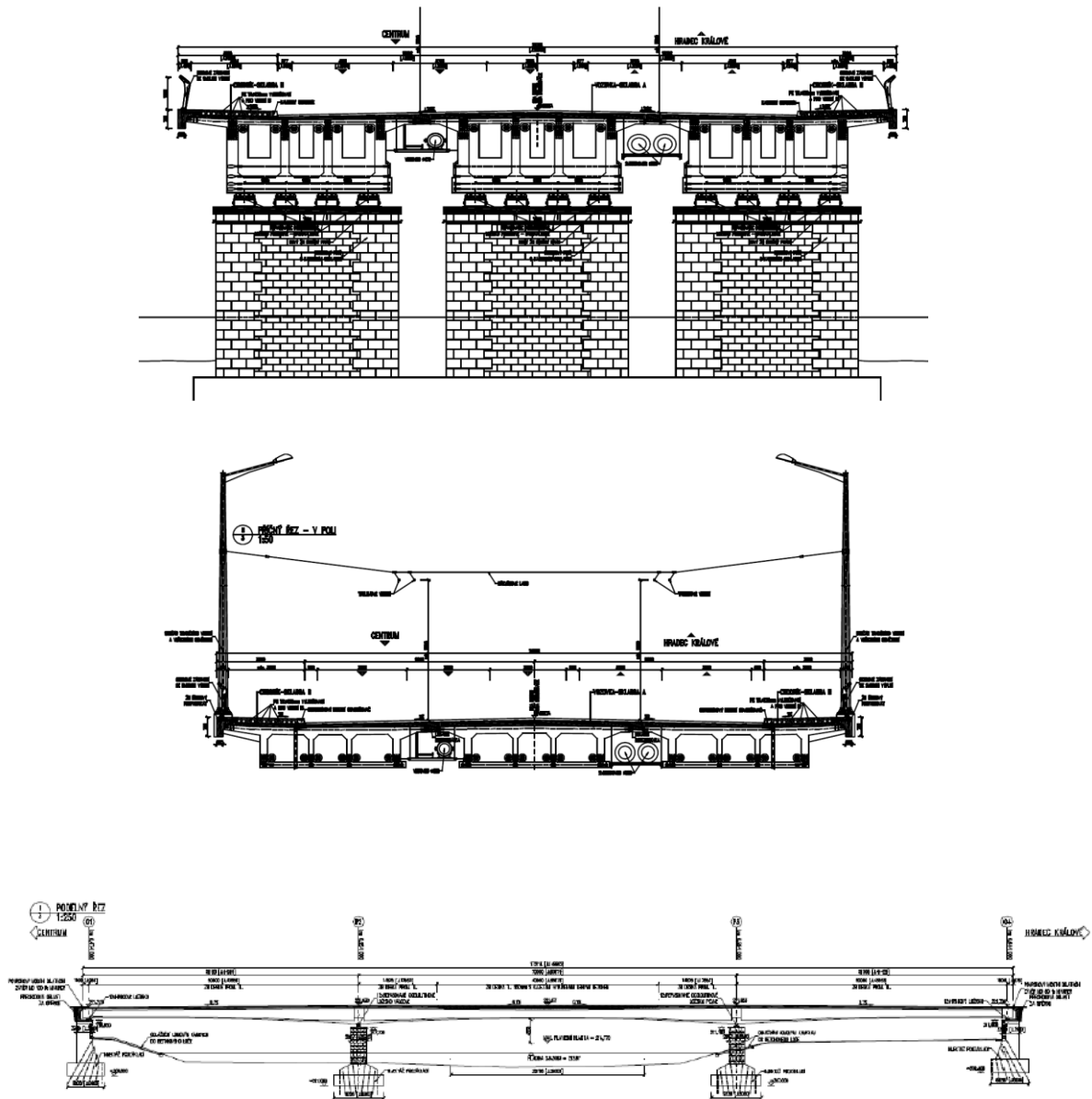


Fig. 2-2: Dimensions of the bridge: drawing of cross section near the pillars, (top picture), mid-span cross section, (middle picture), and side (longitudinal) view of the bridge, (bottom picture)

## 2.1 Monitoring procedure and results

The most suitable locations to install the Spider units and the sensors were determined based on the provided drawings. After installation the Spiders were adjusted and the first bridge transits were used to measure the required lead- and stopping times and to determine thresholds for triggering the measurement.

Direct measurements started immediately afterwards and data was sent to our database.

Trucks weighing 16.63T, 24.36T and 12.24T were used to calibrate the system for the Wonka bridge. Each truck passed the bridge 10 times (22nd August 2018). We selected the most interesting results for this report based on gross vehicle weight and plausibility. One highlight is event 1116 which is a 60 ton truck, we think it has passed the bridge illegally. We strongly recommend that this event is re-analysed with the ATENA software.

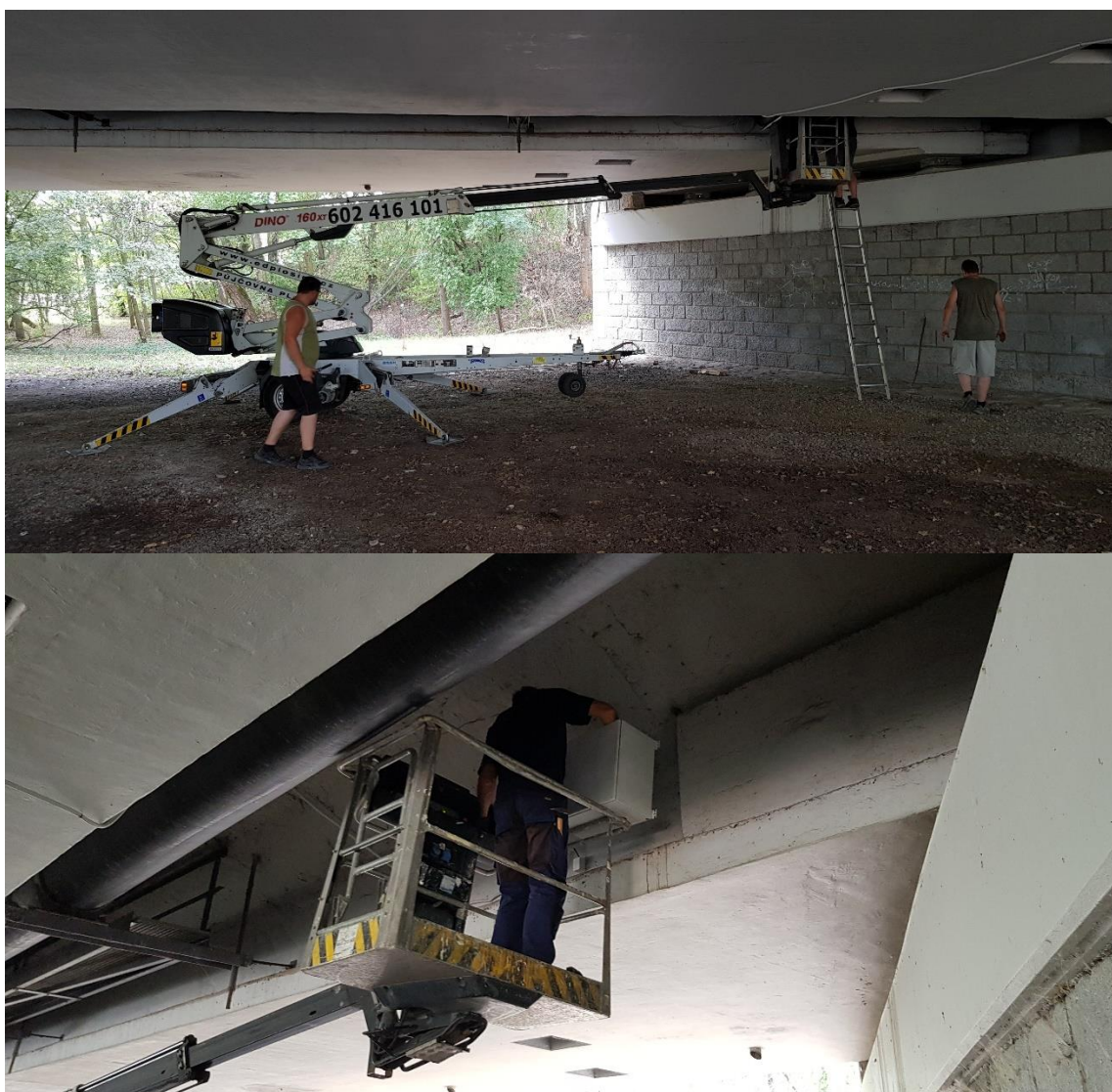


*Fig. 2-3: Installation of BWiM system on Wonka bridge in Pardubice*



*Fig. 2-4: Monitoring installation (left) on Wonka bridge in Pardubice, calibration using trucks with pre-defined weight (top right), laser sensor for detection of vehicles, their location on the bridge and axle distance*

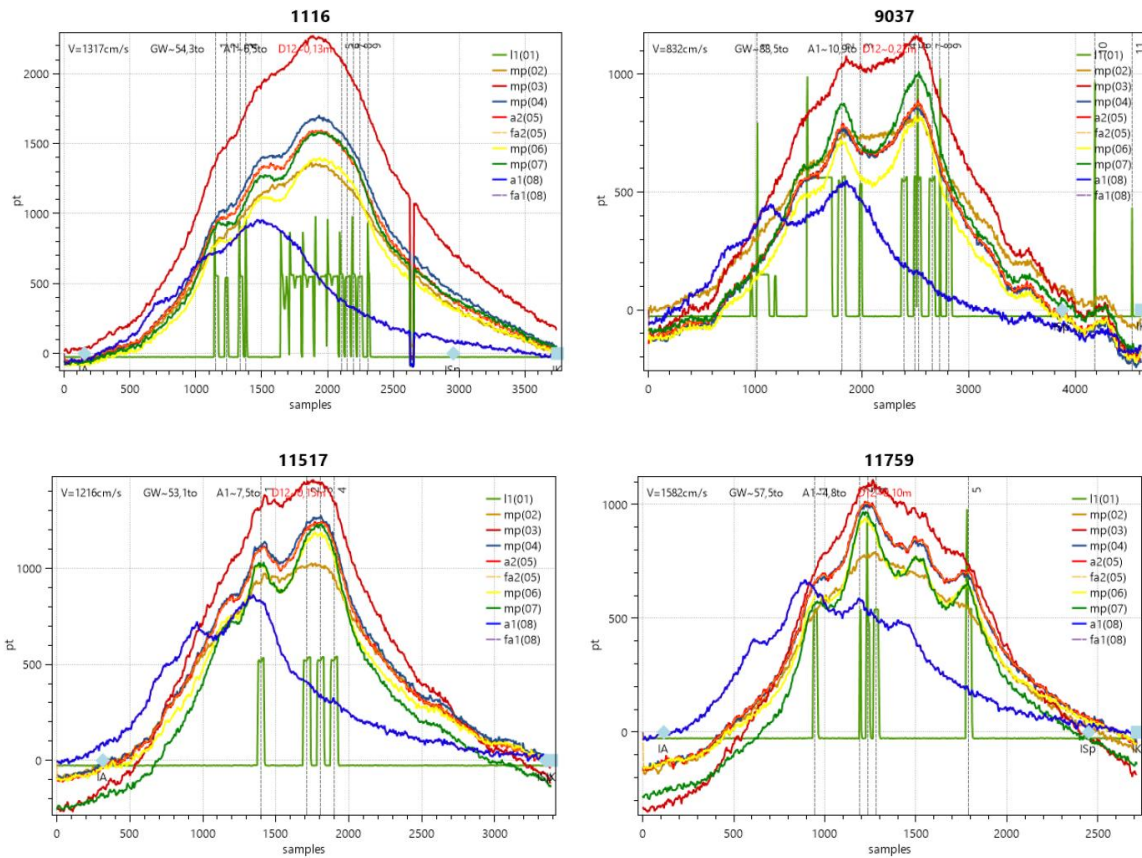


Fig. 2-5: Examples of sensor measurements for selected main events on Wonka bridge

Tab. 2-1: List of events and their measured values

TST	ID	V	AC	VC	GW	Axles	Length	A2A	Q	T	S	y
20180825 07:00:50	1116	47,4	4	80	59,4	18,6 25,4 9,0 6,4	19,96	3,91 12,50 3,55	7	23,7	15,590	4,477
20180917 06:41:04	9037	45,1	2	10	33,7	5,1 28,6	12,97	12,97	18	18,1	8,721	4,366
20180923 10:45:08	11517	43,8	2	41	38,5	37,0 1,5	6,49	6,49	32	18,1	11,589	4,617
20180925 07:07:18	11759	57	2	40	26,9	12,1 14,7	5,09	5,09	24	13,3	8,918	4,567
20180930 06:51:01	13185	52,4	4	62	36,1	16,6 9,7 3,7 6,1	11,14	1,07 4,46 5,62	13	12,2	11,233	4,406
20181010 00:07:30	16626	54	2	41	26,3	9,4 16,9	7,82	7,82	15	14,3	6,625	4,477
20181018 05:10:13	19252	53,5	3	60	28,9	20,8 4,6 3,5	14,94	10,76 4,18	8	16,0	7,932	4,046
20181110 19:18:26	28248	46,9	2	140	37,1	26,1 10,9	11,67	11,67	19	11,8	11,761	4,887
20180923 10:46:40	11519	53,8	2	40	28,9	27,4 1,5	3,89	3,89	34	18,4	9,583	4,296
20181018 05:10:13	19252	53,5	3	60	28,9	20,8 4,6 3,5	14,94	10,76 4,18	8	16,0	7,932	4,046
20180925 07:07:18	11759	57	2	40	26,9	12,1 14,7	5,09	5,09	24	13,3	8,918	4,567
20181010 00:07:30	16626	54	2	41	26,3	9,4 16,9	7,82	7,82	15	14,3	6,625	4,477
20181005 13:42:31	15506	67	3	101	25,8	1,5 1,5 22,8	12,49	6,65 5,84	33	13,2	5,807	3,976
20180822 14:34:51	123	52,4	3	101	25,7	20,9 1,5 3,3	8,71	6,38 2,33	23	26,4	7,537	3,535
20180822 14:45:56	129	61,3	3	140	25,6	20,6 1,5 3,5	10,7	9,92 0,78	27	26,4	6,962	3,565
20181020 08:35:57	20199	50,1	2	41	25,5	24,0 1,5	5,51	5,51	35	14,0	9,480	4,256
20180923 15:23:55	11586	64,5	2	41	24,1	19,4 4,7	7,13	7,13	19	18,4	6,647	4,467
20181019 14:17:24	20025	55,2	2	10	23,6	12,8 10,8	13,28	13,28	16	14,7	5,946	5,268
20181015 10:29:19	18105	58,9	2	40	23,1	21,3 1,8	5,20	5,20	27	18,0	7,742	4,296
20181009 06:45:26	16219	45,8	3	140	22,8	14,9 6,4 1,5	18,76	6,58 12,18	20	13,0	7,213	4,286
20181025 14:15:01	22070	64,1	2	10	21,9	13,5 8,4	11,16	11,16	14	11,8	6,113	4,677
20181023 13:41:57	21110	54,5	2	10	21,8	11,6 10,2	11,54	11,54	19	11,1	5,623	4,777
20181018 15:25:15	19554	57,7	2	10	21,4	16,5 5,0	10,79	10,79	13	16,4	5,880	4,176
20181016 08:46:17	18529	56,1	4	64	21,2	16,5 1,7 1,5 1,5	12,29	3,93 6,91 1,45	25	16,9	6,373	4,406

Tab. 2-2: Table of symbols for measurements of Wonka bridge

<b><i>Symbol</i></b>	<b><i>Description</i></b>
<i>TST</i>	Local time stamp
<i>ID</i>	Record number
<i>V</i>	Velocity (km/h)
<i>AC</i>	Axle count
<i>VC</i>	Vehicle class
<i>GW</i>	Gross vehicle weight (to)
<i>Axles</i>	List of axle weights (to)
<i>Length</i>	Distance between first and last axle (m)
<i>AZA</i>	Axle to axle distances (m)
<i>Q</i>	Quality of fit (%)
<i>T</i>	Temperature at bridge (°C)
<i>S</i>	Average strain (mS)
<i>y</i>	Lateral distance

## 2.2 Analysis of Preliminary Measurements

### 2.2.1 Introduction

In this the dataset acquired between 22/08/2018 and 22/10/2018, 14240 events over 60 days are presented

The objective of this section are the following tasks:

- First we test whether our measurements are biased, i.e. are we more likely misclassify certain types of vehicles.
- Secondly, we will use the data to infer information about the type and characteristics of vehicles traversing the bridge.
- Thirdly, we will identify and interpret temporal patterns in the traffic flow.

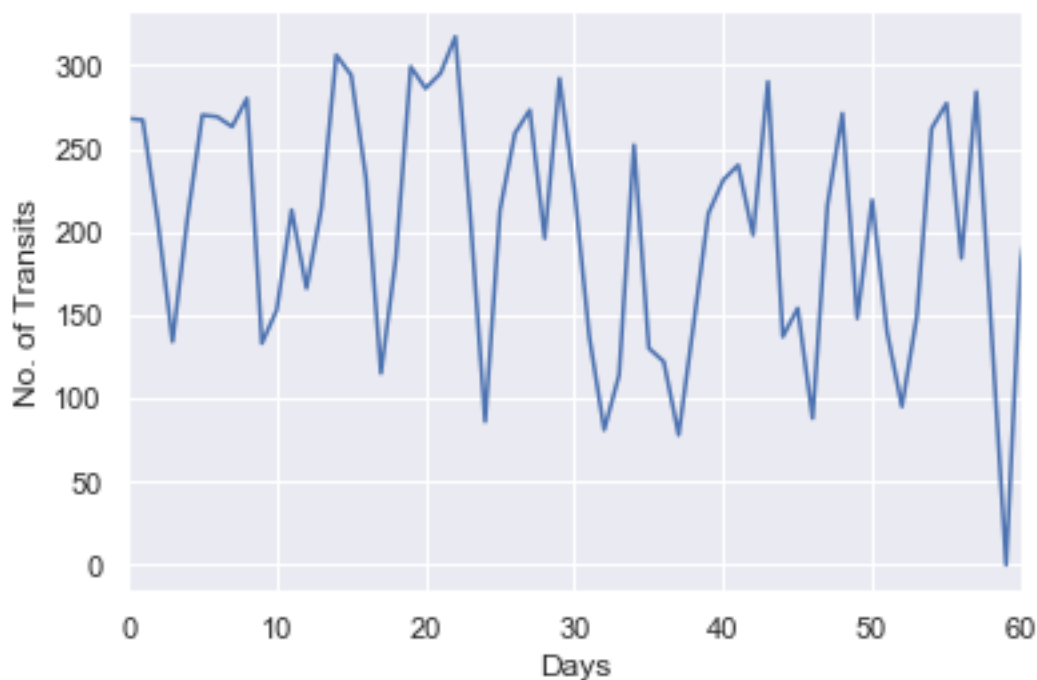


Fig. 2-6: Number of vehicles crossing Wonka bridge for each day of the measurement period.

### 2.2.2 Is our data set biased?

In previous work we have established that, once calibrated, the iBWIM system can accurately infer the weight, speed, and axle distribution of individual test vehicles. With the acquired data set we can now undertake a more statistical assessment. Ideally we would have a ground truth data set, acquired by other measurement methods, with which we could compare our results. Unfortunately this is not available. However, we do have a Quality value ( $Q$ ) that indicates how well our model fits the measured data.

The Quality metric is obviously an imperfect metric—there may be several different models that fit the measurement. However, it is a useful indicator for our purposes. The question we would like to answer in this subsection is whether the iBWIM system performs better for some classes of vehicle than others—if it does this will bias our analysis. We answer this question by seeking any correlation between the quality metric and vehicle characteristics, such as gross weight, Speed and Length, see Fig. 2-7. The scatter plots and  $R^2$  values indicate there is no significant correlation and we will assume that there is no systematic error in our measurements and that our analysis is unbiased.

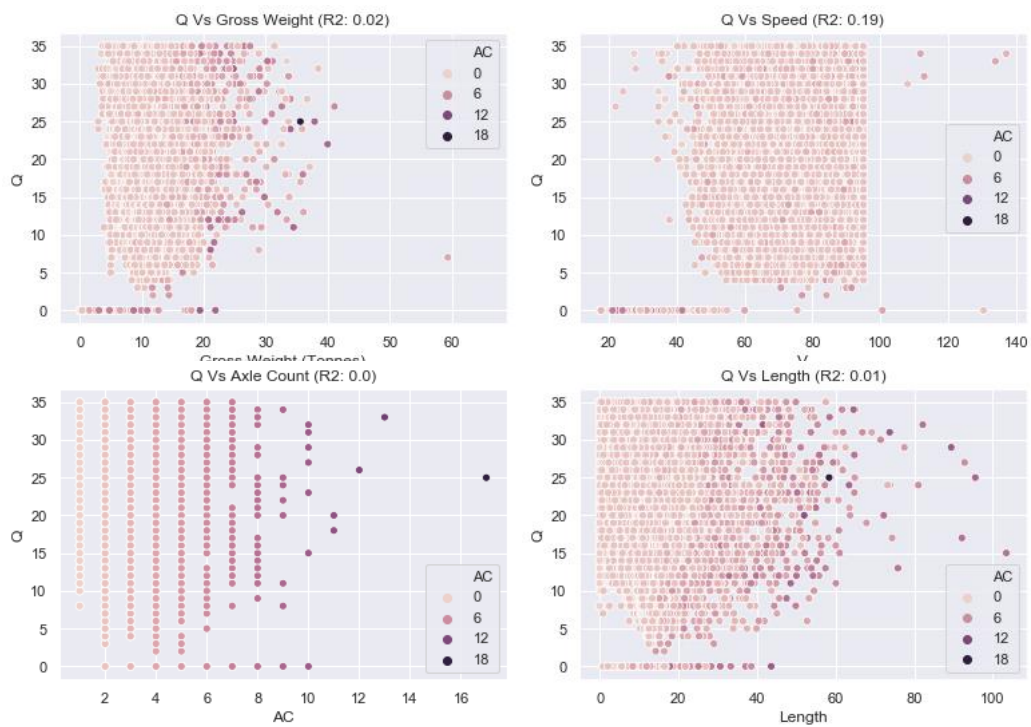
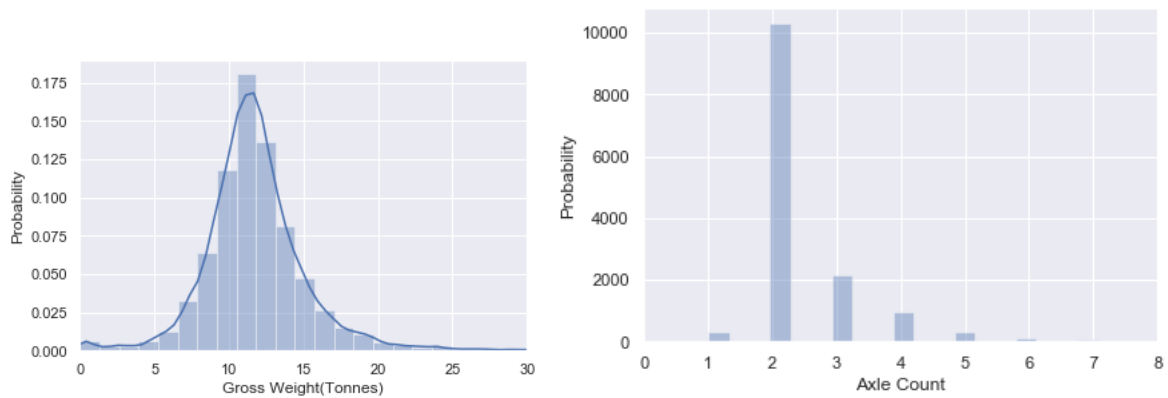


Fig. 2-7: Correlations between quality metric and various parameters of the model for the Vogelsang bridge

### 2.2.3 Vehicle Description



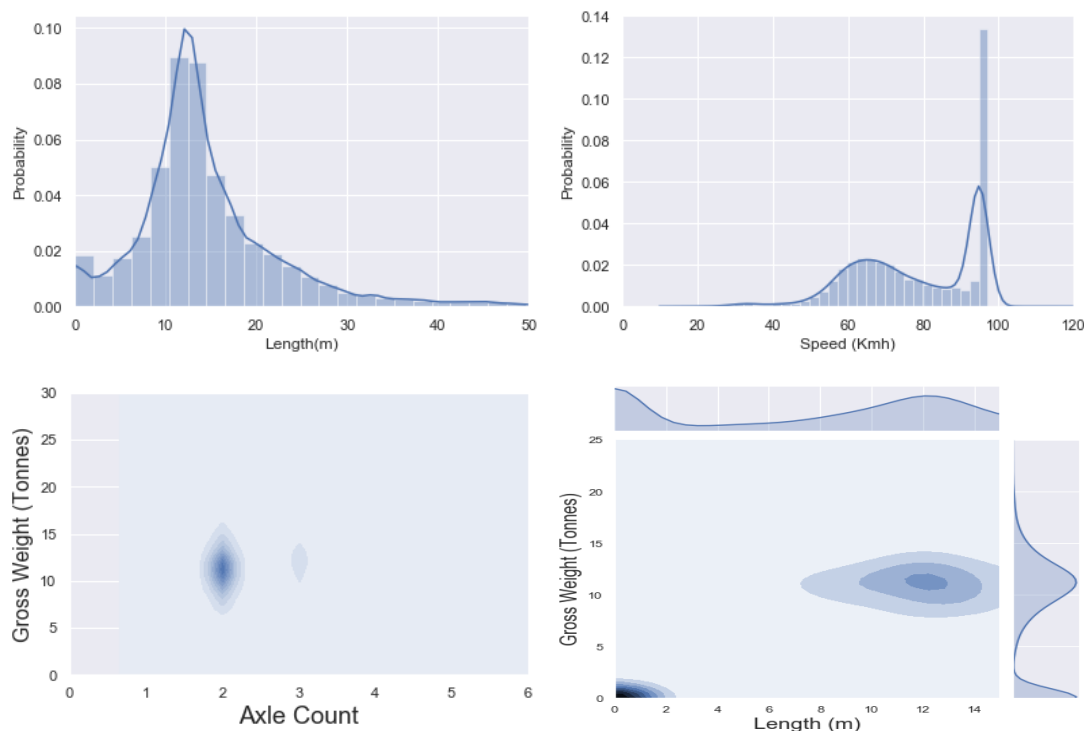


Fig. 2-8: Probability of vehicle Gross Weight, Length and Speed, Wonka bridge

### 2.2.4 Temporal patterns

In Fig. 2-6 we noted a strong weekly periodicity in the number of vehicle crossings, plotting this by week day, Fig. 2-6, we can see that during the working week we can expect 250 or more vehicle crossings a day, which falls to around 100 crossings during the weekend.

It is possible to evaluate diurnal patterns, Fig. 2-10 . There is no significant change in weight distribution of traffic over the course of the day—beyond the variation in vehicle frequency. There is, however, a more noteworthy effect in vehicle speed, Fig. 2-10 (right). The majority of traffic is moving at 90Km/h, however, between 06:00 and 18:00 there is a significant likelihood that vehicles will be travelling at around 60Km/h—presumably due to congestion.

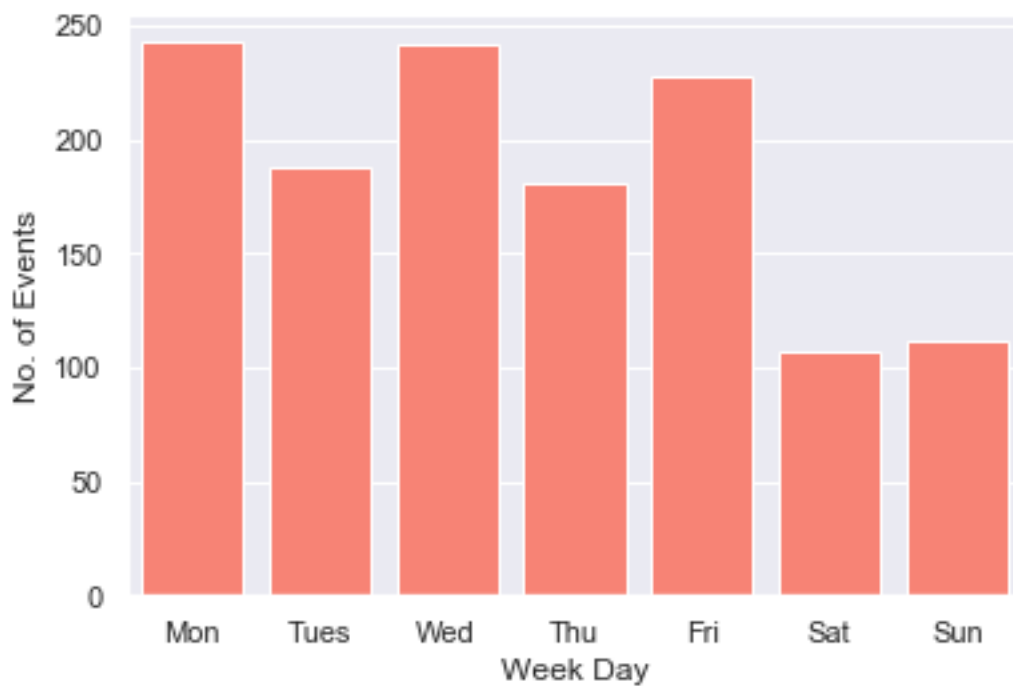


Fig. 2-9: Vehicle transits by week day, Wonka bridge

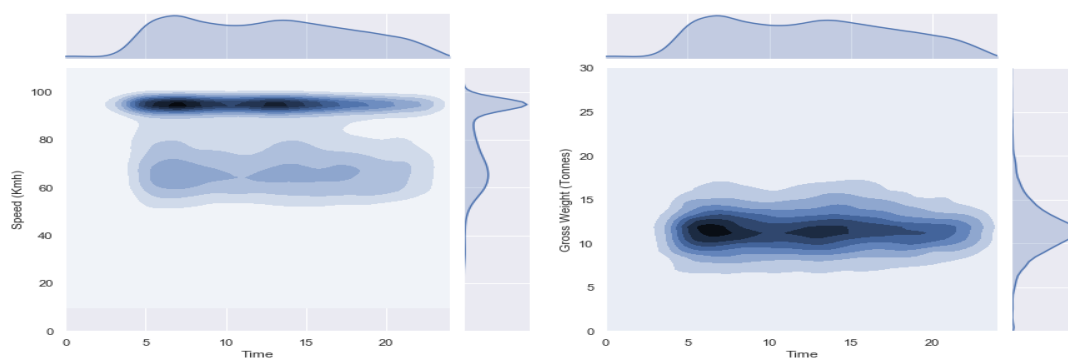


Fig. 2-10: Diurnal patterns for vehicle weight and speed, Wonka bridge

### 2.2.5 Damage description

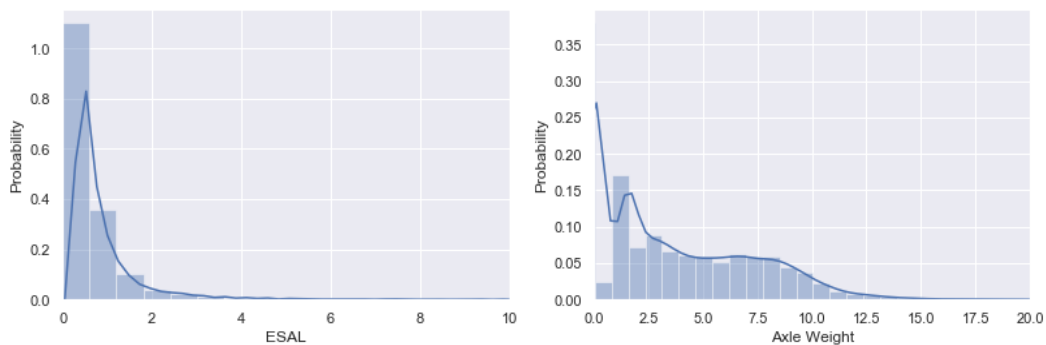


Fig. 2-11: Damage metrics, Wonka bridge

### 2.3 Development and calibration of the numerical model

Three-dimensional model was developed in ATENA [3]. The bridge is modelled by 4512 layered shell elements. The structure near supports and some other details are modelled by hexahedral and wedge solid elements. The pre-stressed tendons are realized by 3022 external cable truss elements, while the conventional reinforcement is introduced by embedded reinforcement within shell elements (see Fig. 2-12).

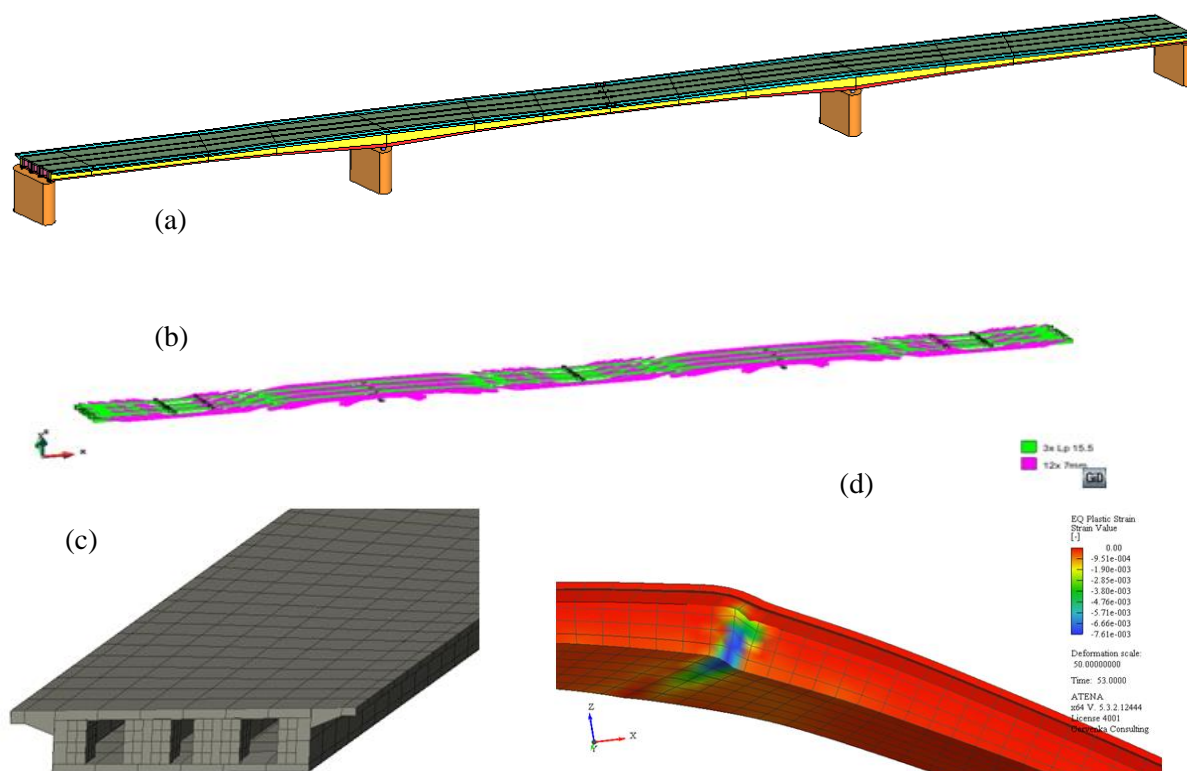


Fig. 2-12: (a) Geometrical model of P. Wonka bridge, (b) geometry of pre-stressing cables, (c) the finite element model of the end segment, (d) failure mechanism at peak load near the right middle support during overloading up to failure

### 2.3.1 Initial calibration using bridge load test data

The numerical study involved several analyses. First the model was calibrated using the known results from the bridge load test performed after the bridge rehabilitation in 2006, see Tab. 2-3 and Tab. 2-4.

Tab. 2-3: Model calibration results based on the bridge load test from 2006

	2006 load test	analysis
Mid span deflection	14.36 mm	14.23 mm

Tab. 2-4: Used values of elastic modulus and calibrated prestressing values for cables in the box girder walls

Elastic modulus	Prestressing in box girder walls	
	Prestressing force	Prestress
50 GPa	450 kN	974 MPa (63% of yield strength)

### 2.3.2 Calibration on bridge monitoring

Then the model is further calibrated using the measurement of Petschacher, which was performed in the period August – October 2018, and is described in more detail in Section 2.1.

The Petschacher measurements were also compared with the existing monitoring on this bridge, which is performed by company Bohemian Technology Group (referred to as Botega). This is a long term monitoring. The location of the sensors is described in Fig. 2-16, and the data are available to the cyberBridge project. It is possible to identify the loading events detected by Petschacher on the long term measurements by Botega. It was however necessary to extract the short term data with shorter sampling period from Botega measurement, which normally concentrates on long term response. The comparison and identification of major loading events is shown in Fig. 2-17. When the short term data are extracted from Botega measurements, it is possible to observe the individual loading events that correspond to the passing of heavier vehicles as shown in Fig. 2-18 and Fig. 2-19.

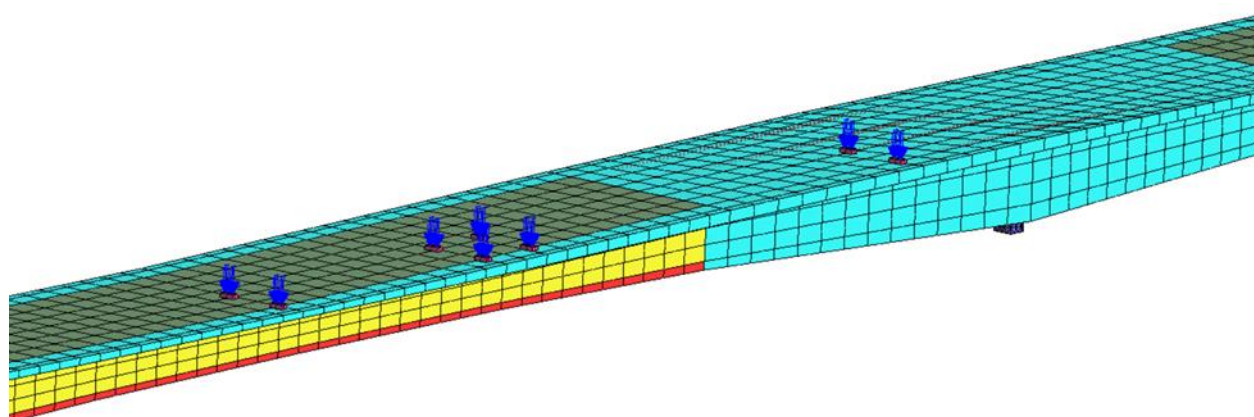


Fig. 2-13: Loading by truck load

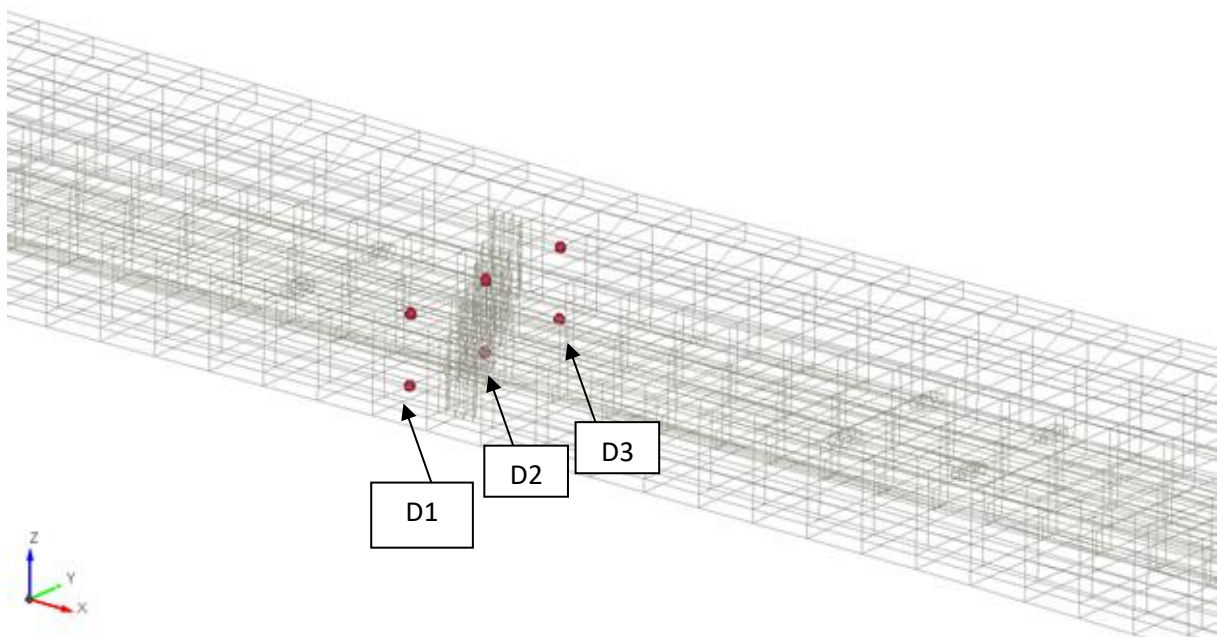


Fig. 2-14: Location of monitoring points for the calibration using Petschacher measurements

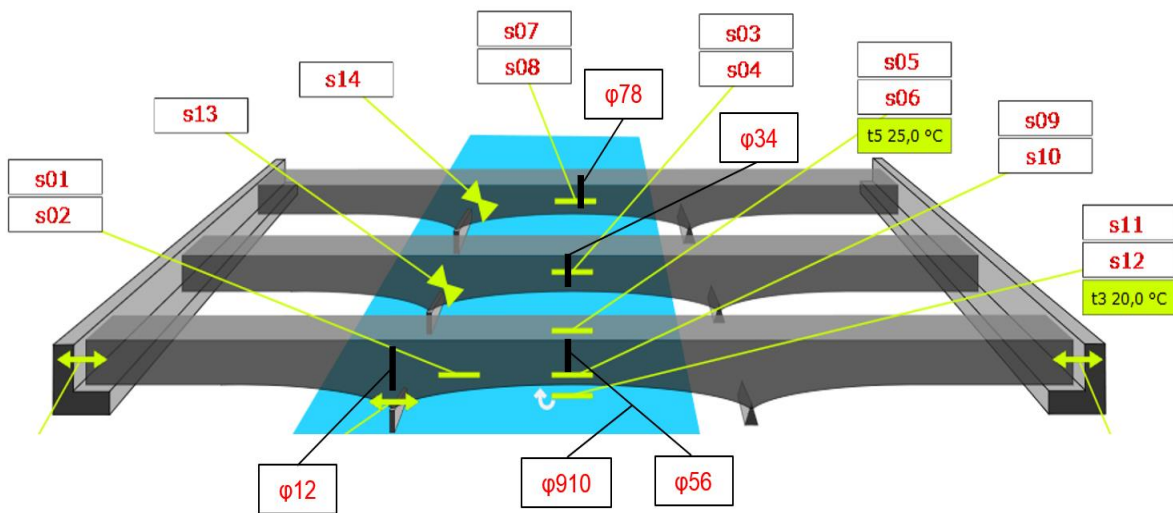


Fig. 2-15: Overview of sensor location in the existing monitoring program of Wonka bridge by Botega

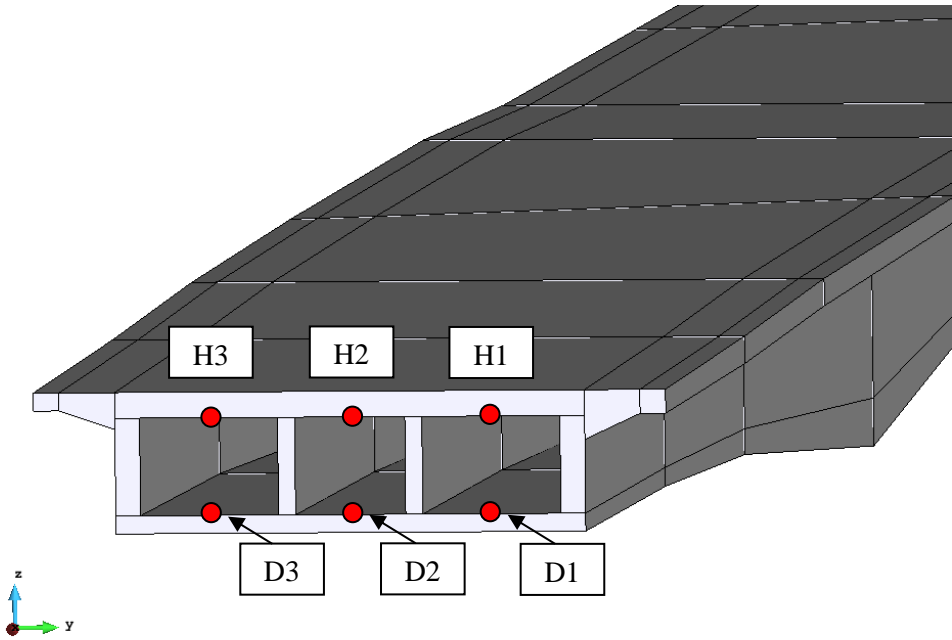
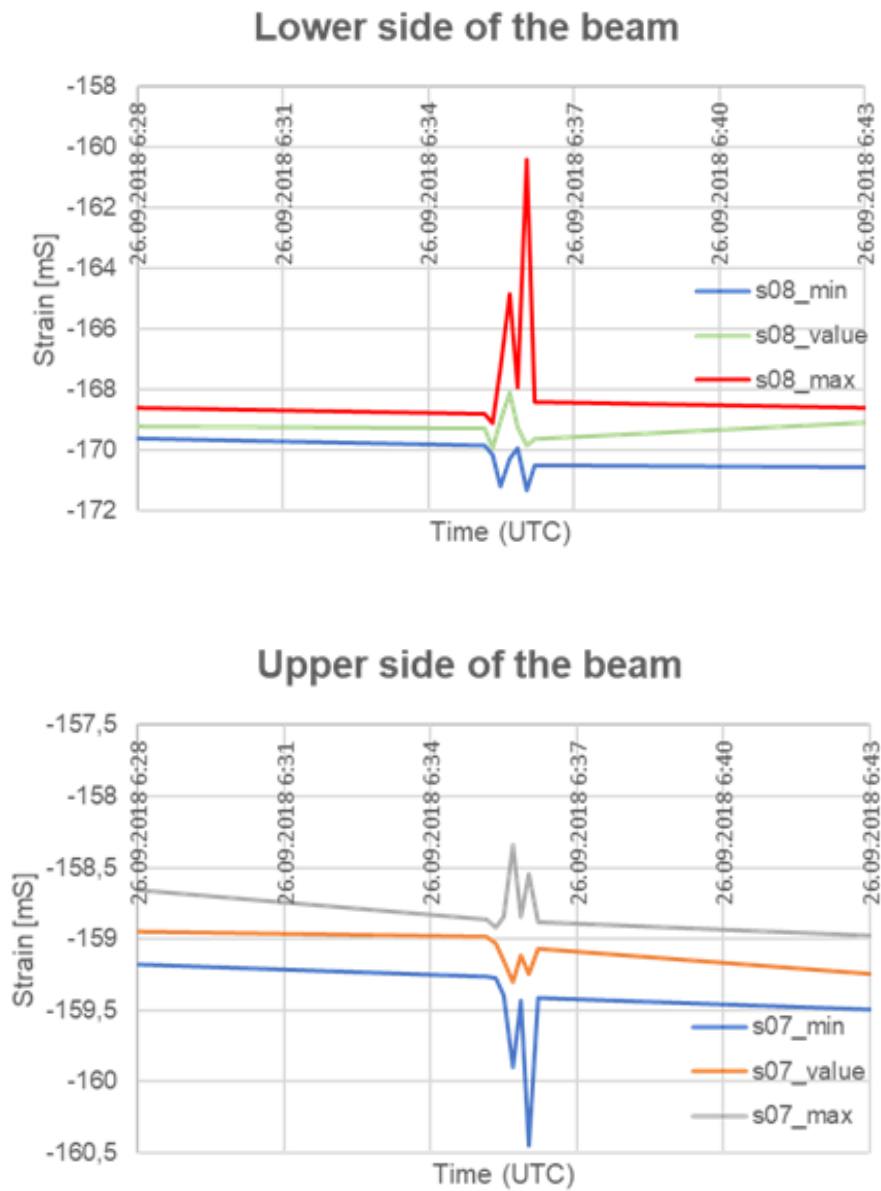


Fig. 2-16: Location of monitoring points for calibration using Botega measurements

Botega measurement						Petschacher measurement									
Monitor	Value	Min	Max	Time UTC	Max-value	TST (Local time, UTC+2h)	Velocity	AC	GW	Length	Te	QE	max. Strain	y	
	[mS]	[mS]	[mS]		[mS]		[km/h]		[t]	[m]	[°]	[%]	[mS]	[m]	
s08_1561	23.17	22.96	28.25	13.09.20186:16	5.08	2018-09-13T08:16:31	95	3	10.22	23.56	21	30	3.055	4.447	
s08_1561	26.19	24.55	34.67	13.09.20189:46	8.48	2018-09-13T11:45:58	68.4	2	10.44	13.92	21.8	6	3.321	4.567	
s08_1561	-33.33	-35.90	-24.19	23.09.20188:45	9.14	2018-09-23T10:45:08	43.8	2	38.47	6.49	18.1	32	11.589	4.617	
s08_1561	-33.84	-36.88	-25.82	23.09.20188:46	8.01	2018-09-23T10:45:55	69.7	2	33.68	3.72	18.2	25	10.554	4.507	
s08_1561	-169.84	-171.35	-160.41	26.09.20186:36	9.44	2018-09-23T10:46:40	53.8	2	28.9	3.89	18.4	34	9.58	4.296	
s08_1561	-149.04	-149.43	-142.52	26.09.201815:46	6.52	2018-09-26T08:36:43	89.1	3	21.59	10.6	12	24	6.204	4.176	
s08_1561	-195.84	-196.07	-189.77	02.10.20186:35	6.07	2018-09-26T17:46:44	29.9	2	0.23	8.85	13.7		2.199	4.096	
s08_1561	-194.80	-195.93	-188.11	02.10.201811:26	6.69	2018-09-26T17:46:54	64.6	2	10.78	13.89	13.7	14	2.830	4.106	
s08_1561	-207.63	-208.46	-199.17	05.10.20186:26	8.45	2018-10-02T08:36:19	80.5	2	11.08	12.65	11.8	16	2.869	4.176	
s08_1561	-161.58	-163.20	-154.26	06.10.201815:35	7.32	2018-10-02T08:36:29	27.9	3	1.43	8.1	11.8		1.945	3.895	
s08_1561	-172.79	-173.97	-166.11	10.10.20187:16	6.67	2018-10-02T13:26:42	33.8	3	1.47	15.99	11.8		2.272	4.346	
s08_1561	-117.12	-117.42	-111.01	15.10.20184:46	6.11	2018-10-05T08:26:16	95	2	29.82	4.52	11.7	29	8.834	4.166	
s08_1561	-119.66	-120.29	-112.01	15.10.20187:06	7.65	2018-10-06T17:35:31	95	3	26.65	16.17	15	16	6.600	4.066	
s08_1561	-122.93	-125.13	-117.55	16.10.20186:46	5.38	2018-10-10T09:16:29	62.7	3	21.09	35.31	13.6	18	5.957	4.296	
s08_1561	-114.18	-114.19	-105.84	16.10.201812:45	8.35	2018-10-15T06:46:36	66.2	2	12.43	14.39	17.8	14	4.030	4.176	
s08_1561	-139.16	-142.15	-130.50	19.10.20183:36	8.66	2018-10-15T06:48:43	95	2	11.36	13.09	18	15	6.162	-	
						2018-10-16T14:44:54	56.1	4	21.2	12.29	16.9	25	6.373	4.4	
						2018-10-16T14:44:55	64.7	2	10.61	7.69	18.2	18	3.336	4.296	
						2018-10-16T14:46:00	55	4	28.46	30.86	18	16	5.852	2.392	
						2018-10-19T05:35:59	77.1	2	10.79	10.29	14.9	26	3.829	4.366	

- Min – minimum value in 10 s of measuring
- Max – maximum value in 10 s of measuring
- Value – average value in 10 s of measuring
- Max-value – difference between Max and Average value
- s08 monitor – monitor on the lower side of the beam
- AC – Axle count
- GW – Gross vehicle weight [t]
- QE – Quality of fit [%]
- Y – lateral distance [m]

Fig. 2-17: Comparison of measurement from Botega and Petschacher



- Sensor s08 is placed on the top of the beam and sensor s07 on the bottom.
- s08\_min and a07\_min are minimum values on the 10 second interval
- s08\_max and a07\_max are maximum values on the 10 second interval
- s08\_value and a07\_value are average values on the 10 second interval

Fig. 2-18: Identification of truck passing on 26.9. 2018 in Botega monitoring

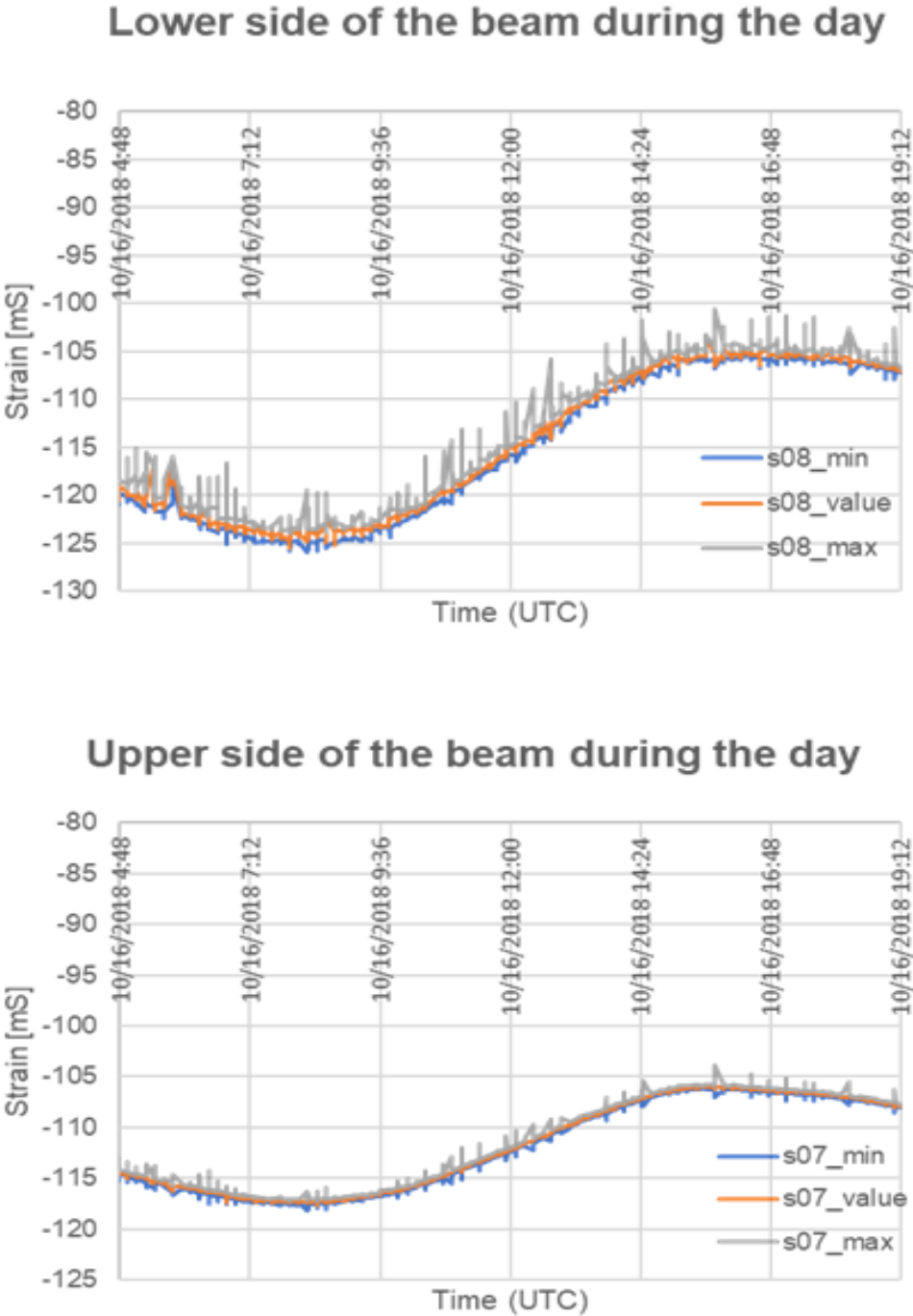


Fig. 2-19: Identification of major loading events (vehicle passing) in Botega measurements for a selected day of Oct. 16, 2018

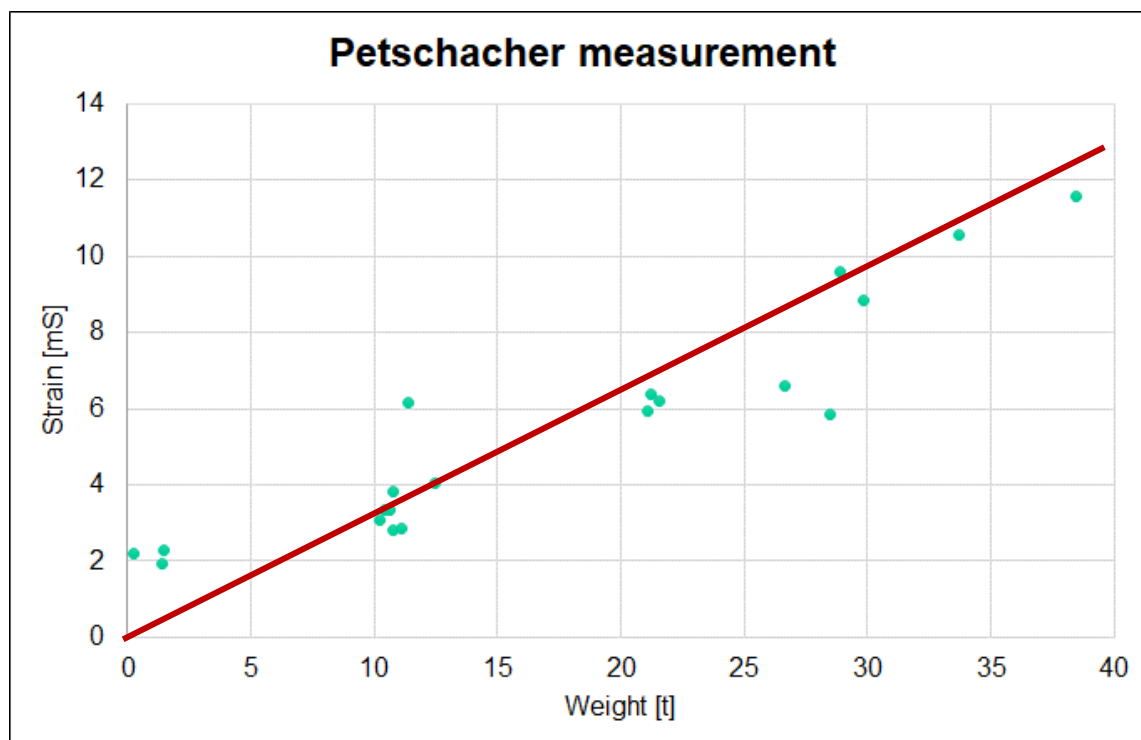


Fig. 2-20: Strain measurements with respect to the vehicle load in Petschacher measurement

It is possible to develop a comparison of strain measurements as a function of vehicle load. The vehicle load is obtained from Petschacher iBWIM system. It was then possible to identify the major loading events by the heaviest vehicles in the long term measurement by Botega. These relationships are shown for the selected monitors S07 and S08 (for location see Fig. 2-15) in Fig. 2-21 and Fig. 2-22. It can be seen that the relationship deviates from the expected linear relationship namely for the cases with lower vehicle weight. This can be explained by the effect of other traffic on the bridge, which is more significant for the cases with smaller and less heavy vehicles. This relationship is almost linear for the case of Petschacher iBWIM model. This is quite natural as this model was used to derive the vehicle weight.

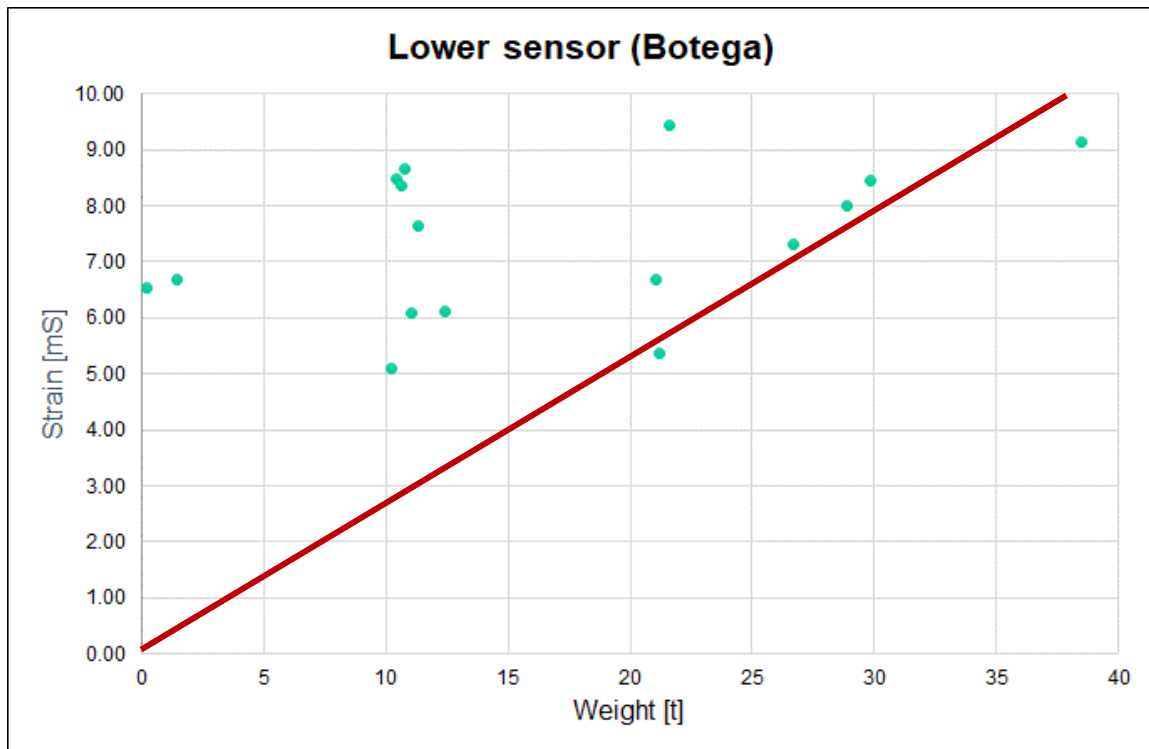


Fig. 2-21: Strain measurements at sensor 08 from Botega correlated with vehicle weight from Petschacher measurement

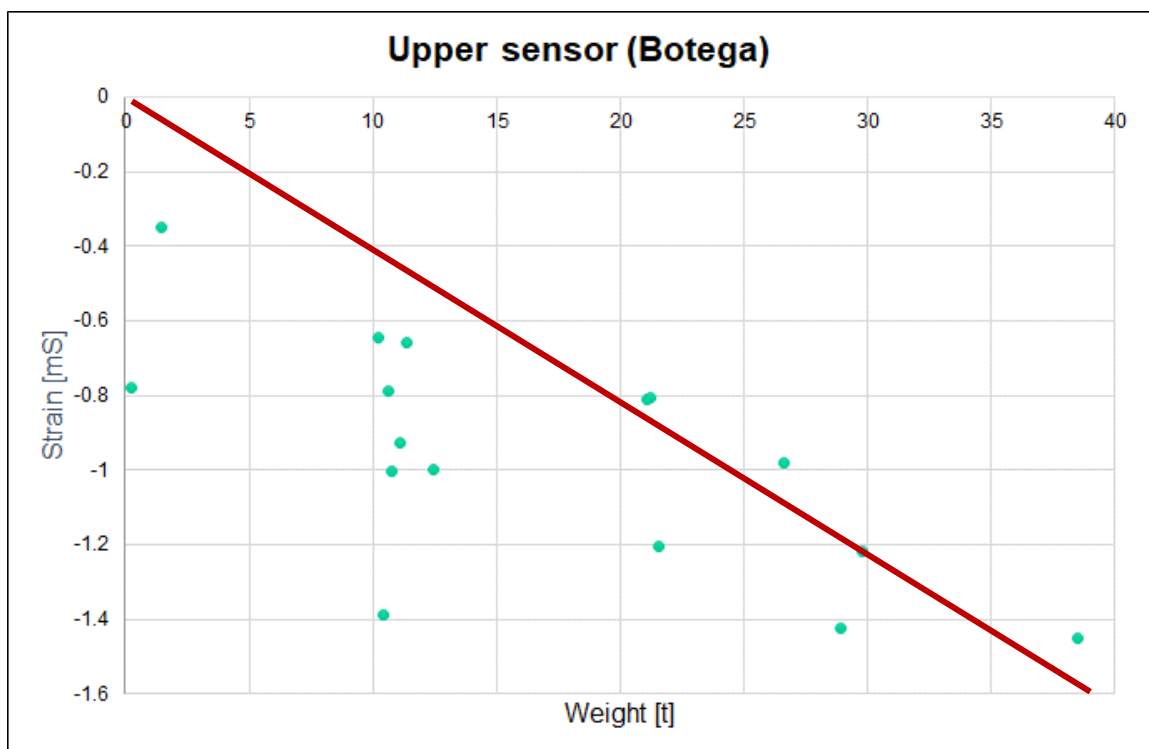


Fig. 2-22: Strain measurements at sensor 07 from Botega correlated with vehicle weight from Petschacher measurement

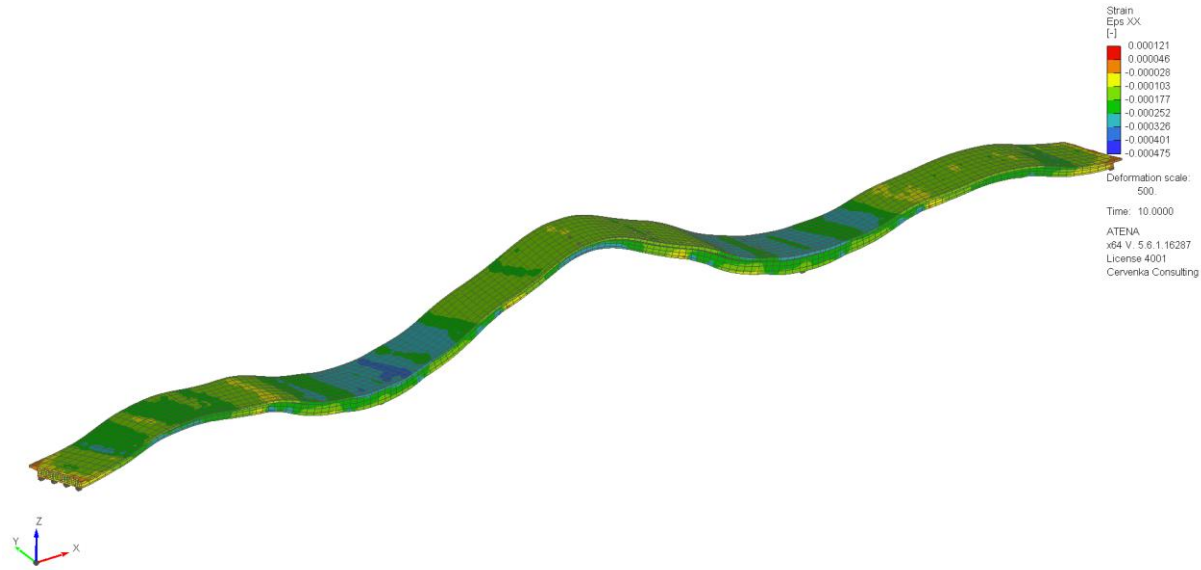


Fig. 2-23: Deformed shape (500x-scaling) and longitudinal strains in concrete after the application of prestressing and self-weight

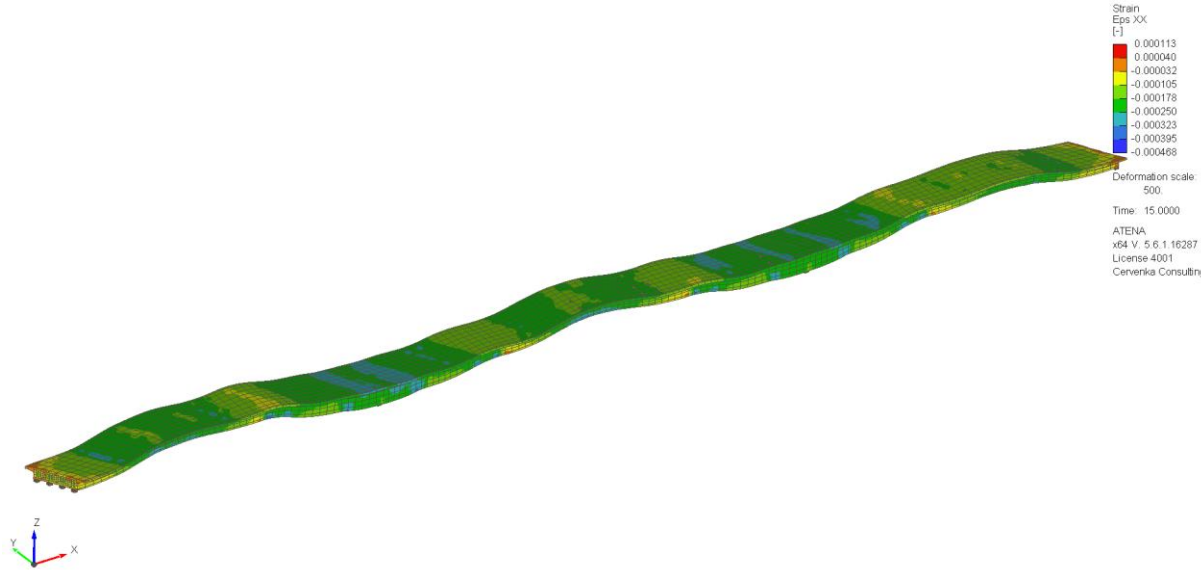


Fig. 2-24: Deformed shape (500x-scaling) and longitudinal strains after additional dead load application

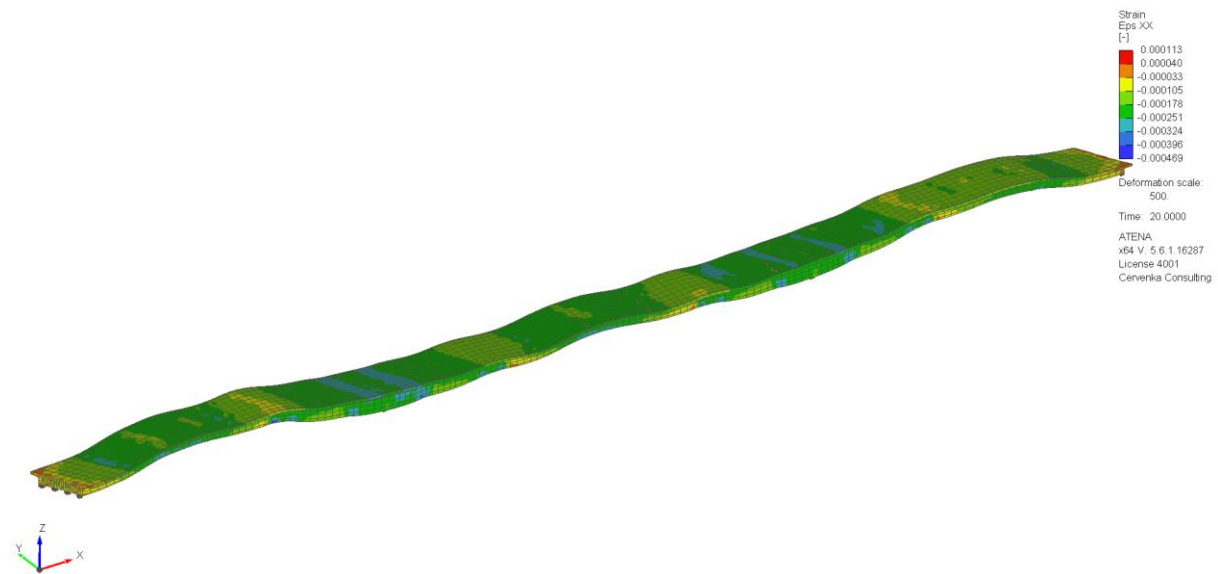


Fig. 2-25: Deformed shape (500x-scaling) and longitudinal strains after loading by the measured vehicle with the weight of 28.46 t

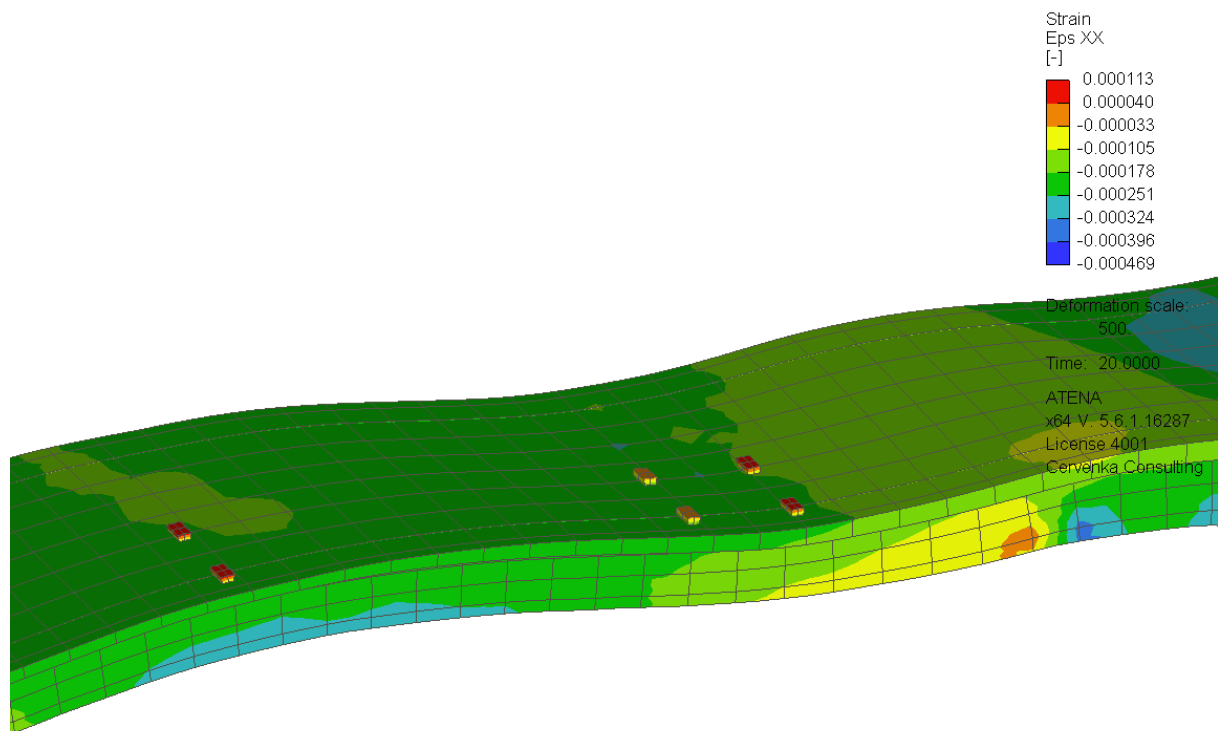


Fig. 2-26: Deformed shape and longitudinal strains at the measured location for vehicle load of 28.46t.

These monitored data were used to perform the final calibration of the model as shown in Fig. 2-23 to Fig. 2-27 and Tab. 2-5.

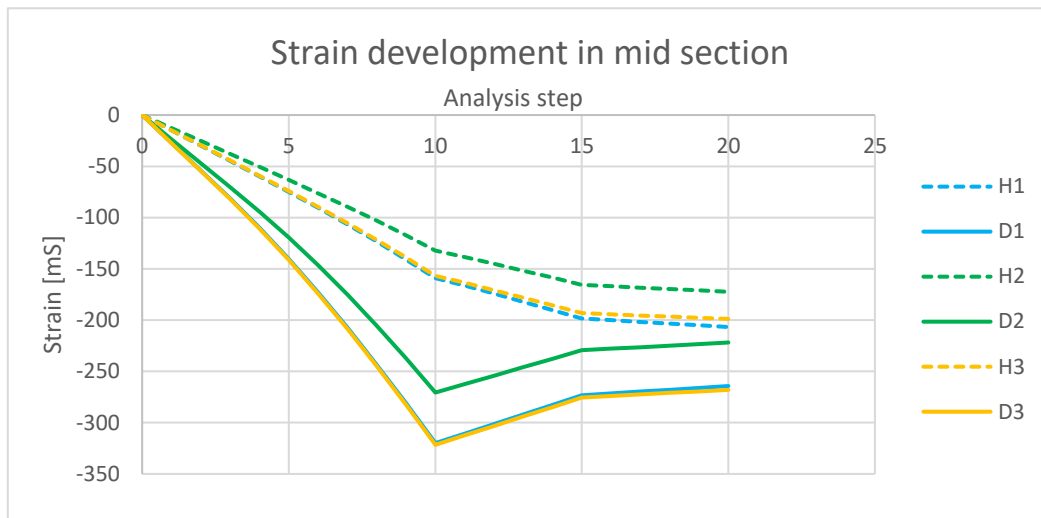


Fig. 2-27: Plot of strain development at the top and bottom bridge slab, vehicle 28.46t loading is applied from step 15-20

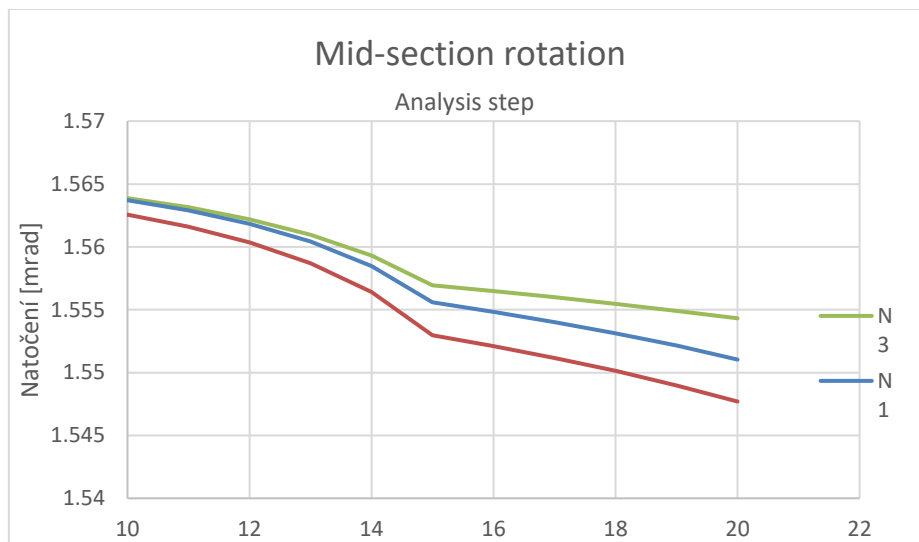


Fig. 2-28: Mid-section rotation during the loading history

In order to compare the strain due to vehicle loading the strain at the monitored location should be calculated by subtracting the values of step 15 from those of step 20. These values were used in the calibration process and the final comparison is shown in Tab. 2-5.

Tab. 2-5: Final calibrated strain values using Petschacher vehicle measurement data

Monitor	ATENA analysis	Petschacher measurement
	[ $\mu$ strain]	[ $\mu$ strain]
Average D1-D3	8.88	8.35

2.3.3 Prognosis of bridge load carrying capacity and durability modelling

Fig. 2-30 This section contains the main results from the evaluation of the bridge load capacity. Fig. 2-29 shows the bridge load carrying capacity for various positions of the design traffic load for the calibrated model and the original model before the calibration using the monitoring data. During the monitoring process in 2017-2018 it was discovered that one of the deviators is broken as shown in Fig. 2-31. Fig. 2-30 shows the comparison of the bridge strength considering the broken deviator and disabling one of the prestressing cables. It shows that the deactivation of one tendon does not significantly affect the load carrying capacity of the bridge.

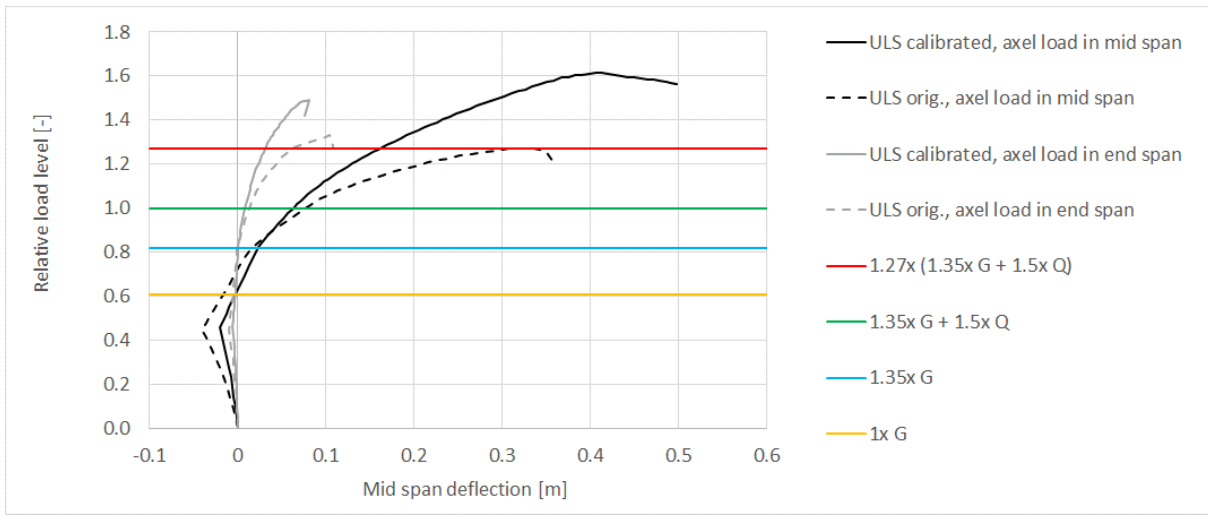


Fig. 2-29: Evaluation of load-carrying capacity of Wonka bridge

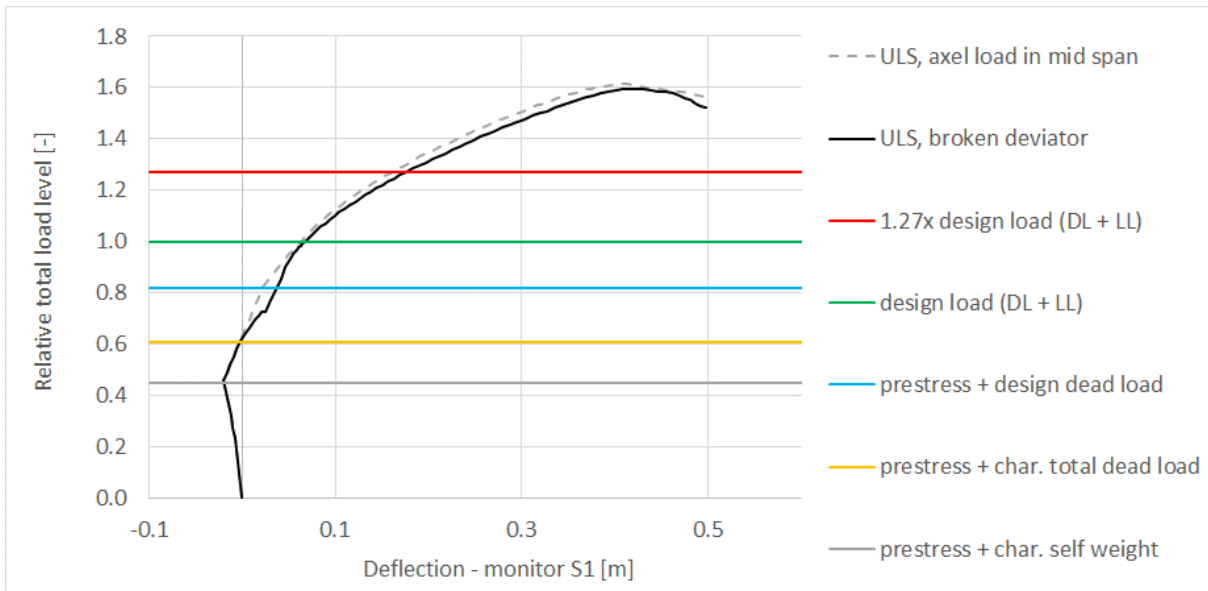


Fig. 2-30: Evaluation of load-carrying capacity of Wonka bridge considering the damaged deviator



Fig. 2-31: Photo of the damaged deviator

The long term durability of the Wonka bridge structure was also analyzed by ATENA with the newly implemented durability models. The bridge is modelled by 4512 layered shell elements. The structure near supports and some other details are modelled by hexahedral and wedge solid elements. The pre-stressed tendons are realized by 3022 external cable truss elements, while the conventional reinforcement is introduced by embedded reinforcement within shell elements (see Fig. 2-12).

The numerical study involved several analyses. First the model was calibrated using the known results from the bridge load test performed after the bridge rehabilitation in 2006 as shown in Section 2.3.1. In the subsequent analysis the bridge is loaded by the permanent load and then it is subjected to the environmental actions: **carbonation**:  $C_p = 350 \text{ kg/m}^3$ ,  $SCM = 0$ ,  $W = 175 \text{ kg/m}^3$ ,  $CO_2 = 0.00036$ ,  $RH = 0.60$ . Progressive period  $a_1 = 7.44e-5 \text{ m}$ ,  $a_2 = 7.30e-6 \text{ m}$ ,  $a_3 = -1.74e-5 \text{ m/MPa}$ ,  $f_{i, ch} = 3.5 \text{ MPa}$ ,  $d_{ini} = 0.001 \text{ m}$ , pitting corrosion  $R_{corr} = 1$ , corrosion rate after spalling  $30 \text{ } \mu\text{m/year}$ , **chlorides**:  $D_{ref} = 1.19e-7 \text{ m}^2/\text{day}$  (mean value would be  $D_{ref} = 7.72e-13 \cdot 86400 = 6.67e-08 \text{ m}^2/\text{day}$ ),  $t_{Dref} = 3650 \text{ days}$ ,  $m_{coeff} = 0.37$ ,  $t_{mcoeff} = 10950 \text{ days}$ ,  $C_s = 0.103$ ,  $Cl_{crit} = 0.0185$ . Progressive period  $a_1 = 7.44e-5 \text{ m}$ ,  $a_2 = 7.30e-6 \text{ m}$ ,  $a_3 = -1.74e-5 \text{ m/MPa}$ ,  $f_{i, ch} = 3.5 \text{ MPa}$ ,  $w_d = 0.001 \text{ m}$ , pitting corrosion  $R_{corr} = 3$ , corrosion rate after spalling  $30 \text{ } \mu\text{m/year}$ . third part of the analysis is devoted for durability study.

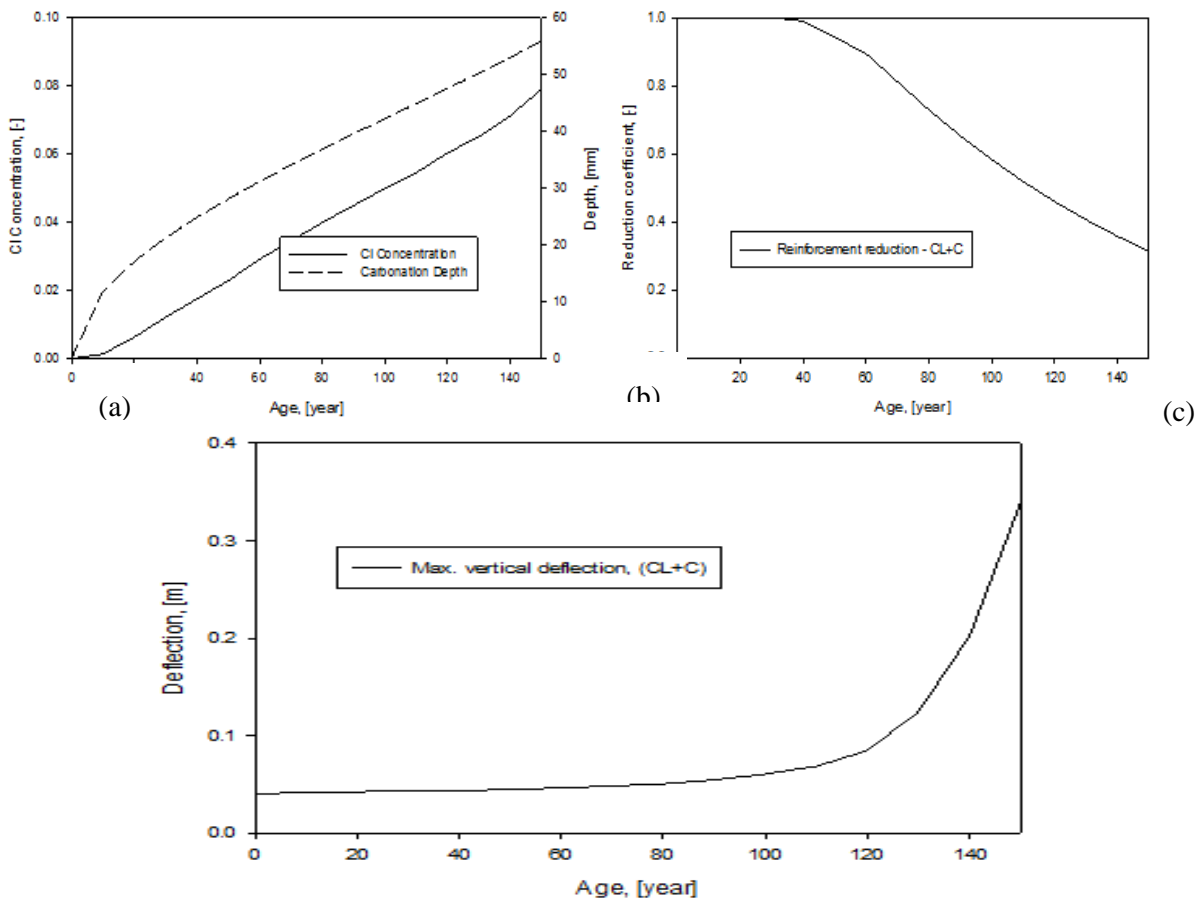


Fig. 2-32: (a) Concentration of chlorides and carbonation at tendon depth, (b) tendon cross-sectional area reduction due to corrosion, (c) deflection increase in time

Chloride ingress assumed concentration of sea water on the surface; this resembles situation when salt brine water had leaked through insulation and the Cl concentration rose up substantially. Also, 90% confidence was considered for diffusivity  $D_{ref}$ , which is about twice higher than the mean value for this concrete strength class.

The main results are summarized in Fig. 2-32, which shows that carbonation depth is about 55 mm for 150 years on uncracked concrete. The induction period for chlorides is approximately 45 years for uncracked concrete with concrete cover of 60 mm. Fig. 2-32b depicts calculated reduction coefficient for a pre-stressing tendon with concrete cover 100 mm. For the first 40 years, the tendon do not corrode, but at the age of 100 years about 50% of the tendon’s cross section area has corroded away. Fig. 2-32c shows also the maximum vertical displacement of the bridge vs. age of the structure. Note that the significant increase of the deflection at later times is due to tendons corrosion only as creep is neglected in computation and the force load is kept constant. It shows that the bridge is currently in a very good shape, without significant cracking and the possible service life of about 40 years.

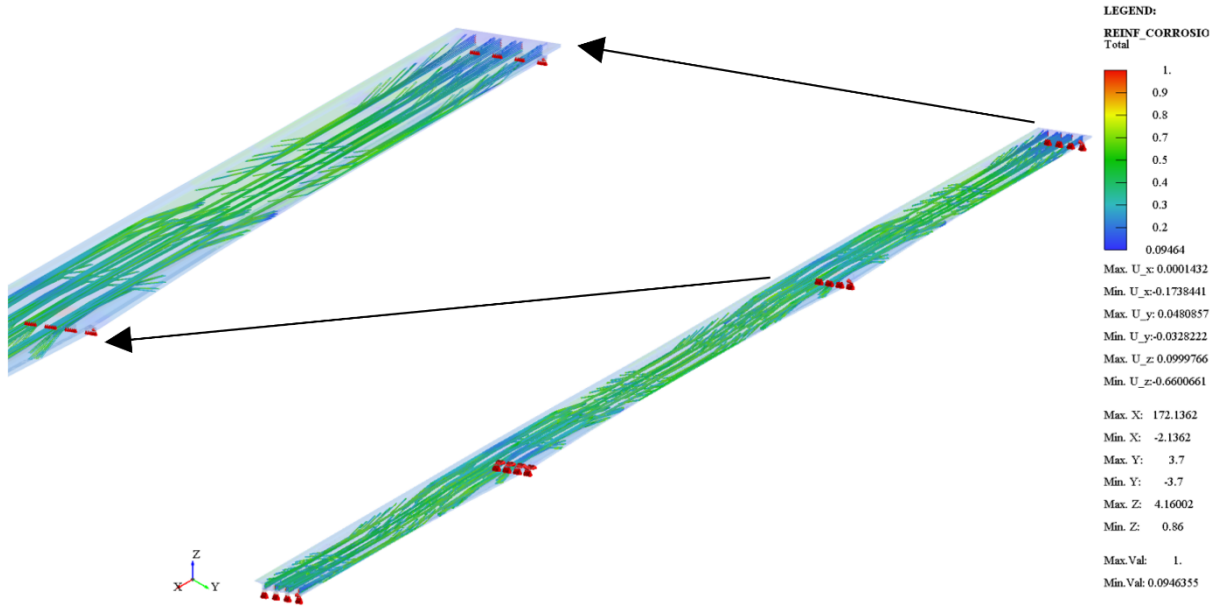


Fig. 2-33: Reinforcement corrosion after 150 years during the prognosis simulation

## 3 Vogelsangbrücke Esslingen, Germany (LAP)

### 3.1 Overview

This pilot bridge is a concrete bridge over the Neckar River in the city of Esslingen, Germany. It is a major part of the city's infrastructure with a high impact on the regional traffic. The bridge consists of eight partial structures built in three different construction types. The bridge was built between the years of 1971 and 1973. The total length is approx. 595m and it has a total area of 9,744m<sup>2</sup> including ramps.



*Fig. 3-1: Aerial image of Vogelsangbrücke Esslingen, Germany [source: maps.google.com]*

During the last major check, many damages have been detected, that influence the structural safety, the safety to traffic and the durability. Due to the damages, refurbishment is urgently needed.

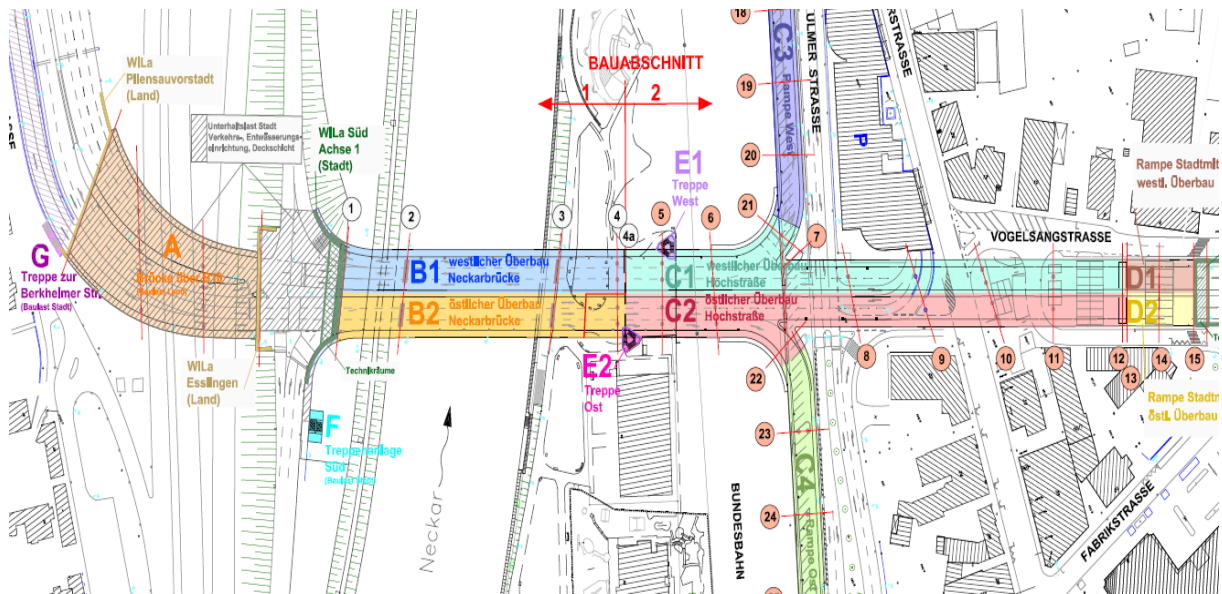


Fig. 3-2: Plan view on the Vogelsangbrücke with its different structures

Beyond that, tendons prone to stress corrosion cracking have been used for the prestressing of the Vogelsangbrücke, which may lead to spontaneous failure of the structure. In a previous feasibility study, a concept was developed, that allows further use for 15 to 20 years by partial strengthening combined with a continuous monitoring system.

### 3.2 Main Bridge B1 & B2 over Neckar River

The main Bridges B1 and B2 are three-span continuous beams out of prestressed concrete with cantilevers attached that connect to the structures C1 and C2. The hollow box sections have been built on falsework. Spans are 24.50m – 58.50m – 24.50m – 3.6m. The construction height varies from 1.60m in midspan to 2.90m at the piers.

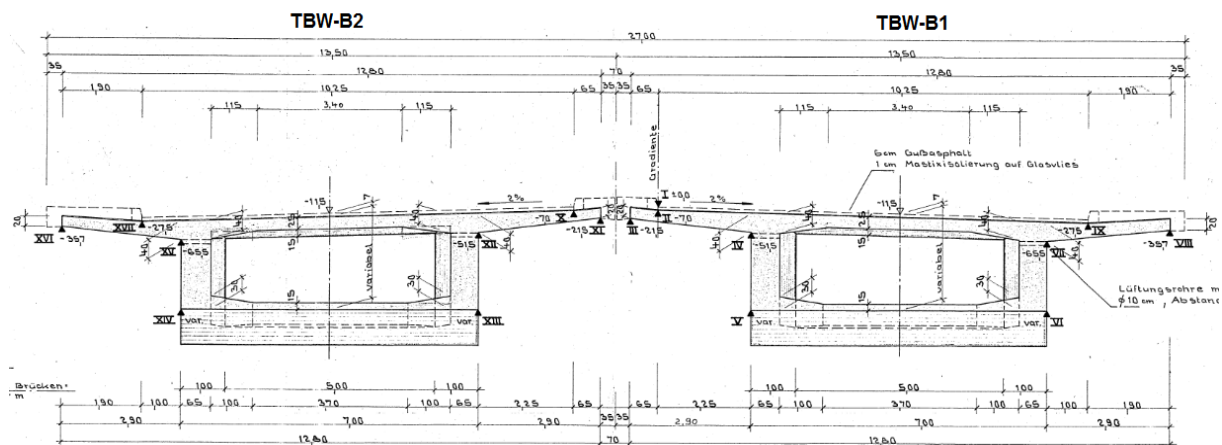


Fig. 3-3: Cross section of the main bridge B1 & B2

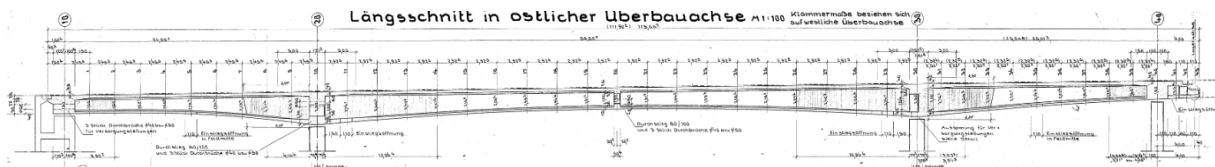


Fig. 3-4: Longitudinal section of main bridge

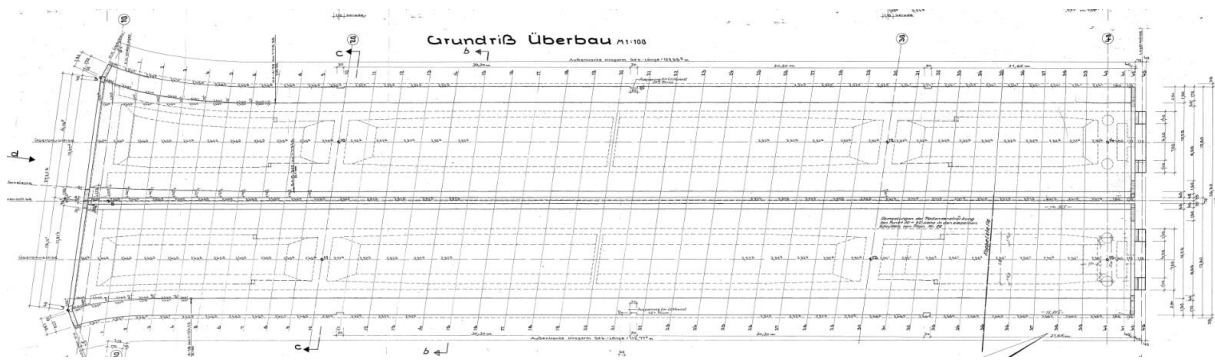


Fig. 3-5: Plan view on main bridge

### 3.3 Ramps C1 – C4

Northbound to the main bridge, the ramps are connected. Superstructure C1 is an eight-span continuous beam with spans of 14.00 – 21.00 – 26.50 – 27.00 – 27.50 – 26.00 – 24.00 – 25.50m. The western junction C3 is attached to C1. It is a five-span continuous beam with spans of 19.00 – 22.00 – 22.50 – 22.50 – 19.50m.

Superstructure C2 is also an eight-span continuous beam with spans of 14.00 – 21.00 – 26.50 – 27.00 – 27.50 – 26.00 – 24.00 – 25.50m. The eastern junction is a five-span continuous beam with spans of 27.50 – 25.50 – 25.50 – 25.50 – 19.50m.

The cross sections are actually T-beam like shaped with hollow tubes for weight reduction between the piers.

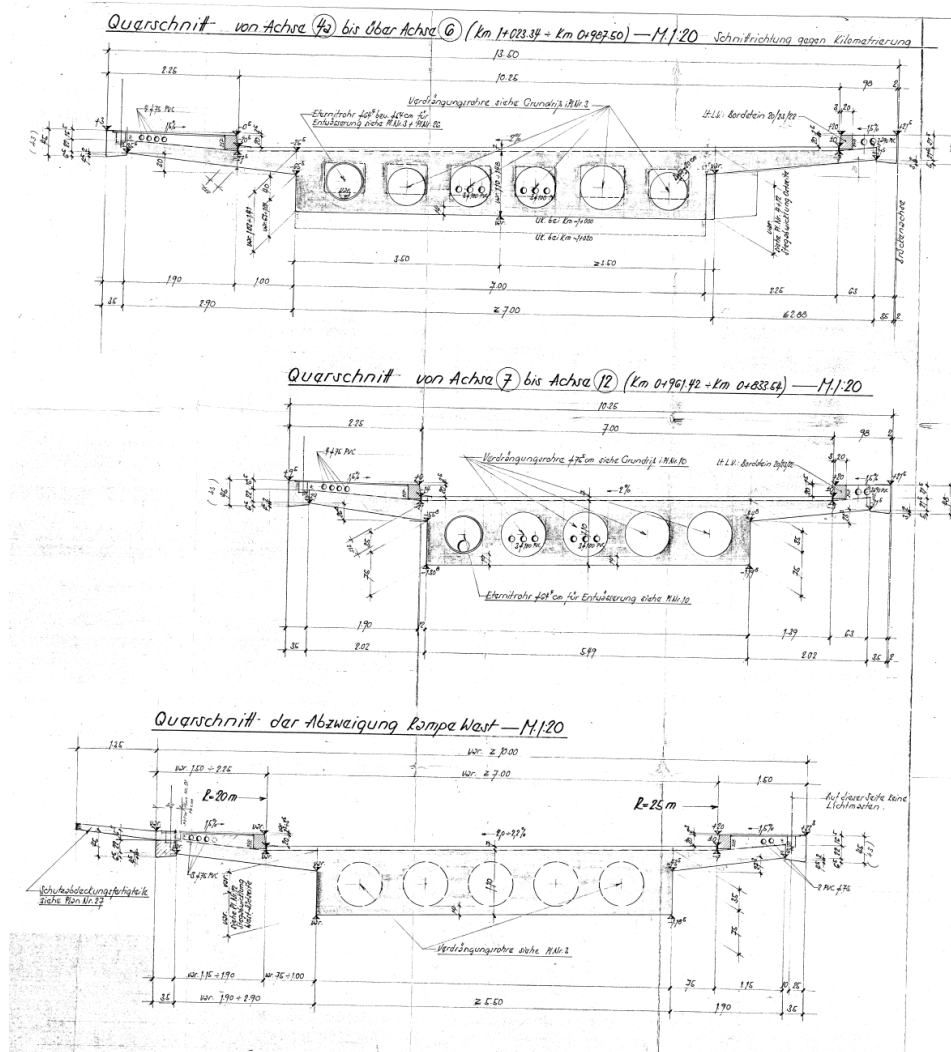


Fig. 3-6: Cross section of ramps

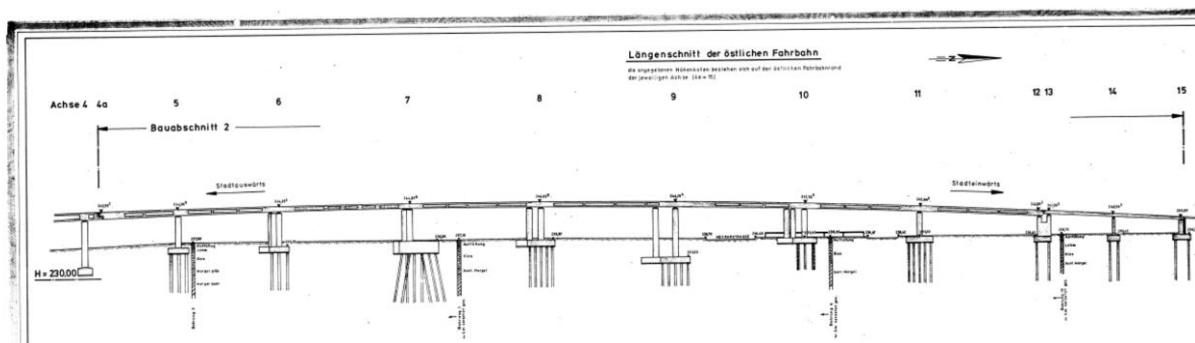


Fig. 3-7: Longitudinal section of ramp C1





*Fig. 3-11: View on two-span bridge from both sides showing good accessibility from underneath*

### 3.5 BIM Model

LAP created a BIM-Modell of the entire building D using the CAD software ALLPLAN, Nemetschek AG. The Model consist of the superstructure, piers, abutments and foundations. For the numeric analysis, the reinforcement of the superstructure was also modelled. The model was transferred to an IFC file, so it could be used to create the numeric model in the ATENA Software.

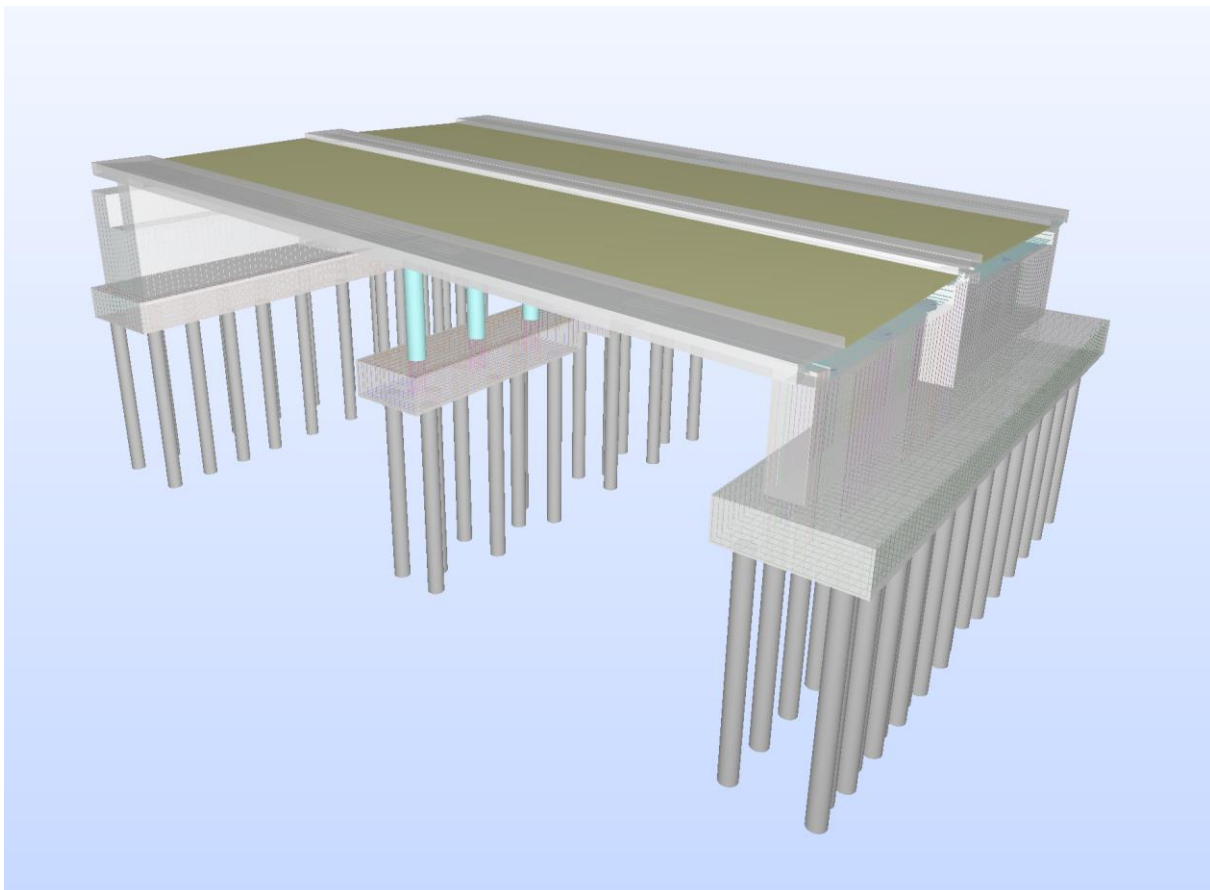


*Fig. 3-12: IFC-Model of Building D*

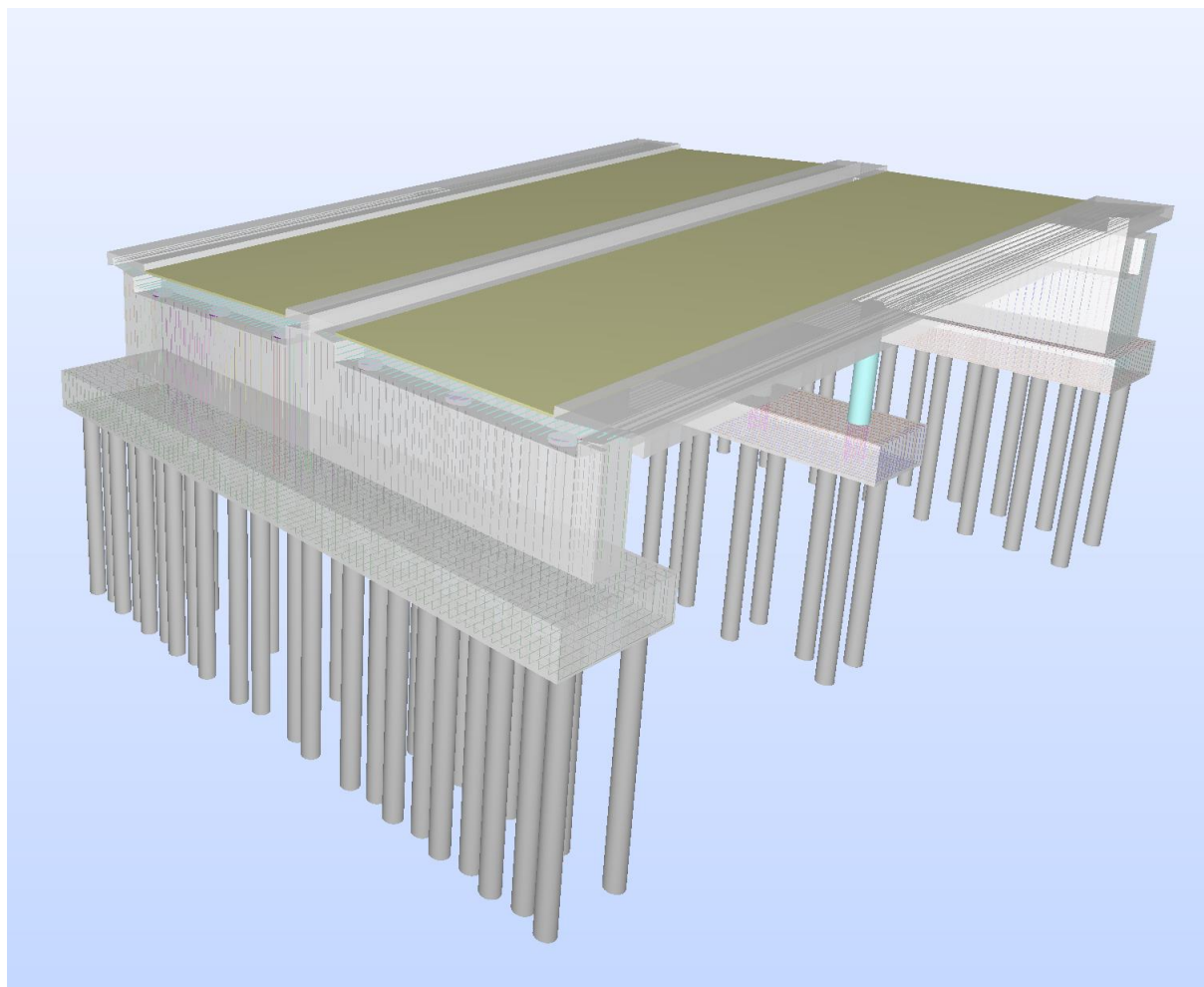


*Fig. 3-13: IFC-Model of Building D*

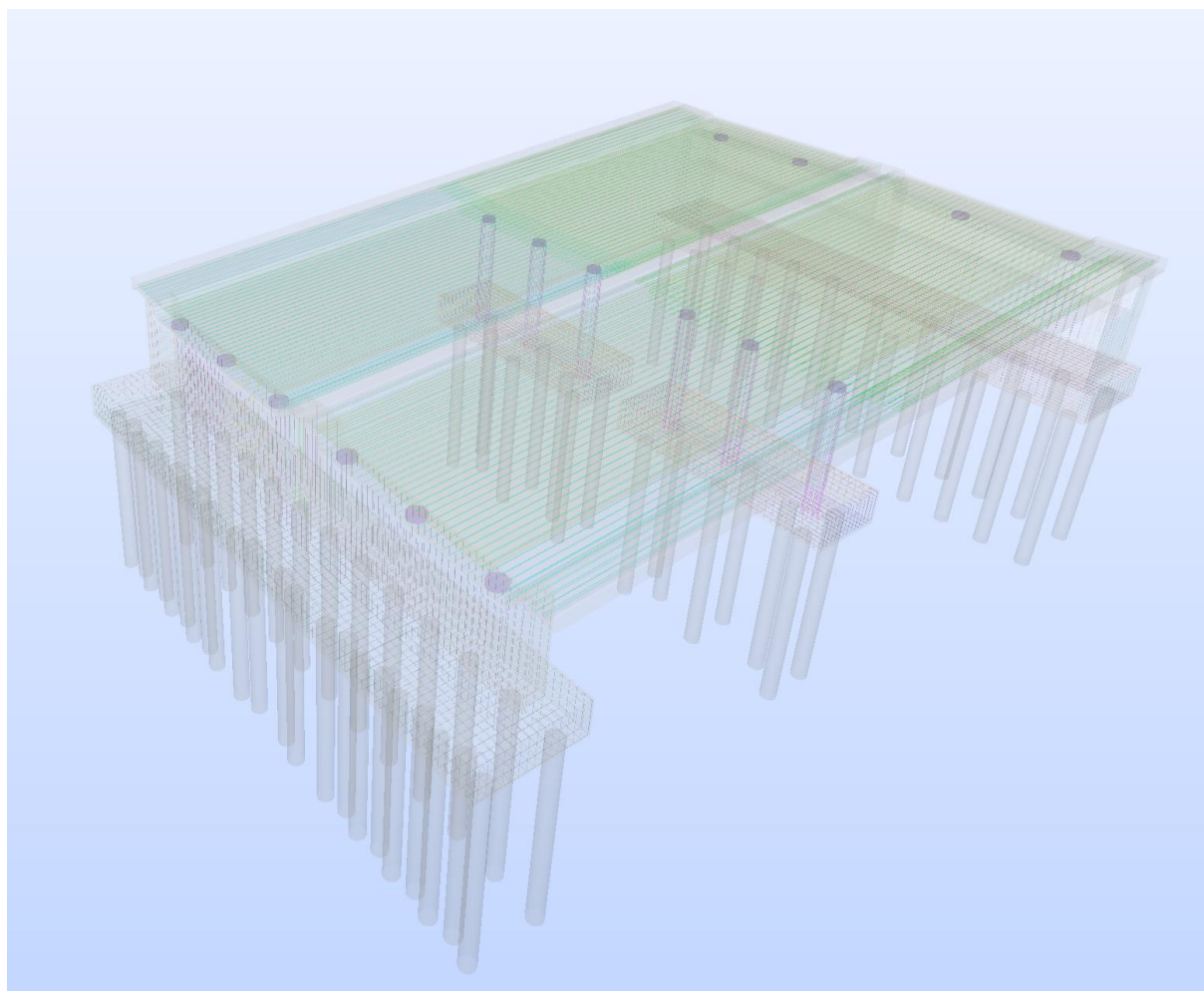


*Fig. 3-14: IFC-Model of Building D - Reinforcement*

### **3.6 Monitoring procedure and results**

One BWIM [5], [7] was used for each lane; each BWIM has a sensor ensemble consisting of one laser rangefinder; five strain gauges arranged in a row transverse to the road; and two strain gauges which are placed on either side of the row. The gauges in the row perform the actual measurement; the two adjacent gauges are used for triggering a measurement and estimating the speed of the vehicle; the laser rangefinder is used to detect and localize the vehicle axles. The spatial arrangement of sensors is shown below. The response of the sensors to a typical event is shown below.

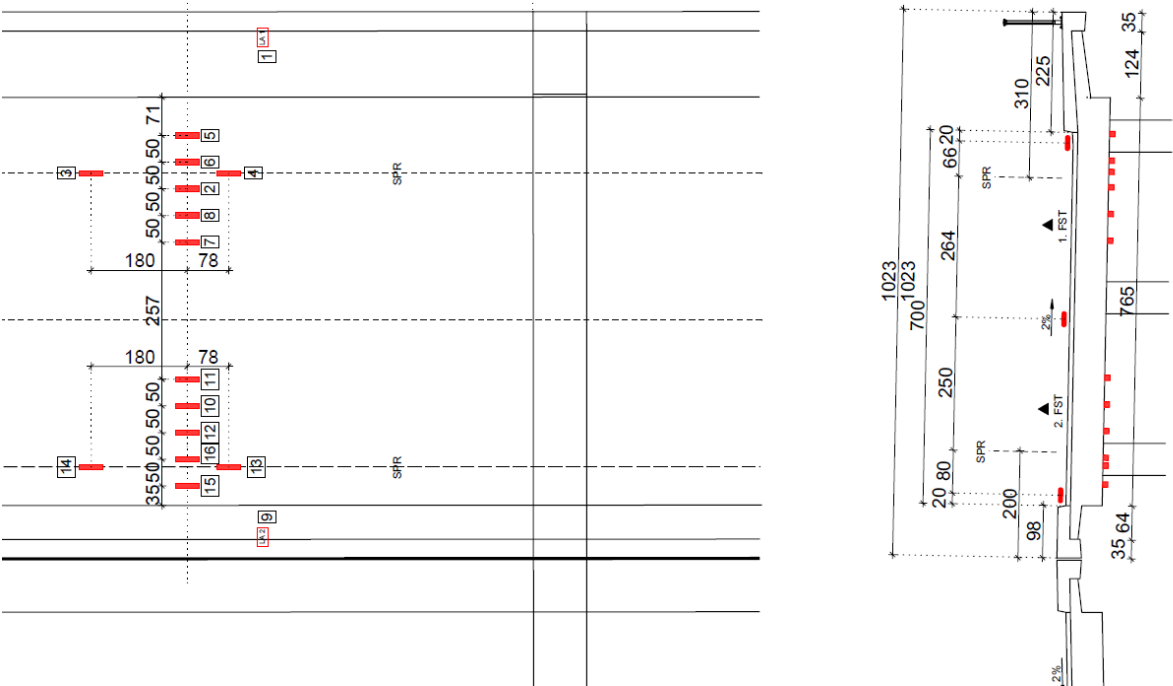


Fig. 3-15: Distribution of strain sensors.



Fig. 3-1: View of the installed sensors

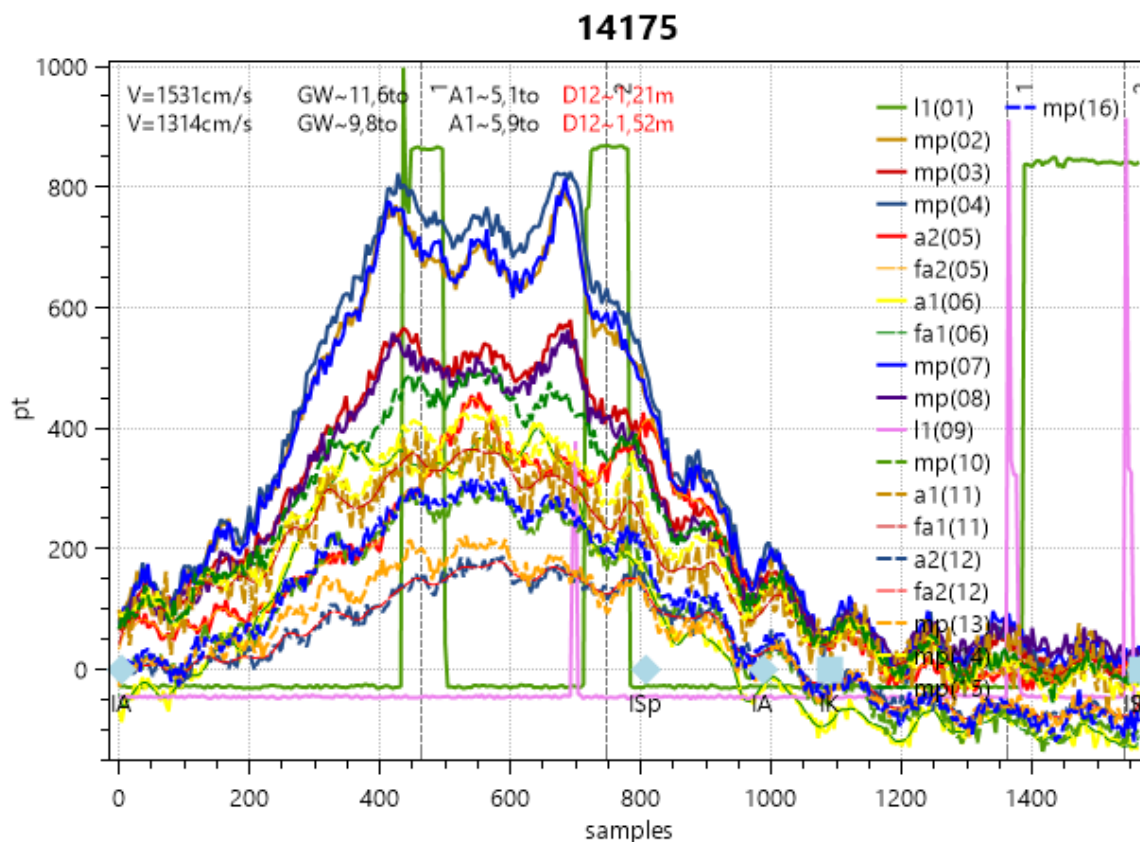


Fig. 3-16: A typical set of measurements from sensor ensemble.

This bridge presents a number of challenges for a BWIM system. First, there are traffic lights at the start of the bridge, a vehicle will often be accelerating as it passes over the sensors, i.e. we cannot assume that velocity is constant. Secondly, the span on which the measurement is made has an inclination of 6%, this further complicates the weight calculation. Furthermore, the bridge is subject to congestion, i.e. traffic may be slow moving or stationary. Combined with the presence of weak harmonics, these factors make the estimation of speed and weight difficult.

The problem of extracting useful information from these measurements can be undertaken in a number of ways: both closed form and optimisation based approaches are available. The approach used here is a “smart” Monte Carlo approach. This is based on an analytical kernel (SVD, though the Moses algorithm may also be used) that is calculated several times with different values of uncertain parameters. The Monte Carlo sampling is based on the uncertainty associated with each parameter, e.g. velocity and axle location. The solution that gives the best fit to the measured data when passed through the forward model is adopted. We define the best fit, in terms of mean square error, and quantify this with a quality factor  $Q$ .

The output of the estimation algorithm are the following parameters:

- Vehicle speed
- Axle locations
- Axle weights

- Quality of fit

From these values we derive:

- Axle count
- Axle spacing
- Gross Vehicle Weight (GVW)
- Vehicle class

These values are recorded in a database along with the following additional data:

- Time stamp
- Record number
- Temperature
- Average starin
- Lateral distance to righthand side of vehicle

Lane B

TST	ID	V	AC	VC	GW	Axles	Length	A2A	Q	T	203	204	201
20190206 13:47:35	20052	50,0	5	73	38,4	7,3 10,6 9,8 2,8 7,9	13,4	5,40 4,19 1,89 1,94	5	2,5	70,47	55,11	1,12
20181113 09:04:43	8393	32,9	5	120	31,8	10,5 1,7 11,8 5,7 1,9	8,3	4,11 1,10 2,08 1,04	7	13,0	82,89	38,99	1,34
20181113 09:47:25	8426	37,7	2	40	27,6	7,2 20,4	5,0	4,95	7	13,0	76,91	30,44	1,35
20190222 15:11:45	24167	35,4	3	52	26,9	8,4 10,1 8,4	7,5	5,77 1,77	7	10,3	66,56	40,74	1,24
20190220 15:29:07	23527	52,0	5	113	25,7	4,6 5,8 5,3 6,0 4,1	10,7	4,29 3,24 1,57 1,55	6	7,9	56,08	72,72	x
20190222 14:25:58	24151	54,2	3	52	25,4	8,9 8,9 7,7	7,8	5,96 1,88	7	10,2	58,83	38,55	1,45
20190305 14:33:31	26853	63,9	2	40	19,4	7,9 11,5	5,0	4,98	6	10,0	53,54	33,93	1,46
20181113 09:12:09	8400	37,5	3	55	19,2	5,0 9,1 5,2	6,5	4,69 1,78	5	13,0	49,47	55,67	x
20190227 15:24:16	25380	60,3	4	103	18,1	6,8 4,1 2,4 4,9	10,9	4,30 5,15 1,48	7	10,9	30,85	20,32	1,35
20181204 06:34:04	13822	67,1	4	124	17,6	2,6 4,3 1,5 9,1	7,9	2,39 1,38 4,14	7	11,6	42,43	29,86	1,43
20190206 13:26:31	20044	45,8	3	51	13,9	7,6 2,2 4,0	5,2	3,81 1,42	6	2,4	35,64	19,76	1,60
20190214 06:18:48	21885	70,2	2	40	11,5	5,9 5,5	5,3	5,29	6	5,2	30,19	21,41	1,34
20190307 08:42:24	27311	73,4	2	40	10,7	3,5 7,2	4,1	4,13	7	11,0	29,62	37,89	1,69
20190228 06:12:02	25509	53,0	2	40	9,4	5,8 3,6	4,4	4,36	5	9,9	26,69	20,25	1,42
20190227 12:31:27	25311	50,1	2	40	22,7	8,7 14,1	4,4	4,42	8	9,8	56,99	33,60	1,44
20190227 12:42:17	25315	60,7	2	40	11,8	5,7 6,1	4,0	4,00	8	9,9	38,20	21,30	1,66
20190227 14:45:59	25369	36,0	2	41	22,5	9,7 12,8	5,8	5,76	9	10,6	56,70	38,30	1,43
20190227 15:54:55	25393	57,7	2	41	16,9	6,8 10,1	5,3	5,31	10	11,1	52,02	32,21	1,64
20190227 17:43:28	25423	61,2	4	61	13,4	3,3 1,6 4,0 4,5	8,6	1,10 6,48 1,06	10	11,3	32,36	24,52	1,74
20190228 08:09:20	25544	59,7	3	101	18,4	7,7 9,0 1,7	13,4	5,87 7,52	10	9,6	44,47	29,24	1,56
20190228 11:04:03	25609	51,1	5	122	38,6	6,5 8,3 10,3 10,7 2,8	9,9	3,52 1,44 3,54 1,44	8	10,0	76,10	51,38	1,43
20190228 15:01:26	25699	57,7	2	41	23,5	9,6 13,9	5,7	5,74	10	12,5	62,00	37,49	1,18
20190304 06:01:03	26398	51,6	3	51	15,1	7,6 6,1 1,5	5,7	4,35 1,37	8	11,2	40,08	32,04	x
20190304 07:47:42	26429	52,0	2	40	9,6	5,4 4,2	4,8	4,84	8	11,1	25,44	19,23	x
20190305 06:27:23	26701	70,9	2	41	16,0	7,9 8,1	5,3	5,34	10	9,9	41,73	25,81	1,37
20190306 06:30:25	26969	61,2	2	40	13,0	6,2 6,8	5,1	5,14	9	8,9	37,76	22,53	1,35
20190306 08:57:31	27013	54,1	2	40	10,2	6,7 3,5	5,1	5,12	8	8,6	26,74	21,62	x
20190306 11:41:17	27083	65,1	2	40	9,2	5,5 3,7	5,2	5,21	8	9,1	24,32	17,96	1,63
20190307 09:38:49	27334	51,4	3	101	13,6	9,1 2,3 2,2	4,1	1,82 2,28	9	11,0	37,91	46,42	1,25
20190312 11:14:08	28432	53,4	2	42	8,7	5,4 3,3	3,5	3,5	9	8,7	26,66	19,11	1,92
20190313 17:00:21	28839	62,4	4	58	13,8	5,3 3,0 2,6 2,9	8,4	6,07 1,28 1,01	8	9,8	30,60	21,67	x
20190314 15:41:37	29094	49,6	3	55	19,5	7,7 3,8 8,1	6,7	4,83 1,82	9	8,4	39,17	57,97	x
20190315 16:24:19	29413	61,2	2	41	14,1	5,2 9,0	6,8	6,75	10	9,2	40,66	22,89	1,33
20190315 23:24:31	29484	56,4	4	62	16,6	7,7 2,3 3,0 3,7	13,2	5,06 2,54 5,61	10	10,1	27,50	15,67	1,65

Fig. 3-2: Table of measured values

### 3.7 Analysis of Initial Data Set

This section analyses data acquired over an uninterrupted period from January 16 2019 to March 17 2019 (61 days), Fig. 3-3. We note the strong weekly periodicity, with weekdays averaging around 200 vehicle transits per day.

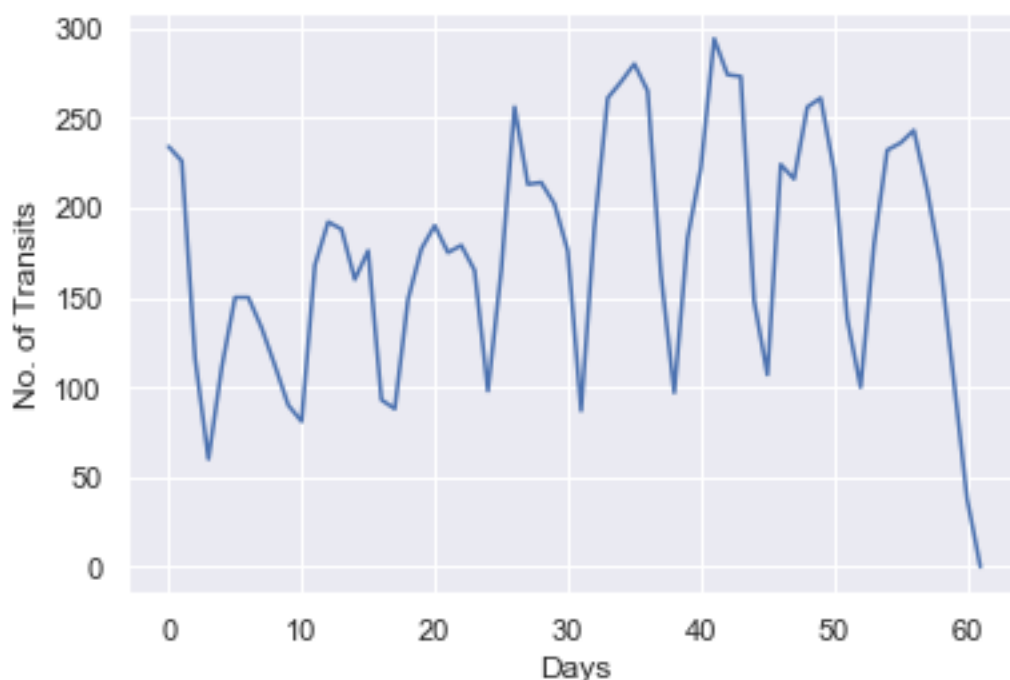


Fig. 3-3: Number of vehicles crossing Vogelsang bridge for each day of the measurement period.

In this section we will do three things:

- First we test whether our measurements are biased, i.e. are we more likely misclassify certain types of vehicles.
- Secondly, we will use the data to infer information about the type and characteristics of vehicles traversing the bridge.
- Thirdly, we will identify and interpret temporal patterns in the traffic flow.

### 3.7.1 Is the data set biased?

In previous work we have established that, once calibrated, the iBWIM system can accurately infer the weight, speed, and axle distribution of individual test vehicles. With the acquired data set we can now undertake a more statistical assessment. Ideally we would have a ground truth data set, acquired by other measurement methods, with which we could compare our results. Unfortunately this is not available. However, we do have a Quality value ( $Q$ ) that indicates how well our model fits the measured data (see Fig. 3-4).

The Quality metric is obviously an imperfect metric—there may be several different models that fit the measurement. However, it is a useful indicator for our purposes. The question we would like to answer in this subsection is whether the iBWIM system performs better for some classes of vehicle than others—if it does this will bias our analysis. We answer this question by seeking any correlation between the quality metric and vehicle characteristics, such as gross weight, Speed and Length, see Fig. 3-5. The scatter plots and  $R^2$  values indicate there is no significant correlation and we will assume that there is no systematic error in our measurements and that our analysis is unbiased.

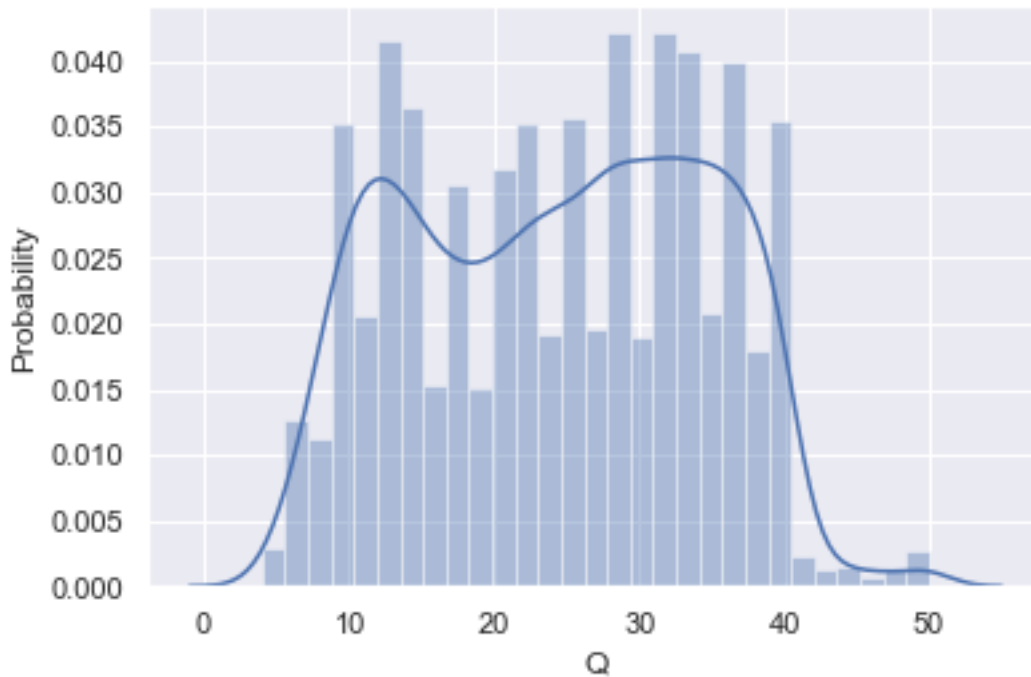


Fig. 3-4: Distribution of Quality metric for Vögelsang bridge dataset

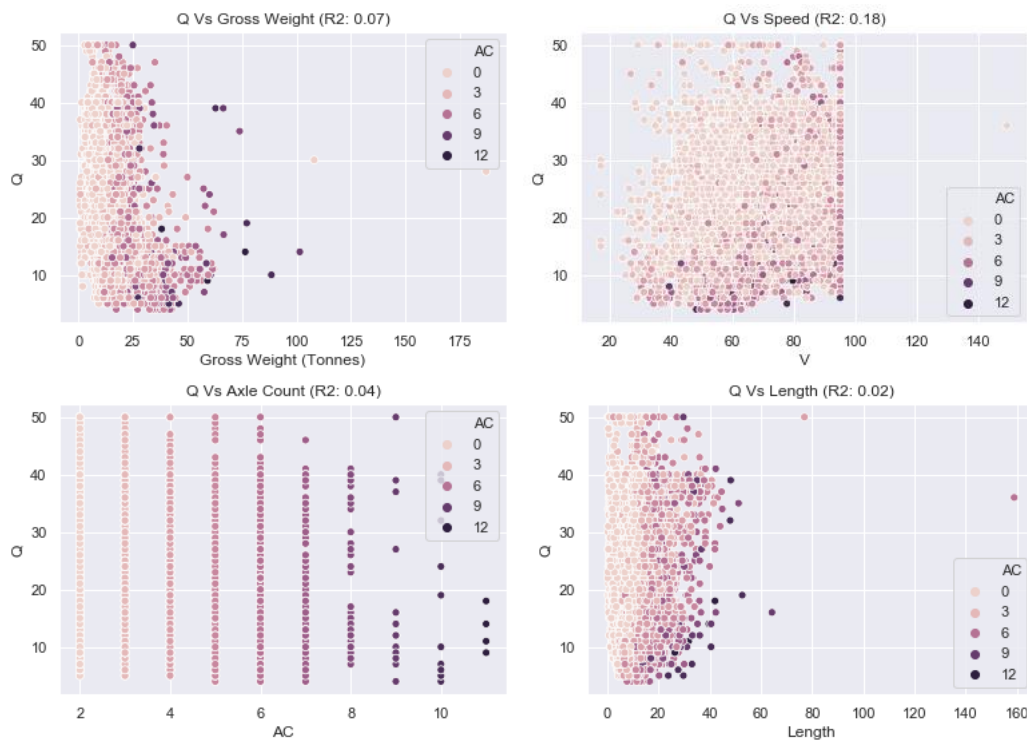


Fig. 3-5: Correlations between quality metric and various parameters of the model for the Vögelsang bridge

### 3.7.2 Vehicle Characteristics

The probability distributions for various parameters are shown in Fig. 3-6.

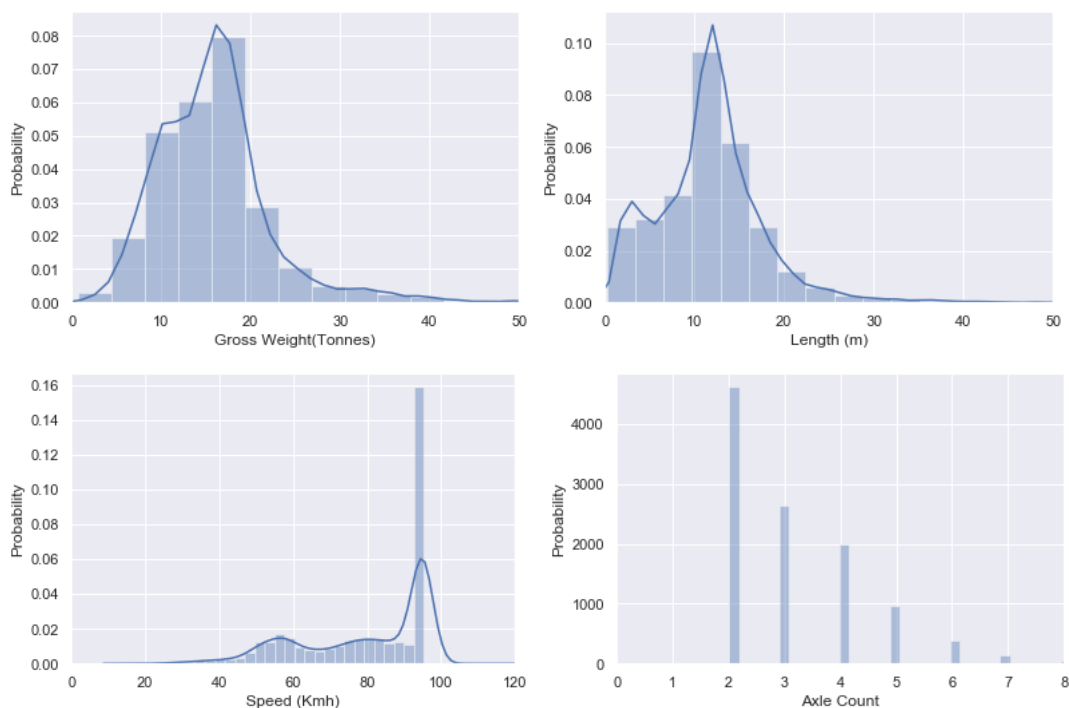


Fig. 3-6: Probability of vehicle Gross Weight, Length and Speed.

If we plot vehicle weight against axle count we unsurprisingly get a weak correlation Fig. 3-7(left). A more interesting result becomes apparent if we restrict ourselves to 2 axle vehicles and plot weight against length, Fig. 3-7 (right). In this graph we can resolve three clusters: small vehicles (intra-axle distance 2m) of around 10 Tonnes, longer vehicles (circa 12m) of either 10 Tonnes or 16 Tonnes.

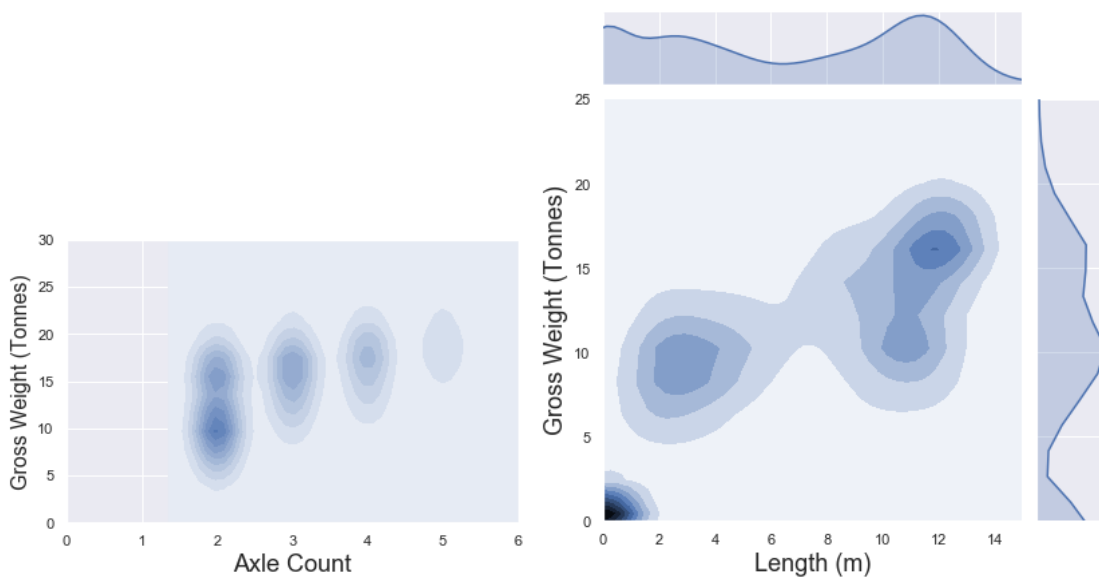


Fig. 3-7: Correlation between Vehicle Weight and axle count, Vogelsang bridge

### 3.7.3 Temporal Patterns

In Fig. 3-3 we noted a strong weekly periodicity in the number of vehicle crossings, plotting this by week day, we can see that during the working week we can expect 200 or more vehicle crossings a day, which falls to around 100 crossings during the weekend.

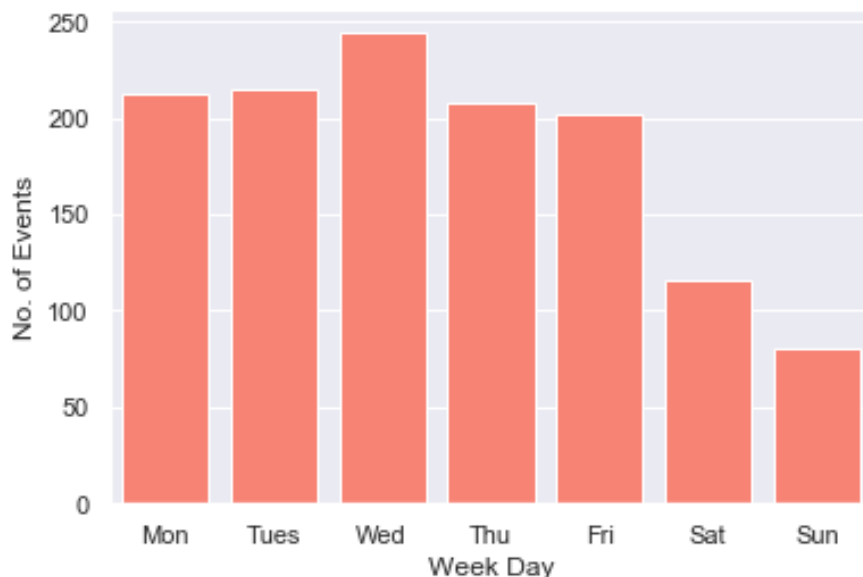


Fig. 3-8: Vehicle transits by week day, Vogelsang bridge

We now consider diurnal patterns, Fig. 3-9. There is no significant change in weight distribution of traffic over the course of the day—beyond the variation in vehicle frequency. There is, however, a more noteworthy effect in vehicle speed, Fig. 3-9 (right). The majority of traffic is moving at 90Km/h, however, between 06:00 and 16:00 there is a significant likelihood that vehicles will be travelling at around 50Km/h—presumably due to congestion.

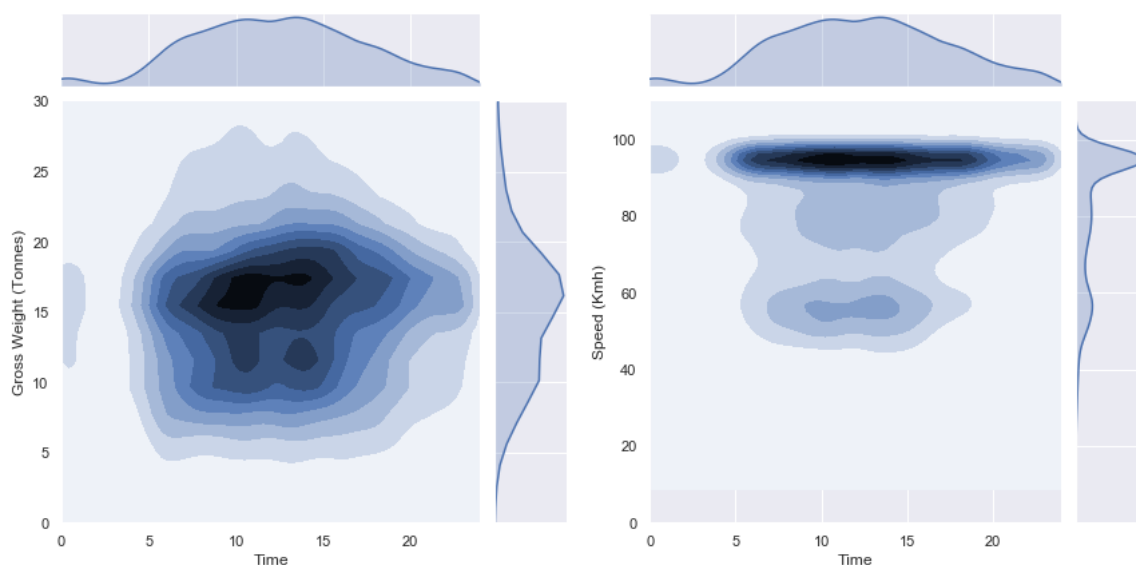


Fig. 3-9: Diurnal patterns for vehicle weight and speed, Vogelsang bridge

### 3.7.4 Damage Metrics

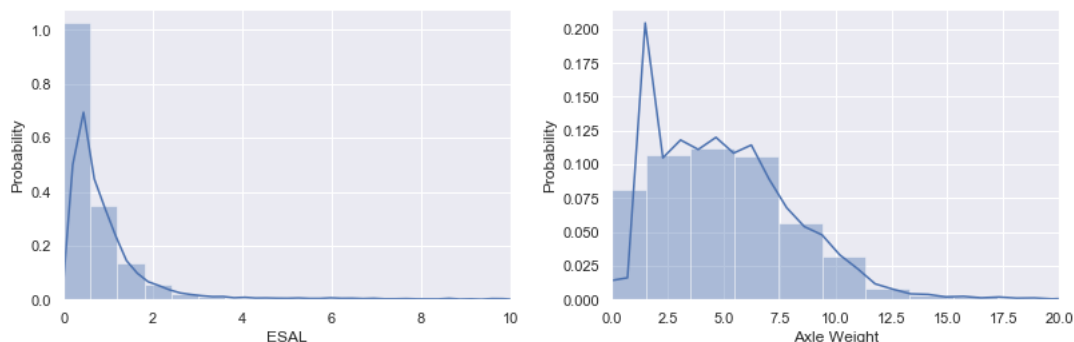


Fig. 3-10: Damage metrics, Vogelsang bridge, ESAL is equivalent single axle load

## 3.8 Development and calibration of the numerical model

### 3.8.1 Model

At the beginning of numerical calculation, model of passing truck were created in ATENA software [3] for determination of critical position on the bridge. In the model were placed monitors for strain at the same position as on the real bridge and if the maximum strain was detected, position of truck was declared as critical.

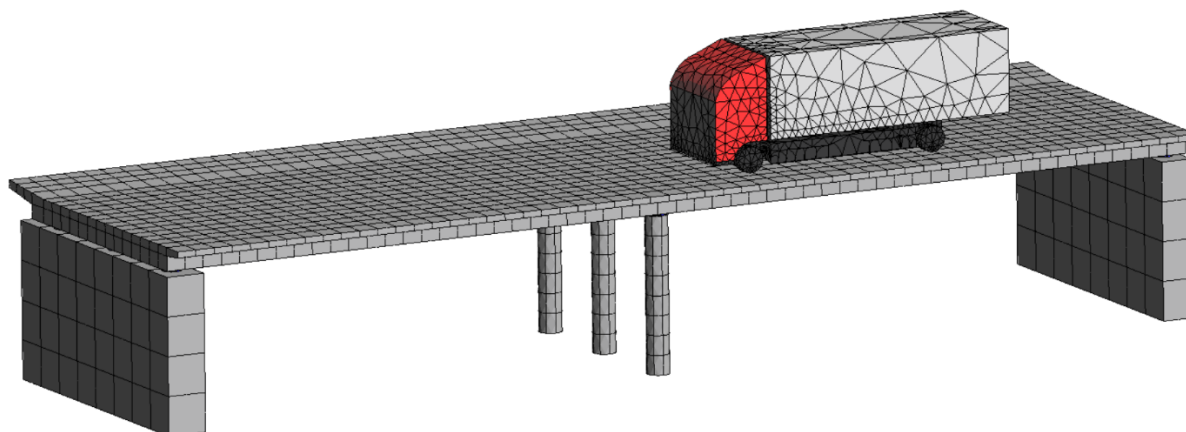


Fig. 3-11: Numerical model of the bridge with moving truck and shown mesh

Numerical model was created as real structure based on dimension from drawings shown in chapter 3.4. Just one half of the bridge was modelled because of symmetry and connecting between two slabs in the middle of the bridge was neglected. For meshing was used hexahedra quadratic mesh sized as 0,5 m. Bridge is supported by nine steel plates fixed to bottom surface of the slab and each steel plate has constraint for middle point. Bridge is 27 m long and first span in 13,2 m and second span is 13,8 m. Height of the slab is 0,6 m and width of one slab is 9,5 m.

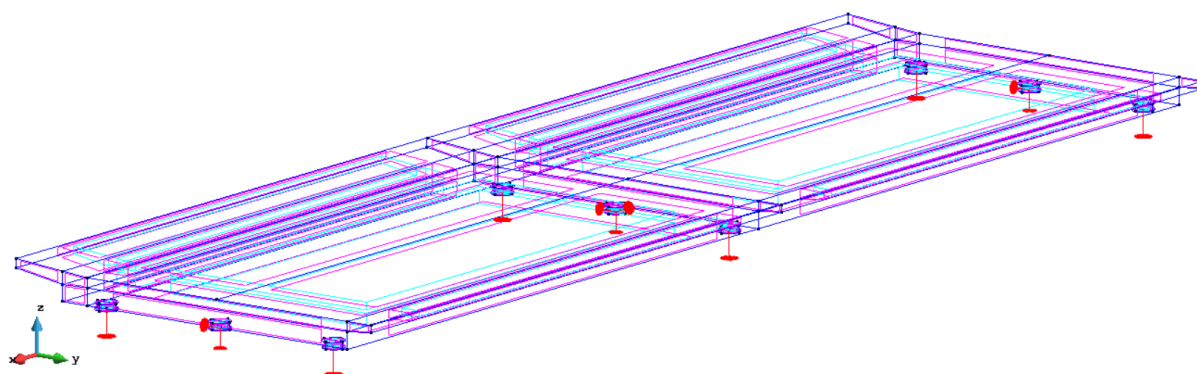


Fig. 3-12: Boundary conditions

Bridge was made from concrete B450 and it is reinforced by steel reinforcement. Reinforcement is modelled as discrete bars based on historical drawings. Straight bars were modelled as lines and curved bars were modelled as polylines. Diameters and material parameters were set individually as material parameters for line.

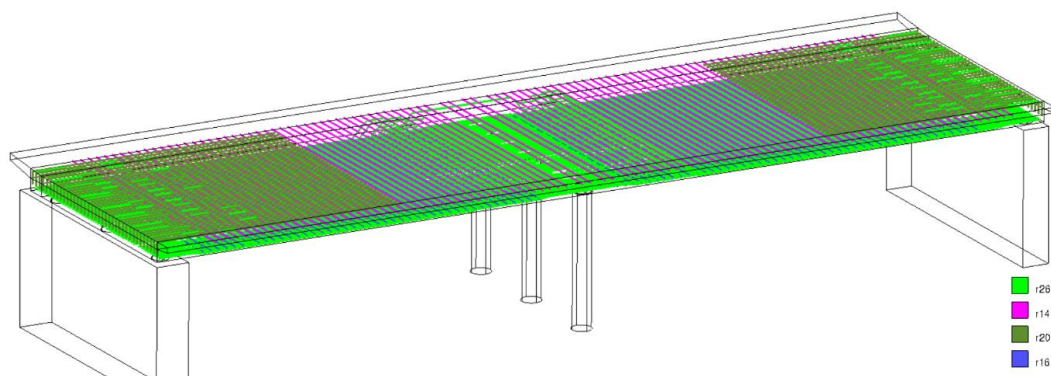


Fig. 3-13: Main reinforcement of the bridge in numerical model

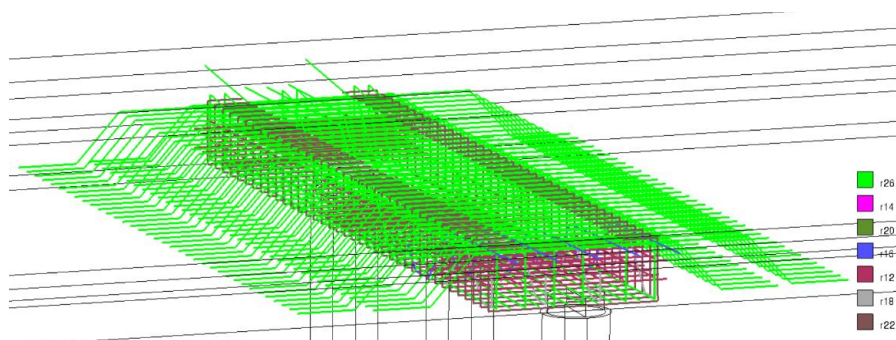


Fig. 3-14: Detail of reinforcement above the middle columns.

### 3.8.2 Material parameters

Material parameters were set based on structural diagnostic. Concrete parameters were determined from cylinder compression test. In historical drawings is written type of used concrete B450 and from compressive test were determined values of compressive strength  $f_{ck,cyl} = 35,5$  MPa and elastic modulus  $E_c = 33,3$  GPa. It corresponds to values of concrete C35/45 and material parameters were generated from this type of concrete.

Tab. 3-1 - Characteristic values of concrete used in the model

Material parameter	Value
Young's modulus $E$ [GPa]	33.3
Poisson's ratio $\nu$ [-]	0.2
Compressive strength $f_c$ [MPa]	-35.5
Tensile strength $f_t$ [MPa]	2.27
Fracture energy $G_f$ [N/m]	139
Plastic strain at compressive strength $\epsilon_{cp}$ [-]	-0.0013
Critical compressive displacement $w_d$ [mm]	-0.5
Reduction of compressive strength due to cracks [-]	0.8

Material parameters of steel were detected from project drawings. Characteristic values of yield strength was 420 MPa, tensile strength 500 MPa and elastic modulus 210 MPa. Maximum plastic strain was 5%.

Tab. 3-2 – Summary of reinforcing bars in the numerical model

Material name	Diameter [mm]
r12	12
r14	14
r16	16
r20	20
r22	22
r26	26

### 3.8.3 Parametric study

After determination critical position of the loading, were modeled real situations from Petschacher measurement. Gross vehicle weight, axle to axle distances, number of axles, velocity, lateral distance etc.. were measured on the bridge. The most interesting situations during the measuring were founded and used for comparison with values of strain measured on the bottom side of the bridge. Load corresponding to one real situation have been modeled in software ATENA and strains calculated in the same position as in real sensors placed on the bridge were compared with strains measured on the bridge.

Because strains didn't correspond accurately to each other, parametric study have been used. Basic parameters have not been changed. But parameters as tensile strength or fracture energy of concrete could be changed to fitting maximum strain in sensors. For fitting was used software SARA which is probabilistic tool of ATENA. SARA automatically changing selected parameters until selected magnitude correspond to defined values. On following pictures are shown influences of some parameters which have been used for parametric study. On each chart are shown two curves showing difference between sides of the bridge. It simulates groups of sensors placed on sides of real bridge.

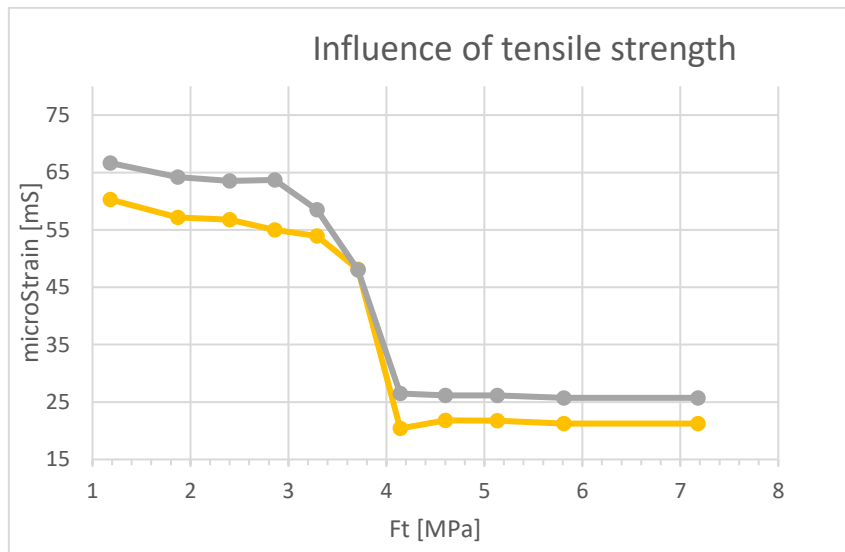


Fig. 3-15: Influence of tensile strength of concrete to strain on the both sides of the slab

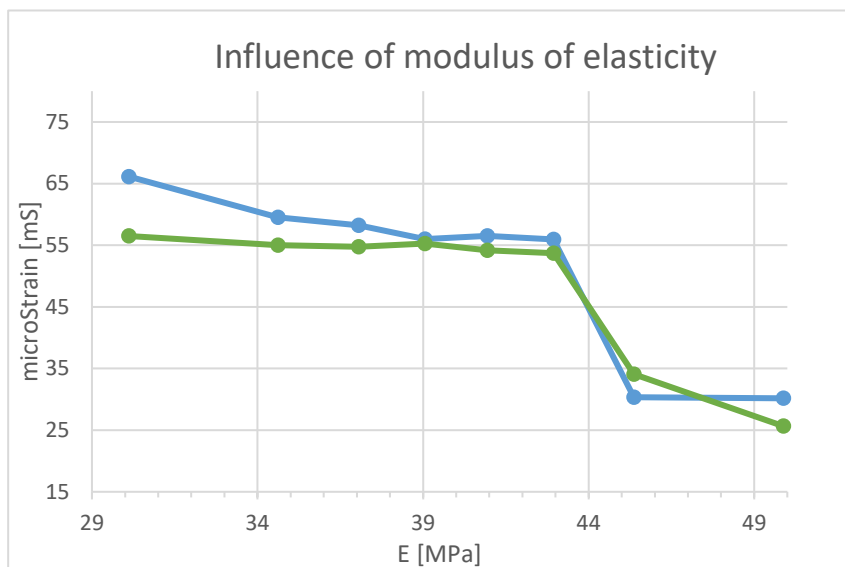


Fig. 3-16: Influence of young's modulus of concrete to strain on the both sides of the slab

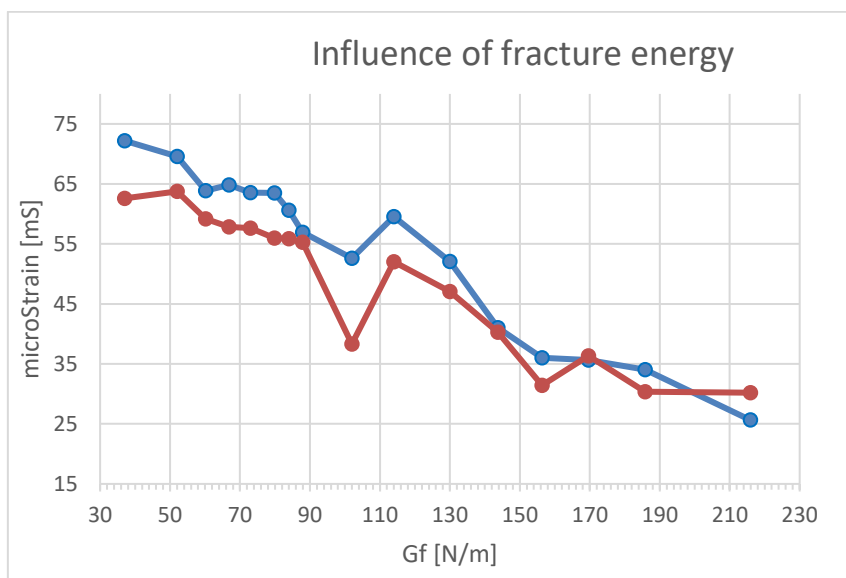


Fig. 3-17: Influence of fracture energy to strain on the both sides of the slab

Based on parametric study have been created numerical model fitted to real structure. Situation marked by ID number 8426 have been modeled. Truck 27,6 tons heavy, 5 meters long passing the bridge by speed 37,7 km/h was used in the model. Value 76,91 mS was determined in the group of sensors “203” and 30,44 mS was determined in the group of sensors “204” during the measurement. After parametric study both values of strains were not fitted accurately, but higher value was fitted better. From numerical analysis were obtained values 76,1 mS for group “203” and 52,2 mS for group “204”. Model with similar material parameters was used for next calculations of load capacity and durability study.

### 3.8.4 Results

Model was loaded by dead load and overloaded to level corresponding to characteristic live-load due to cracking of concrete. After unloading there was applied weight of the truck.

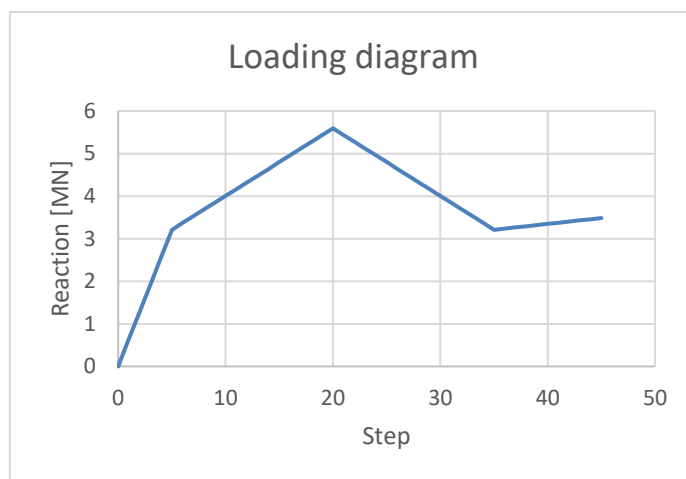


Fig. 3-18: Loading history in steps of analysis

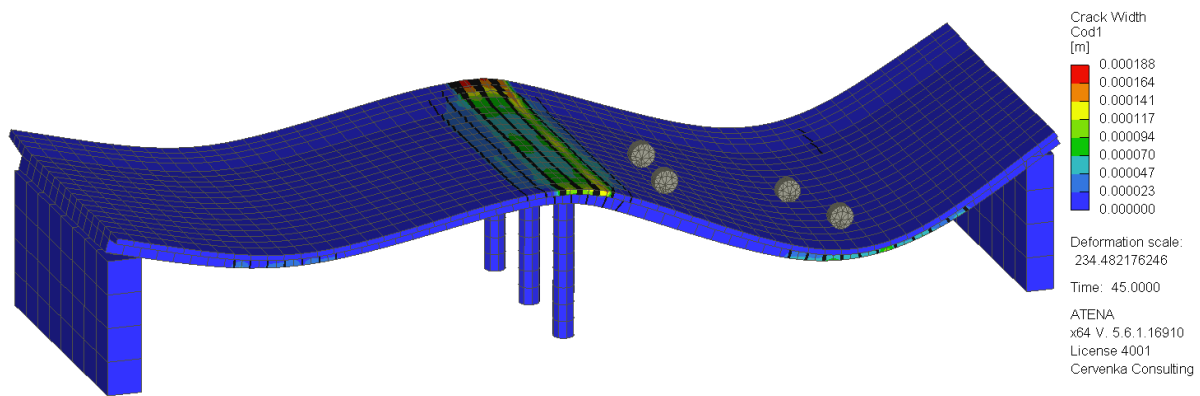


Fig. 3-19: Crack width after loading by weight of the truck.

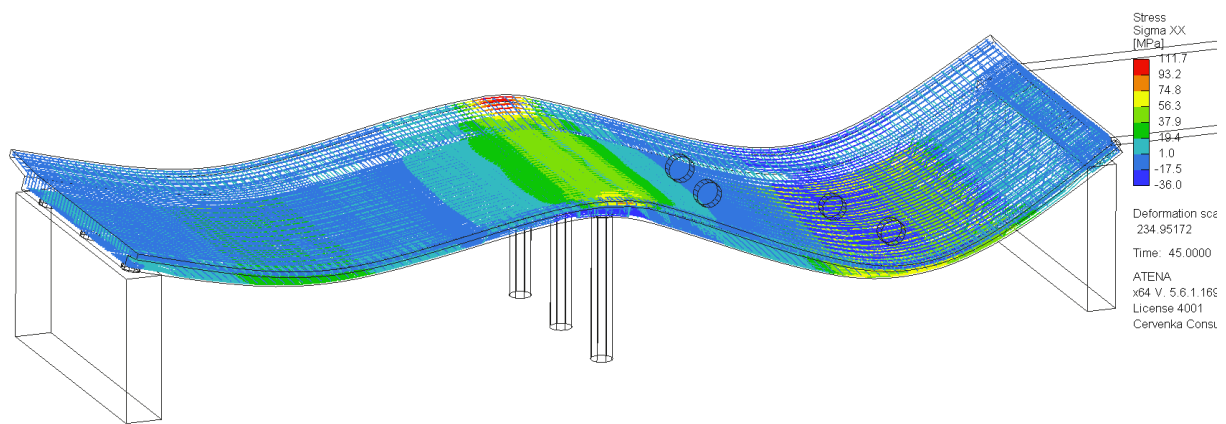


Fig. 3-20: Stress in reinforcement after loading by weight of the truck.

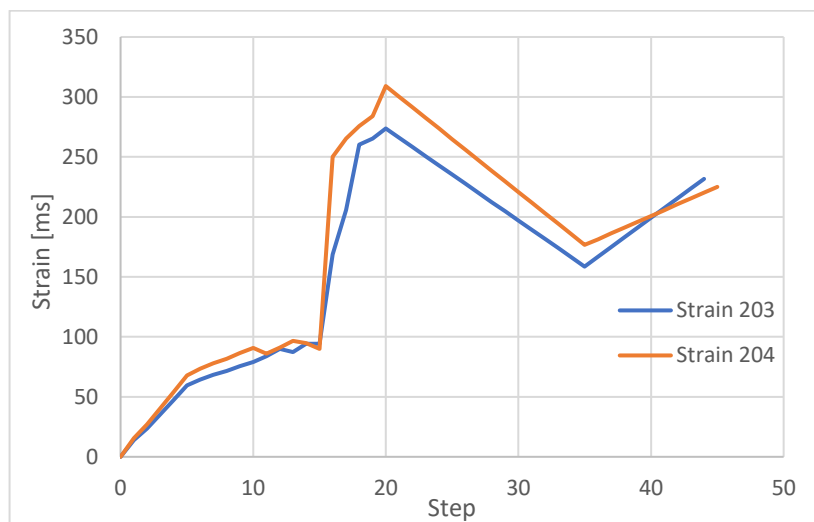


Fig. 3-21: Strain in groups of sensors “203” and “204” during loading

Final value of strain is average value calculated from two sensors placed on the side of the slab and it is difference between step 35 and 45. Last ten steps represent loading by weight of the truck.

## 3.9 Durability Prognosis

### 3.9.1 General

Corresponding to the procedure described in M6.2 “Simulation and Probabilistic Prognosis Model” CER made a lifetime prognosis for die Vogelsang Bridge, building D. Prior to the cyberBridge research project, a remaining life time for the entire bridge of 15 to 20 years was estimated on the base expert knowledge. As several damages on the building are known and building B is prone to stress corrosion cracking, a monitoring system will be installed on the bridge. The goal of the durability prognosis was, to analyze the influence of chloride based corrosion on the load bearing capacity of the bridge.

### 3.9.2 Durability Study

In the first instance was the bridge loaded by permanent load from measurement and results from numerical analysis were validated to measured results. In the subsequent analysis the bridge is loaded by the permanent load and then it is subjected to the environmental actions: **chlorides**:  $D_{ref} = 1.2e-7$  m<sup>2</sup>/day,  $t_{Dref} = 3650$  days,  $m_{coeff} = 0.37$ ,  $t_{mcoeff} = 10950$  days,  $Cl_{crit} = 0.004$ ,  $f_{t,ch} = 3.2$  MPa,  $w_d = 0.001$  m, pitting corrosion  $R_{corr} = 2$ , and  $C_s$  was differed due to position. For top surface  $C_s = 0.009$  and for bottom surface  $C_s = 0.0055$ , corrosion rate after spalling 35 μm/year. Third part of the analysis is devoted for durability study.

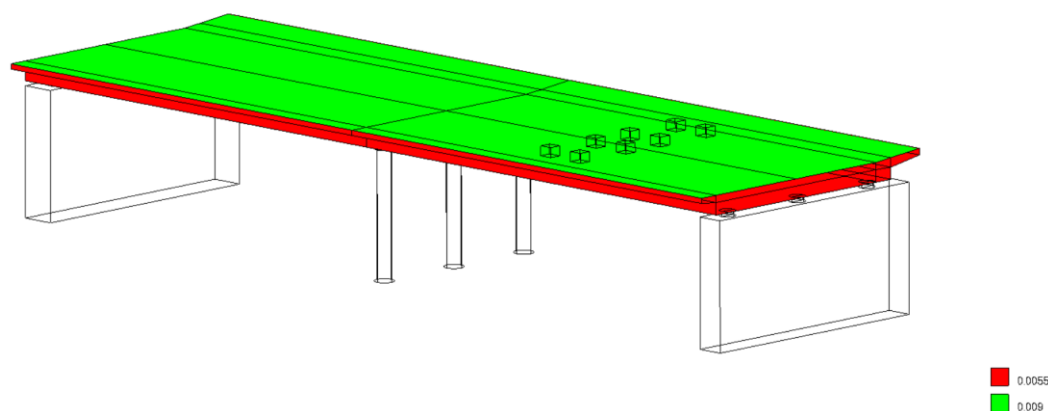


Fig. 3-22: Chlorides applied for surfaces of the bridge

Before application of corrosion bridge was gradually loaded until ULS level in 60 steps. After finishing of loading, corrosion study starts. A few models have been calculated with different time of corrosion. The first model was without corrosion for setting load bearing capacity. Later models were calculated with 25, 50, 75, 100 and 150 years of corrosion. All models have been calculated in two sets of material parameters (characteristic and mean). Later values of design capacity by ECOV method were calculated. On the Fig. 3-24 the influence of the corrosion on the load carrying capacity is shown. Each curve describes different values of material parameters (design, characteristic and mean) and it decreases in time.

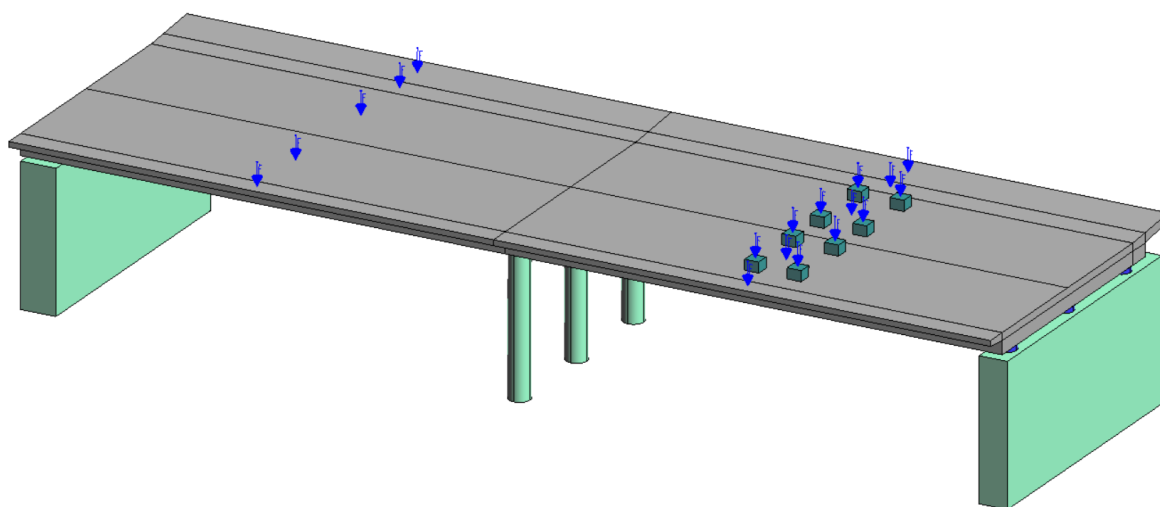


Fig. 3-23: Loading according to ČSN EN 1991-2

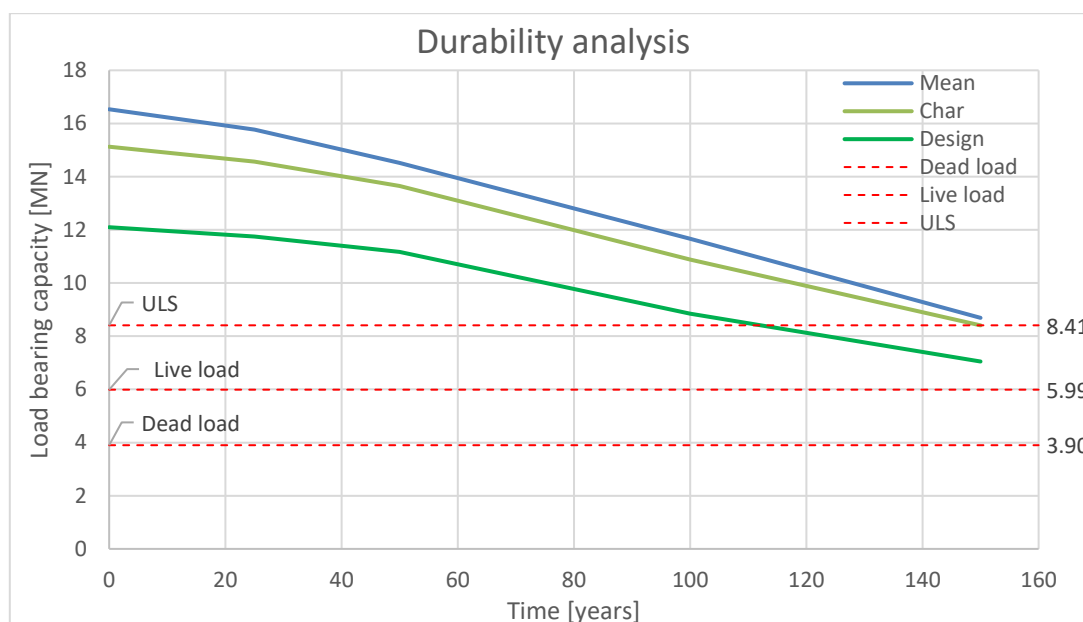


Fig. 3-24: Influence of chlorides for load bearing capacity

Results in Fig. 3-24 show the decrease of the load bearing capacity of the bridge on different levels. The load bearing capacity is reduced by about 40% over the considered time-span of 150 years. This may look dramatic, but considering the design criteria the actual lifetime of the bridge on design (ULS) level is about 100-110 years which fits quite well to state-of-the-art design goals. Considering the actual age of the bridge of about 50 years, another 50 to 60 years of remaining lifetime can be estimated. This is a great benefit compared to the previously estimated remaining lifetime of 15 to 20 years.

### 3.9.3 Prediction of Reinforcement Corrosion in Existing Structure

This section presents the results of the reinforcement corrosion evolution that occurs in the structure in over 150 years of its service life. Following figures show the corrosion of reinforcement for the selected points in time. The values represent the relative loss of the reinforcement cross-sectional area, i.e. 1.0 represents 100% loss of reinforcement and 0.0 no corrosion.



failure. After 150 years of corrosion is visible, that structure cannot bear enough loading for ULS design-level anymore. Corrosion on few parts of reinforcement was 100%.

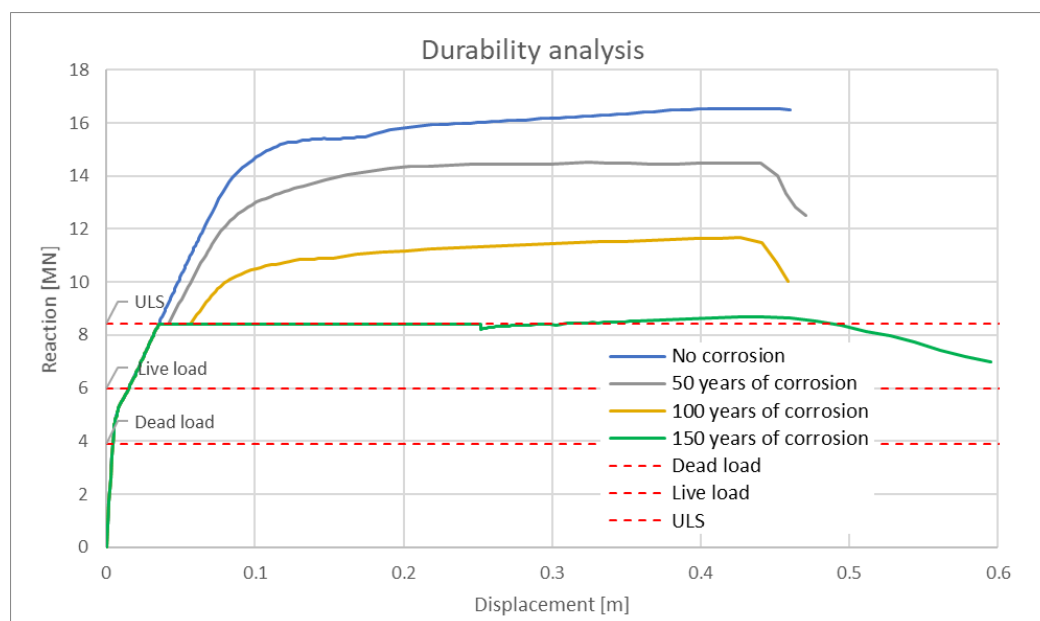


Fig. 3-28: Influence of corrosion to load bearing capacity.

On following figures is shown failure mode. In all models was structural collapse caused by flexural failure. On Fig. 3-29 and Fig. 3-30 is shown model without corrosion. There is visible that equivalent plastic strain of concrete is over maximum level. It caused crushing of concrete and failure of the structure. On the other way Fig. 3-31 and Fig. 3-32 shows model after 150 years of corrosion. Crushing of concrete is concentrated just on one small area and plastic strain of reinforcement exceeds limit value.

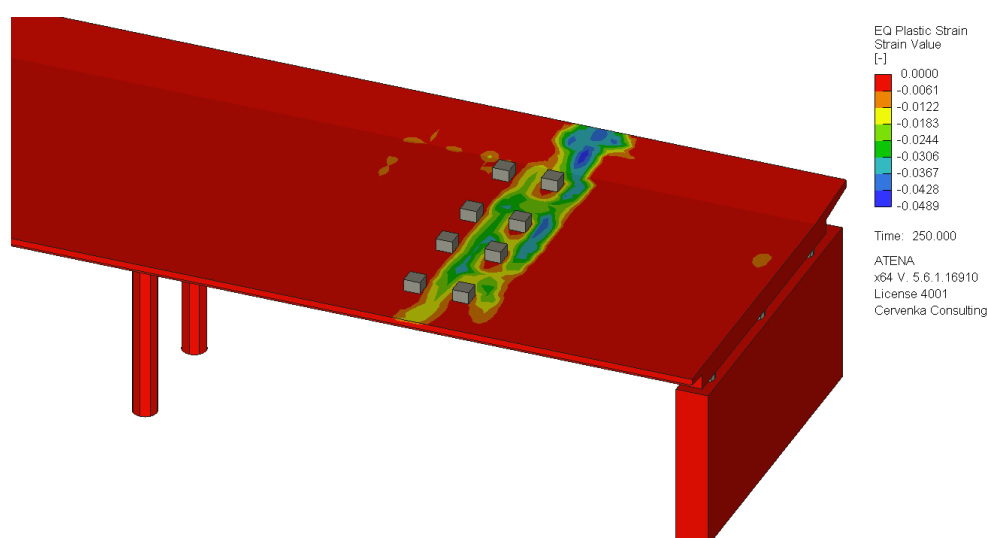


Fig. 3-29: Crushing of concrete during the failure of the structure on the peak of loading.  $\epsilon_{CP} = 0,00123$  (model without corrosion)

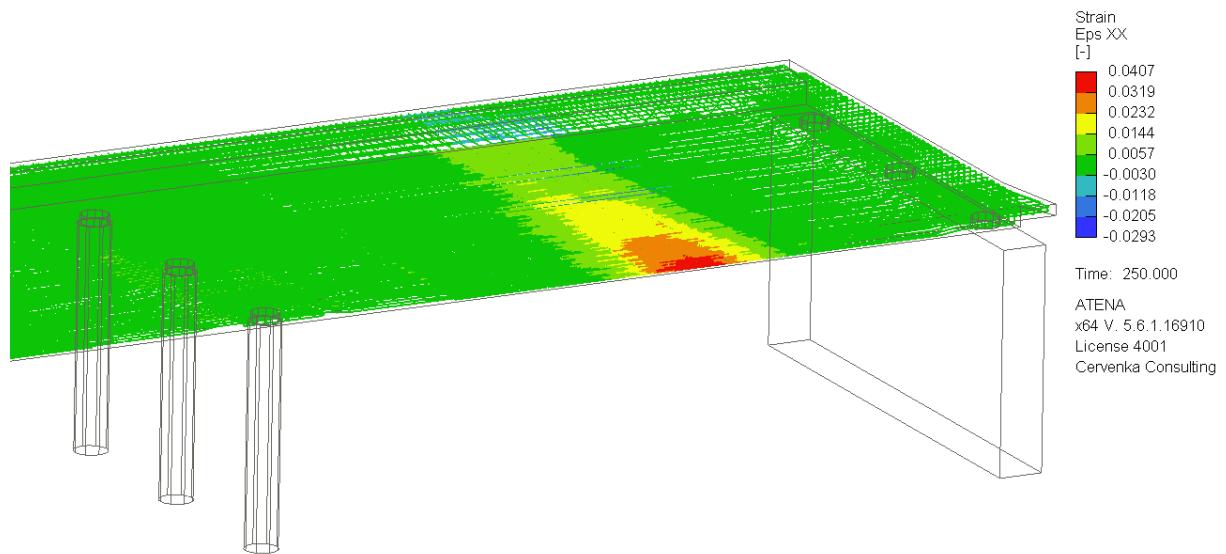


Fig. 3-30: Strain of reinforcement on the peak of loading (model without corrosion)

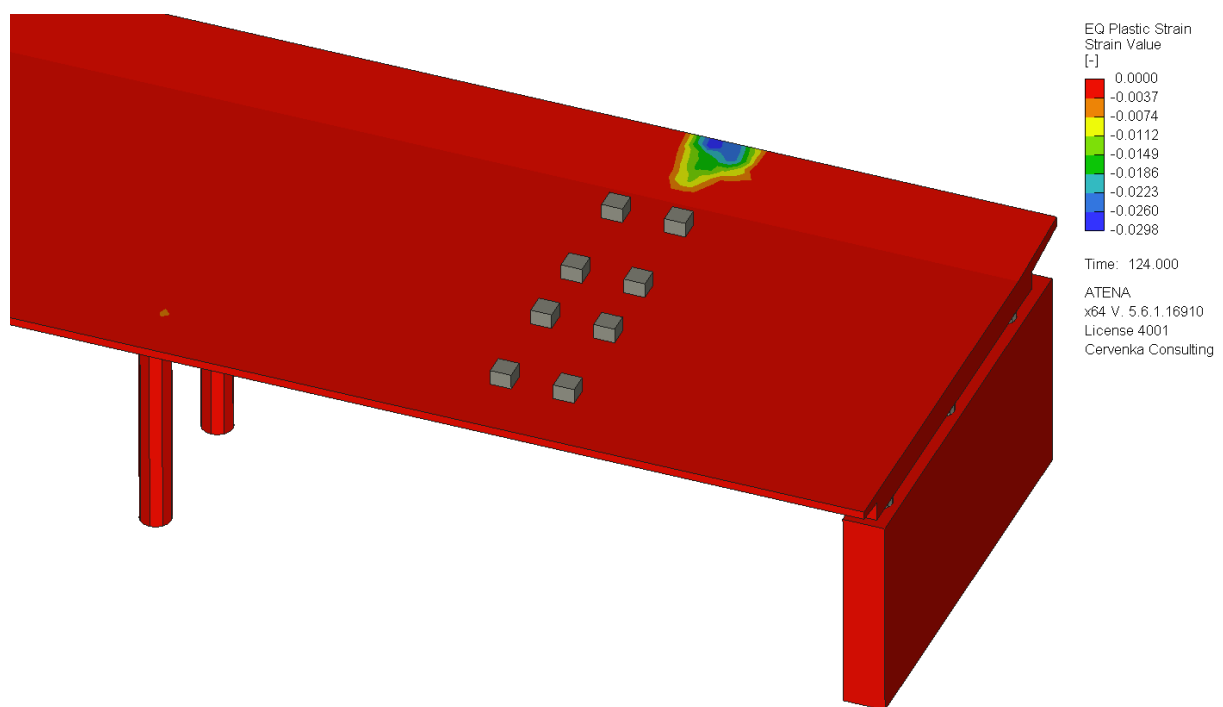


Fig. 3-31: Crushing of concrete during the failure in one part of the structure on the peak of loading.  $e_{CP} = 0,00123$  (model with 150 years of corrosion)

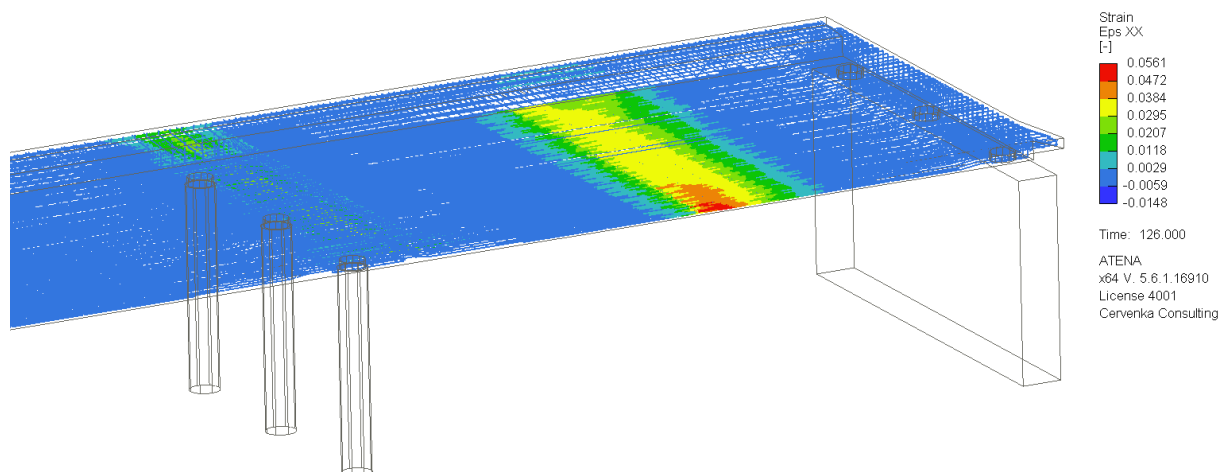


Fig. 3-32: Strain of reinforcement on the peak of loading (model with 150 years of corrosion)

Results of reinforcement corrosion prognosis show on the one hand the influence of reinforcement corrosion on the lifetime of the bridge and on the other hand the failure mode of the bridge due to reinforcement corrosion. Reinforcement on the upper surface of the slab in the support area is most likely to be weakened by corrosion. This leads to increasing rotations and decreasing hogging moments in that area. As a result, the sagging moment in midspan increases until failure of the structure.

#### 3.9.4 Conclusions

The results of the durability studies show a much higher remaining lifetime of the bridge, than previously estimated with less sophisticated methods. Considering Building D alone, the remaining lifetime can be exceeded to approximately another 50 to 60 years from now instead of 15 to 20 years previously predicted. The results also show that chlorides have a great impact on the deterioration of the structure. Therefore, it is very important that the sealing underneath the wearing surface is in good condition so chlorides cannot intrude the concrete.

Ongoing deterioration will lead to great deformations and visible damages especially in the support area of the bridge including spalling of the concrete cover. Typical for a not-prestressed concrete structure the bridge has a very good preparatory behaviour.

Apart from that a monitoring system, especially the iBWIM Method on building D is a very good measure to monitor the traffic on the bridge. Knowing the loading of the bridge in real time is very valuable for the monitoring of the other building parts C and D which are prone to stress corrosion cracking. As the spontaneous cracking of tendons may lead to a collapse without any advance notices, it is very important to know the behaviour of the bridge very well, so that minor changes of gauge signals can be interpreted correctly and the correct measures can be taken.

## 4 Austrian Bridge (PSP)

The bridge selection criteria are specified in COST 323 [4].

			WIM site classes		
			I Excellent	II Good	III Acceptable
<b>Geometry</b>		Longitudinal slope (%)	≤ 1	≤ 2	≤ 2
		Transverse slope (%)	≤ 3	≤ 3	≤ 3
		Radius of curvature (m)	≥ 1000	≥ 1000	≥ 1000
<b>Rutting (3m beam)</b>		Rut depth max. (mm)	≤ 4	≤ 7	≤ 10

Tab. 4-1: Classification and criteria of WIM sites

Criteria	Optimal	Acceptable
Bridge type	Steel girders, reinforced concrete girders, steel orthotropic decks	Concrete slab, prestressed concrete girders
Span length (m)	10 – 24	5 – 10; 24 – 35
Traffic density	Free traffic – no congestion (traffic jam)	
Skew (°)	≤ 10	≤ 25 or ≤ 45

Tab. 4-2: Bridge selection criteria based on COST 323, adapted by PSP

The accuracy classes of different bridge types can be determined with , different bridge lengths are given with recommended sampling rates for the Spiders. The aim is to always use the lowest sampling rate which can be achieved at long bridges. The achievable accuracy classes also depend on the bridge condition.

The table answers the question if our system is able to reach a specific accuracy class, presupposed the class I or II in Tab. 4-1 can be fulfilled.

Tab. 4-3: Accuracy classes

L (m)	5-10	11-23	24-35	≥ 36
Rec. sampling rate (Hz)	1000	800	500	500
<b>Slab</b>	B(10)	B(10)	B(10)	-
<b>Frame</b>	B+(7)	A(5)	B+(7)	-
<b>Beam</b>	-	A(5)	B+(7)	-
<b>Steel box girder</b>	-	-	-	B(10)

We are looking for potential bridges on the A10 Tauernautobahn in the area of Kellerberg. There is a place where the police is undertaking weight controls at the end of the Kroislerwandtunnel at km 166.611 on the left side, on the opposite a motorway station is currently built which could be a possible place for static weighing in the future. The evenness criteria for weight control regarding to STVO is not given there.

The following potential bridges (Tab. 4-4) are available for Pilot measurements in Austria. We chose these bridges also with the aim to use them in a type approval test later on.

Tab. 4-4: Potential bridges for iBWIM application in Austria

	<b>D35A</b>	<b>D36</b>	<b>D42</b>
<b>Station [km]</b>	164.825	166.108	170.350
<b>Length [m]</b>	8.7	8.6	8.7
<b>System</b>	Slab	Frame structure	Slab
<b>Rut [mm]</b>	< 4	< 4	< 4
<b>Evenness (APL<sup>(1)</sup>)</b>	9	9	9
<b>Longitudinal slope [%]</b>	0.5	0.5	1.1
<b>Transverse slope [%]</b>	4.6	2.6/4.0	2.5
<b>Skewness [g]</b>	100	100	100
<b>Radius of curvature [m]</b>	≥ 1000	≥ 1000	≥ 1000
<b>Traffic flow</b>	free	jam	free
<b>Supply</b>	?	Tympanum	SOS telephone
<b>H<sub>max</sub> [m]</b>	5.7 fixed	≈ 5.0 fixed	> 6.0 fixed
<b>Pictures</b>			

<sup>(1)</sup> The evenness is specified with *Analyseur de Profil en Long* (APL). The assessment is quantifying the logarithm of energy dissipation in one of the three wavelength ranges: SW = small wavelengths (0.7 ... 2.8 m), MW = medium wavelength (2.8 ... 11.3 m) and LW = large wavelengths (11.3 ... 45.2 m). The scale is reaching from 10 for the smallest energy or excellent evenness up to 1 for highest energy or worst pavement.

Design of Experiments:

The base for preparing a test plan are given in COST 323 [4]. In chapter 8 there is a reference to test plan 4, for which the environmental condition E3 (full environmental reproducibility) and test conditions R3 (limited reproducibility conditions) are required.

The concept for a test plan contains the assignment in groups, 4 vehicle types are randomly allotted to 4 seasons. One vehicle type is used per season, assumed that there are no significant interdependencies at vehicle type and season.

The influence from seasons is determined with an additional checkpoint, the same vehicle drives on each test day or on one of the two following days.

The procedure of the test per group is done with a variation of velocities (two to three), the use of each lane and the use of the checkpoint.

The aim is to receive at least 120 test events per lane, prior-ranking the slow lanes per driving direction.

*Tab. 4-5: Summary of test plan vehicles*

Vehicle type	Weight	Lane	Velocity [km/h]	Runs
	empty	1	75	10
			60	10
		2	75	10
			60	10
	full	1	75	10
			60	10
2		75	10	
		60	10	
	empty	1	75	10
			60	10
		2	75	10
			60	10
	full	1	75	10
			60	10
		2	75	10
			75	10

#### 4.1 Monitoring procedure and results

The sensor arrangement is similar to the one used on the Vögelsangbrücke. The strain measurements were made by six strain gauges mounted in a row under each lane. Two additional strain gauges were placed on either side of the row for triggering and speed estimation. Laser sensors on each lane detected and located vehicle axles.

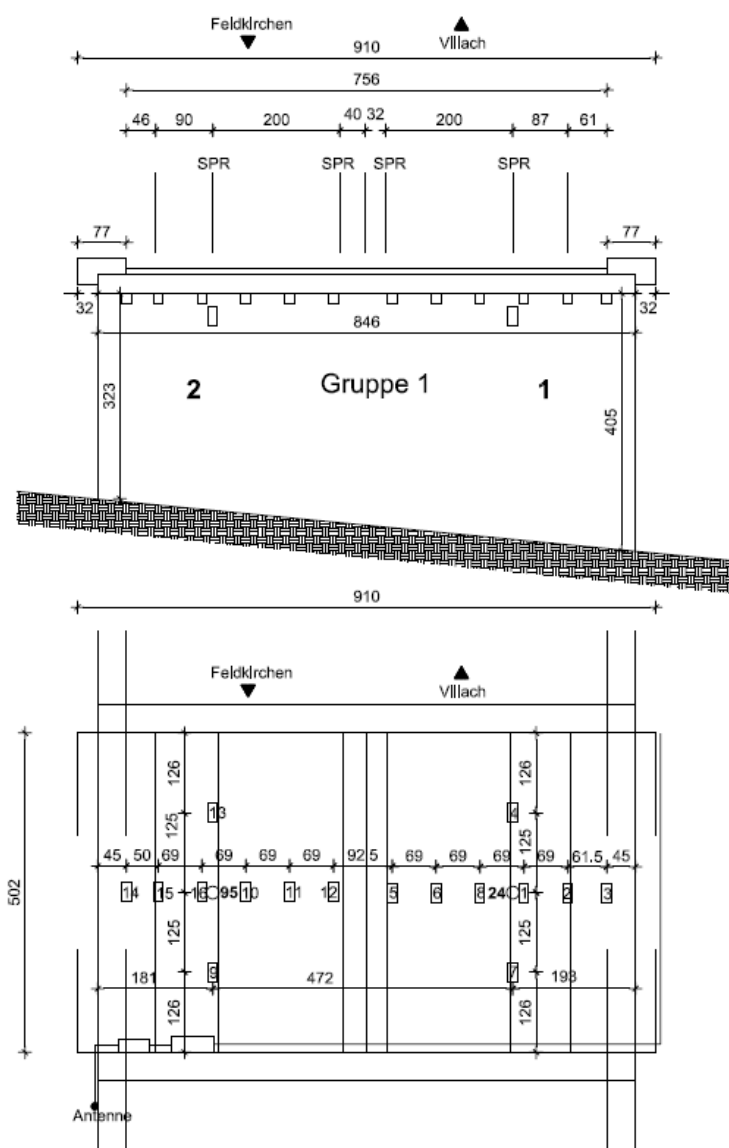


Fig. 4-1: Sensor arrangement for Tiffen bridge.

The most significant difference from the Vögelsangbrücke set up is due to power management. As with many BWIM [5], [7] installations, the Tiffen bridge is relatively remote from a power supply. There is a market for systems that combine solar power, large battery capacity and low power consumption. These are much more independent and flexible than a system that requires a mains supply. We implemented a system that uses a 1m<sup>2</sup> solar cell, a 120 Ah battery and a new low power embedded system. By shifting the computational burden from the embedded system to a central server we were able to use a less power embedded system and significantly reduce power consumption.

Initial tests of this approach were promising. In retrospect a 1m<sup>2</sup> solar cell was an underestimate—particularly since the trials were conducted over the winter months. This notwithstanding the system performed well: when the battery level fell below a set level, the system automatically entered a sleep mode and came back online when the voltage was sufficiently restored by the solar cell. The new

combination of a lightweight embedded system and computational server worked well. We also found it added significantly to our ability to modify and tailor the system to suit the bridge.

## 4.2 Development and calibration of the numerical model

The modelling and calibration of this pilot has not yet been completed and will be reported in the final version of this report.

## 4.3 Initial Analysis of Data Set

### 4.3.1 Introduction

Unlike the Vögelsangbrücke and the Wonka bridge, the bridge at Tiffen is intended as a development platform rather than a monitoring station. For this reason we cannot guarantee continuous coverage during the measurement period. It follows that the results reported in our temporal patterns must be treated with caution.

In any case, the measurements for the 60 day measurement period are shown in Fig. 4-2. Here in addition to the weekly periodicity observed on the other bridges, we also have the system outages affecting the graph. Nonetheless, it is not uncommon for more than 300 vehicles to cross the Tiffen bridge in a day.

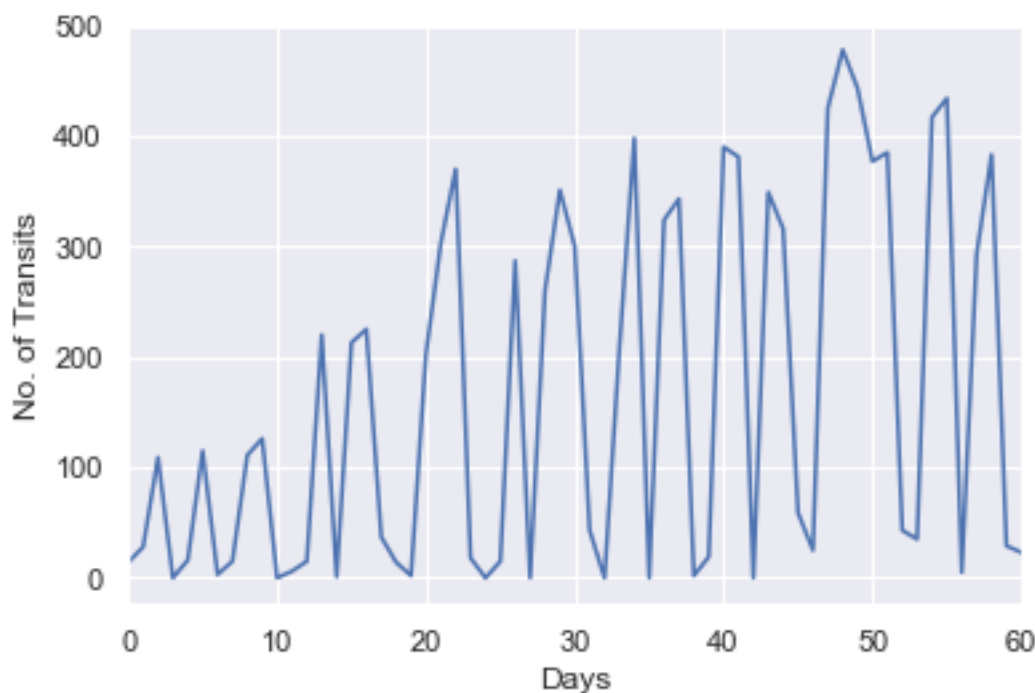


Fig. 4-2: Recorded transits during measurement period.

### 4.3.2 Bias

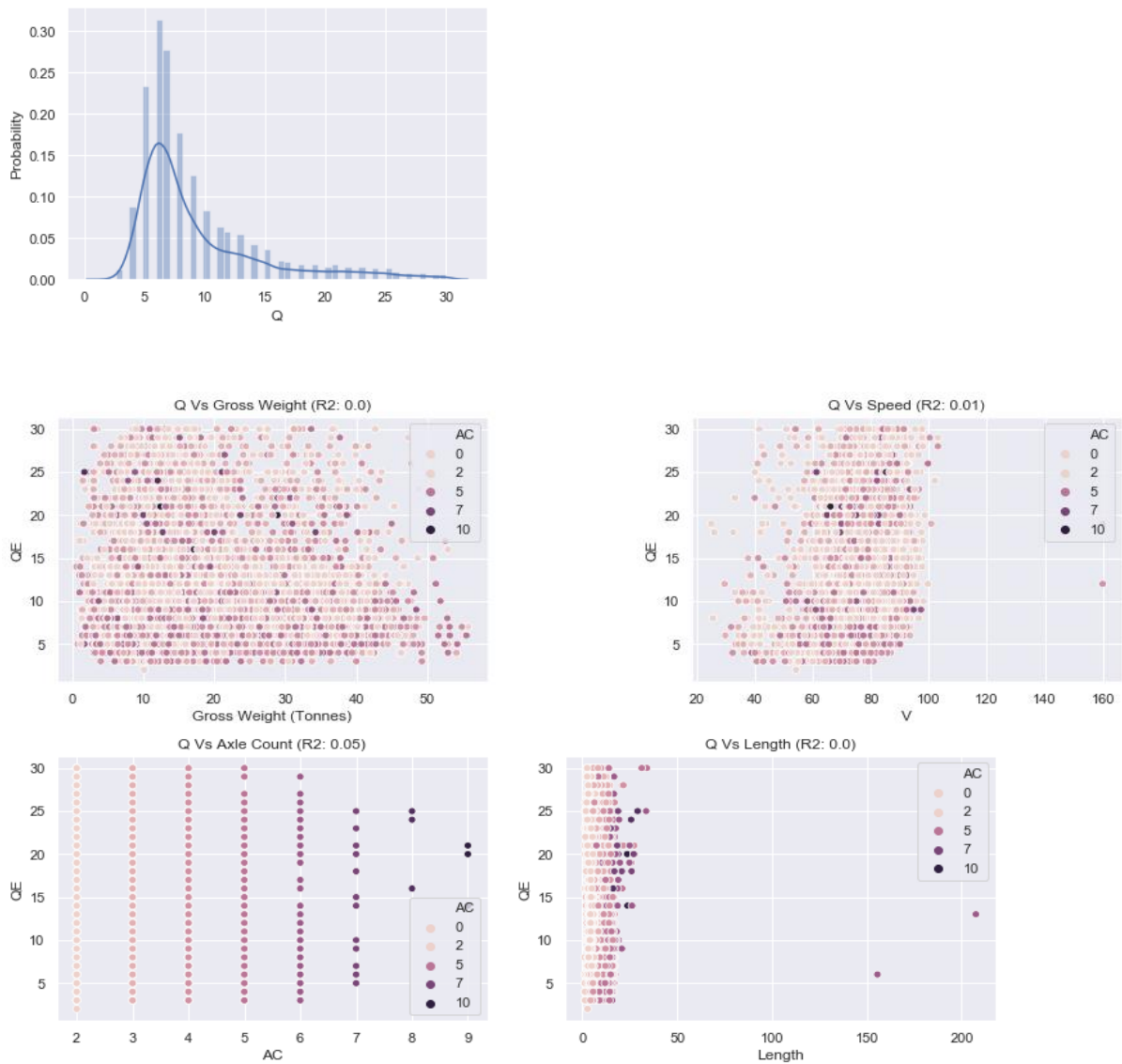


Fig. 4-3: Correlating quality metric with vehicle characteristics.

### 4.3.3 Vehicle Characteristics

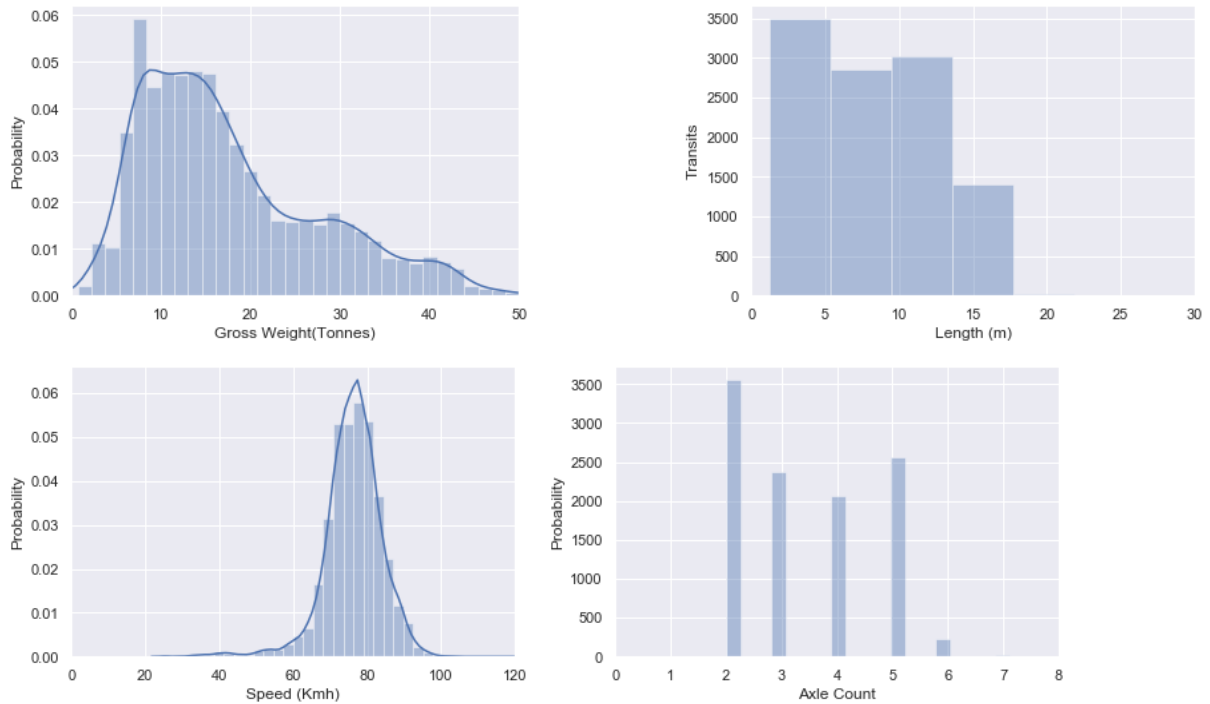


Fig. 4-4: Characteristics of vehicles crossing the Tiffen bridge

### 4.3.4 Temporal Patterns

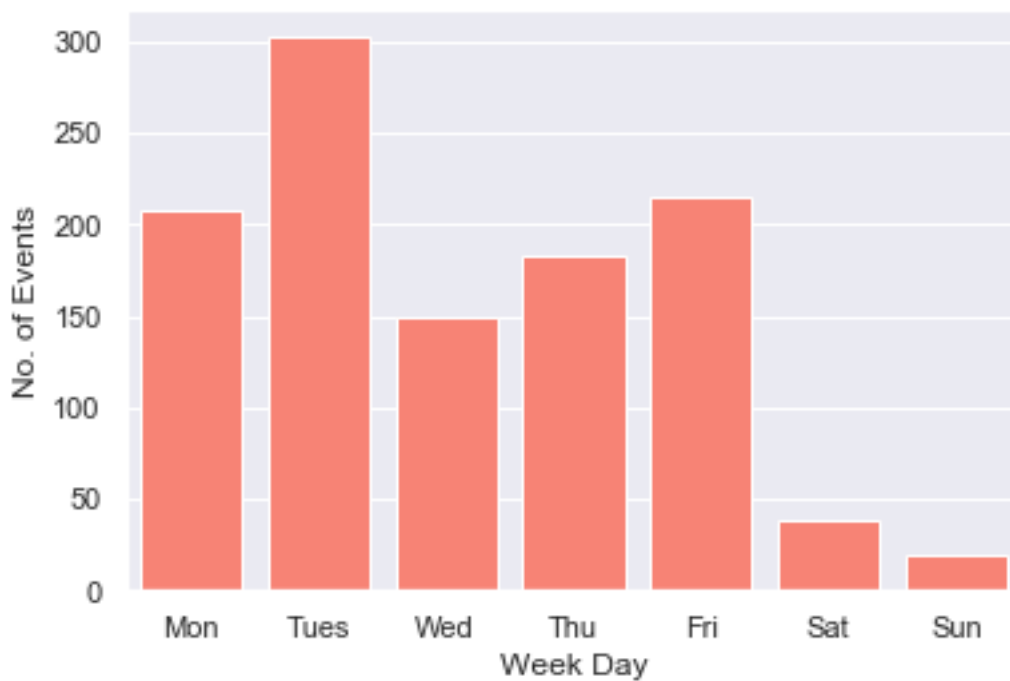


Fig. 4-5: Traffic over Tiffen bridge as a function of week day.

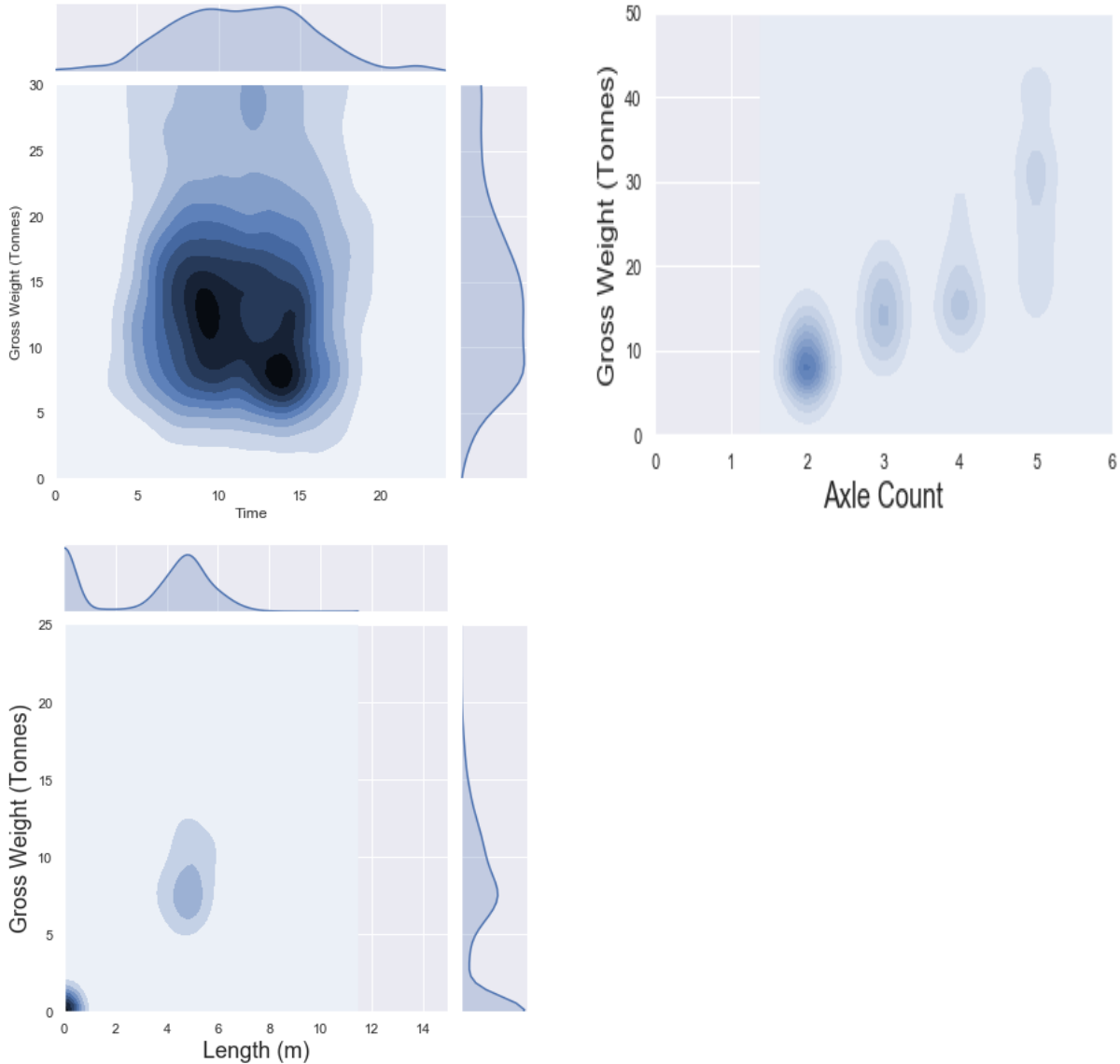


Fig. 4-6: Correlation between Vehicle Weight and axle count, Tiffen bridge

### 4.3.5 Damage Metrics

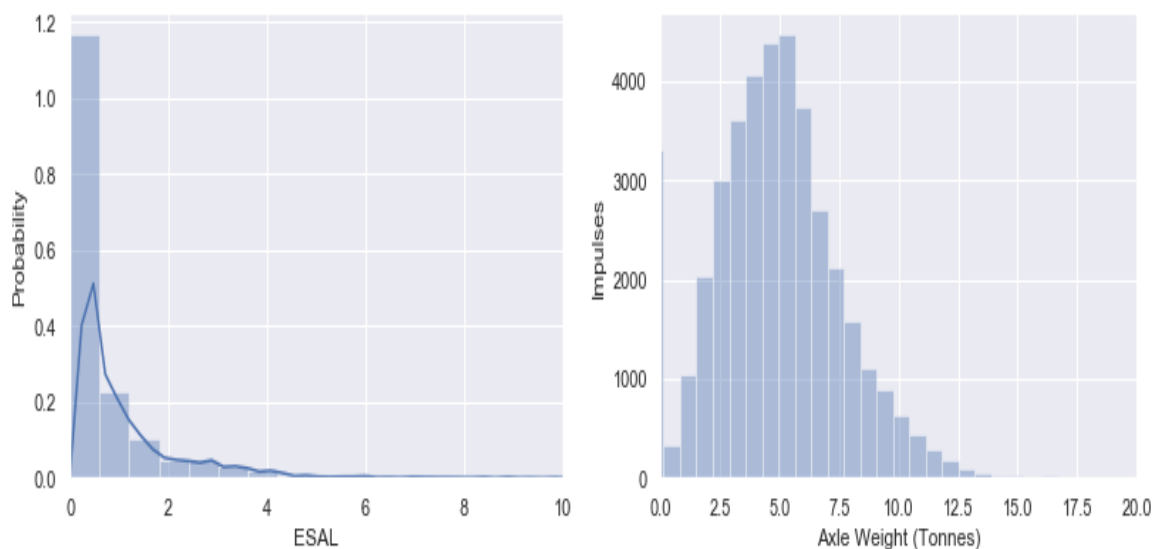


Fig. 4-7: Damage metrics, Vogelsang bridge, ESAL is equivalent single axel load

## 4.4 Ethical Issues

The Bridge Monitoring systems are deployed on public roads and detect actions made by members of the public. However, it is not possible to identify a vehicle purely with its strain signal. If combined with video surveillance it would be possible to read the license plate of vehicles, identify brands of commercial vehicles and, at least in theory, identify the drivers. However in this report we have not used video surveillance and these issues do not arise. Beyond the scope of the project we note that if CCTV is used the necessary civil authorities must be notified and the data can be retained only for a limited time period.

## 5 References

- [1] *fib* Model Code for Concrete Structures 2010. Wilhelm Ernst & Sohn, Berlin, Germany, (2013), ISBN 978-3-433-03061-5.
- [2] Cervenka, V., Reliability-based non-linear analysis according to fib Model Code 2010, Structural Concrete, Journal of the *fib*, Vol. 14, March 2013, ISSN 1464-4177, (2013) 19-28, DOI: 10.1002/suco.201200022.
- [3] V. Červenka, J. Cervenka, L. Jendele, Atena Program Documentation. V5.8, Part 1-7, Červenka Consulting, Prague, Czech Republic, 2000-2020.
- [4] COST 323. European Weigh-in-Motion Specifications, Version 3.0. Technical report, LCPC, Paris, 1999
- [5] M. Petschacher. Bridge-Weigh-in-Motion. ISSN 0379-1491. FSV, Wien, 2010
- [6] J. Červenka,, M. Petschacher, T. Mansberger,, M1.2 – Requirements for Project Pilots, Version 3.0, cyberBridge project, 22. 1. 2019
- [7] M. Petschacher, M3.2 – Sensor Implementation, PSP – Petschacher Software und Projektentwicklungs GmbH, Feldkirchen, Austria
- [8] J. Červenka, T. Mansberger, M6.2 – Simulation and Probabilistic Prognosis Model, Version 1.0, cyberBridge project, 4.9.2019
- [9] T. Mansberger, J. Červenka,, M. Petschacher, M8.1 – Preliminary Survey of the Pilots, Version 1.0, cyberBridge project, 22. 1. 2019

## Acknowledgements

This document was created within the Eurostars project cyberBridge E!10925. The financial support of the Eurostars program and national funding agencies in Czech Republic, Germany and Austria are greatly appreciated.

The partners in the project are:

Cervenka Consulting s.r.o. ....	CER
Petschacher Software und Projektentwicklungs GmbH.....	PSP
Leonhardt, Andrä und Partner, Beratende Ing. VBI AG.....	LAP
Institut für Bauinformatik, TU Dresden.....	TUD

This report owes to a collaborative effort of the above organizations.

## More information

Public cyberBridge reports are available through:

cyberBridge public web site <a href="http://www.cyberBridge.eu">http://www.cyberBridge.eu</a>
---

## Copyright

© cyberBridge Consortium 2018, 2019, 2020

© Cervenka Consulting s.r.o. 2018, 2019, 2020

© Petschacher Software und Projektentwicklungs GmbH 2018, 2019, 2020

© Leonhardt, Andrä und Partner, Beratende Ing. VBI AG 2018, 2019, 2020

© Institut für Bauinformatik, TU Dresden 2018, 2019, 2020